
THE UNIVERSITY
*of* EDINBURGH

**THE UNIVERSITY of EDINBURGH**
**Institute of Materials and Processes**
**School of Engineering**


# *Electrochemical machining: towards 3D simulation and application on SS316*

Ares Argelia Gómez Gallegos

**A thesis submitted to the University of Edinburgh**
**for the Degree of Doctor of Philosophy, 2015**

# *Declaration*

The candidate hereby confirms that the work submitted is her own, except where otherwise stated in this thesis. The contribution of the candidate and other authors to this work has been explicitly indicated. The candidate confirms that appropriate credit has been given where reference had been made to the work of others. The candidate confirms that the work has not been submitted for any other degree or professional qualification.

Ares Argelia Gómez Gallegos

# *Acknowledgements*

I gratefully acknowledge the scholarship from CONACYT during the development of the present work and to pECM systems Ltd. for supporting the experimental work.

I would like to thank my supervisors, Dr. Frank Mill and Prof. Andy Mount, for their guidance and advice, they were invaluable during this project, and to my examiners, Dr. Vasileios Koutsos and Dr. David Clifton, for the time you dedicated to this work, and your comments and insights.

I want to express my gratitude for the immense support that my PhD fellow students (and friends) provided me. Although there are far too many to name, there are some that deserve a particular mention: Alex, Alex, Apostolos, Dani, Davide, Dimitris, Dimitris, Dursun, Enzo, Helen, Ilka, Matt, Mike, Olga, Pedro, Patrick, and Zoe; you all taught me more than you could ever imagine and transformed my everyday routine, inside and outside the office, into an enjoyable and enriching experience. I cannot imagine how I could have finished my PhD without you. Thank you. To Charitea, Esme, Nelly, Nick and Sofia, thank you for your encouragement in the darker moments of my writing up. Furthermore, I would like to express my gratitude towards all members of IMP and Engineering School for making the Sanderson Building a constructive and inspirational work environment.

I want to make a special mention to my Italian family, who adopted me and provided me with an inexhaustible source of love and friendship. Franci and Simo, thank you for making our flat a home. And to my Mexican friends, in Mexico, Japan and Edinburgh, for being a constant support albeit the distance.

Quiero agradecer especialmente a mi familia: a mis papás, Héctor y Argelia, por todo el apoyo y compresión durante esta aventura. Sé que en muchas ocasiones fue más difícil para ustedes que para mí. A mi hermana, Airé, por tu ejemplo y cariño. Lo logramos de nuevo!. A Jorge, por ser parte de mi familia y cuidar de ella mientras estoy lejos. Y a la familia Gallegos y Gómez por estar siempre al pendiente de mí. Gracias.

And finally, to God.

# Abstract

Electrochemical machining (ECM) is a non-conventional manufacturing process, which uses electrochemical dissolution to shape any conductive metal regardless of its mechanical properties and without leaving behind residual stresses or tool wear. Therefore, ECM can be an alternative for machining difficult-to-cut materials, complex geometries, and materials with improved characteristics, such as strength, heat-resistance or corrosion-resistance. Notwithstanding its great potential as a shaping tool, the ECM process is still not fully characterised and its research is an on-going process. Various phenomena are involved in ECM, e.g. electrodynamics, mass transfer, heat transfer, fluid dynamics and electrochemistry, which occur in parallel and this can lead to a different material dissolution rate at each point of the workpiece surface. This makes difficult an accurate prediction of the final workpiece geometry. This problem was addressed in the first part of the present thesis by developing a simulation model of the ECM process in a two-dimensional (2D) environment. A finite element analysis (FEA) package, COMSOL multiphysics® was used for this purpose due to its capacity to handle the diverse phenomena involved in ECM and couple them into a single solution.

Experimental tests were carried out by applying ECM on stainless steel 316 (SS316) samples. This work was done in collaboration with pECM Systems Ltd® from Barnsley, UK. The interest of studying ECM on stainless steels (SS) resides on the fact that the application of ECM on SS typically results in various different surface finishes. The chromium in SS alloys usually induces the formation of a protective oxide film that prevents further corrosion of the alloy, giving the metal the special characteristic of corrosion resistance. This oxide film has low electrical conductivity; hence normal anodic dissolution often cannot proceed without oxide breakdown. Partial breakdown of the oxide film often occurs, which causes pits on the surface or a non-uniform surface finish. Therefore the role of the ECM machining parameters, such as interelectrode gap, voltage, electrolyte flow rate, and electrolyte inlet temperature, on the achievement of a uniform oxide film breakdown was evaluated in this work. Experimental results show that the resulting surface finish is highly influenced by the overpotential and current density, and by the characteristics of the electrolyte, flow rate and conductivity. The complexity of experimentally controlling these parameters emphasised the need for the development of a computational model that allows the simulation of the ECM process in full.

The simulation of ECM in a three-dimensional (3D) environment is crucial to understand the behaviour of the ECM process in the real world. In a 3D model, information that was not visible

before can be observed and a more detailed realistic solution can be achieved. Hence, in this work a computer aided design (CAD) software was used to construct a 3D geometry, which was imported to COMSOL Multiphysics® to simulate the ECM process, but this time in a 3D environment. This enhanced simulation model includes fluid dynamics, heat transfer, mass transfer, electrodynamics and electrochemistry, and has the novelty that an accurate computational simulation of the ECM process can be carry out *a priori* the experimental tests and allows the extraction of enough information from the ECM process in order to predict the workpiece final shape and surface finish. Moreover, this simulation model can be applied to diverse materials and electrolytes by modifying the input ECM parameters.

***Lay Abstract***

Electrochemical machining (ECM) is a manufacturing process in which the material of a workpiece is removed by electrochemical dissolution, often characterised as "reverse electroplating". It is normally used to shape extremely hard metals, complex geometries, and special materials used in aerospace, medicine and other high value industries. ECM is a complex process that involves various phenomena occurring in parallel, thus making difficult the correct control of the process and the accurate prediction of the final workpiece geometry. In this thesis, this problem was addressed by developing a two-dimensional (2D) computational simulation model of the ECM process, in which ECM can be carried out virtually before the actual process is implemented.

Experimental work was performed in collaboration with pECM Systems Ltd® from Barnsley, UK, where ECM was applied on the interior face of commercial stainless steel 316 (SS316) pipes. The ECM machining parameters, e.g. interelectrode gap, voltage, electrolyte flow rate, and electrolyte inlet temperature, were varied in order to evaluate their role on the ECM results, specifically in the quality appearance of the pipe surface (surface finish). The complexity of experimentally controlling these parameters emphasized the need for a computational model that allows the simulation of the ECM process in full and the correct prediction of the final workpiece shape and surface finish before the experimental work.

The simulation of ECM in a three-dimensional (3D) environment is crucial to understand the behaviour of the ECM process in the real world. In a 3D model, information that was not visible before can be observed now and a more detailed solution can be achieved. Hence, a new ECM simulation model was built in a 3D environment giving a better understanding of the process and more accurate results. Moreover it allows the extraction of enough information from the ECM process in order to predict accurately the workpiece final shape and surface finish. Furthermore, this simulation model can be applied to diverse materials and electrolytes by modifying the input ECM parameters. This potentially will increase the applicability of ECM in industry.

# Table of Contents

# Table of figures

# Acronyms and Symbols

| | |
|---|---|
| 2D | two dimensional |
| 3D | three dimensional |
| BEM | boundary element method |
| CAD | computer aided design |
| CNC | computer numerical controlled |
| ECM | electrochemical machining |
| EDM | electrodischarge machining |
| FD | finite difference |
| FE | finite element |
| FEA | finite element analysis |
| FEM | finite element method |
| LBM | laser beam machining |
| pECM | pulse electrochemical machining |
| SS | stainless steel |
| SS316 | stainless steel 316 |
| USM | ultrasonic machining |
| WJC | water jet cutting |

| | |
|---|---|
| $A$ | cross sectional area of the electrode |
| C | electrolyte specific heat |
| $dx$ | x-displacement |
| $dy$ | y-displacement |
| $dz$ | z-displacement |
| $E$ | electric field within the electrolyte |
| $F$ | Faraday's constant |
| $f$ | tool feed rate |
| $I$ | electric current |
| $J$ | current density |
| $k$ | electrolyte thermal conductivity |
| $K_1$ | electrochemical constant |
| $k_e$ | electrolyte electric conductivity |
| $l$ | characteristic length of the channel |
| $m$ | material dissolved |
| $M$ | molar mass |
| $nJ_{side}$ | normal current density at the sides of the interelectrode gap |
| $Nu$ | Nusselt number |
| $P$ | power |

| | |
|---|---|
| $p$ | pressure |
| $Q$ | electrolyte flow |
| $q$ | Joule heat |
| $R$ | resistance of the conductor |
| $Re$ | Reynolds number |
| $T$ | electrolyte temperature |
| $t$ | time |
| $T_e$ | entrance electrolyte temperature |
| $T_{out}$ | exit electrolyte temperature |
| $U$ | maximum electrolyte velocity |
| $u$ | mean electrolyte velocity |
| $V$ | voltage |
| $V_0$ | overvoltage |
| $V_1$ | voltage applied |
| $y$ | interelectrode gap |
| $z_n$ | valence |
| $\delta T$ | temperature difference |
| $\eta$ | electrochemical machining efficiency |
| $\nu$ | electrolyte kinematic viscosity |
| $\dot{\nu}$ | volumetric material removal rate |
| $\rho$ | electrolyte electric resistance |
| $\rho_a$ | anode density |
| $\rho_e$ | electrolyte density |
| $\varphi$ | electric potential distribution |
| $\varphi_{anode}$ | electric potential at workpiece |
| $\varphi_{cathode}$ | electric potential at tool |

# Chapter 1

## *Electrochemical machining background*

*If the questions don't make sense,*

*neither will the answers.*

*-Kurt Vonnegut*

## 1.1. *Introduction*

The continuous development of new materials with enhanced characteristics, in terms of their properties and performance, has led to the progress in manufacturing processes. These new and usually non-conventional manufacturing processes aim to shape these materials for their applications in aerospace, medical, energy and other high value industries. Conventional manufacturing processes are characterised by the application of a sharp/hard tool for the removal of material from a softer workpiece, while non-conventional manufacturing processes harness energy (mechanical, electrical, chemical, or a combination of them) for removing the excess material [1], making possible the manufacturing of these new high performance materials.

Electrochemical machining (ECM) is one of these non-conventional processes, which uses electrochemical dissolution to shape any conductive metal regardless of its mechanical properties [2] and without leaving behind residual stresses or tool wear [3]. Therefore, the implementation of ECM in industry emerges as an alternative for machining difficult-to-cut materials, complex geometries and materials with improved characteristics, such as strength, heat-resistance or corrosion-resistance, which otherwise would be impossible or not economically viable to machine with conventional techniques. ECM applications include the fabrication of blades used in gas turbine engines [4]–[6], biomedical implants [7] and everyday products [8]. However, there are still many challenges to overcome in order to increase the ECM use as a manufacturing alternative, such as material removal forecast and control, tool design, and environmentally friendly electrolyte and products disposal. [9]–[12].

The ECM system comprises an electric circuit formed by the tool (cathode) and the workpiece (anode) connected to an external electrical source. The electrodes are submerged in an electrolyte bath that closes the circuit. When electric current passes through the circuit, the metal ions from the anode travel towards the cathode (anodic dissolution). In ideal cases, this ions movement from the workpiece surface leaves behind a negative imprint of the tool profile [13], [14]. The electrolyte is pumped through the interelectrode gap flushing away the dissolved metal ions from the workpiece before they can deposit on the tool surface and at the same time mitigating the temperature increase of the system.

ECM is based on the concept of electrolysis, which laws were established by Faraday in 1833 [13]. This machining technique was reported for first time in 1929 by V. N. Gusseff [15], and developed as an industrial manufacturing option in 1959 by Anocut Engineering Company [16]. By 1990, ECM was already employed in many industries, *e.g*. automotive, offshore petroleum,

aerospace and medical engineering [13]; nonetheless the ECM process is still not fully characterised and its research is an on-going process. The main research areas can be divided as following: numerical simulation, optimization of the specification and machine operation conditions, tool design, electrochemical micromachining, and new application practices of the process (such as ECM jet machining, ECM wire machining, ECM by a universal–tool, etc.).

Various phenomena are at play in ECM, e.g. electrodynamics, mass transfer, heat transfer, fluid dynamics and electrochemistry [2]. These phenomena occur in parallel and this can lead to a different material dissolution rate at each point of the workpiece surface [17], thus making difficult a correct prediction of the final workpiece geometry. Furthermore, one of the main advantages of the ECM process, the potential of shaping complex geometries, is constrained by the complexity of the tool design techniques. In order to solve these problems, diverse theoretical studies of the ECM, e.g. numerical solutions [18], [19], two-dimensional computational models [17], [20], [21], and three-dimensional computational models [22]–[24], had been developed. In parallel, experimental investigation in areas such as surface finish [25]–[27], cathode design [28]–[30], and micro- and nano- machining [31]–[33], had been carried out. The outcomes of these investigations have made evident the need for a computational simulation model that could explain and forecast the ECM process. Several works have been published about the simulation of ECM on two-dimensional (2D) geometries, however there are still few authors who had succeeded in the ECM simulation in a three-dimensional (3D) environment.

For these simulations usually a tool with fixed geometry is used to shape a static workpiece. The dissolution of the workpiece surface profile obeys ECM theory and the corresponding equations can be solved by finite difference (FD) [17], [34], boundary element method (BEM) [22], [35]–[37], or finite element method (FEM) [38]–[40]; however these studies were limited by the complexity of setting up the problem or the technological limitations at the time the studies were done. Therefore an accurate prediction of the resulting workpiece shape is still one of the main limitations for the application of ECM in the industry. To this extent, in the first part of the present thesis, this problem was addressed by developing a simulation of the ECM process in a 2D environment. A finite element analysis (FEA) package, COMSOL multiphysics® was used for this purpose due to its capacity to handle the diverse phenomena involved in ECM and couple them into a single solution.

In the second part, experimental tests were carried out by applying ECM on stainless steel 316 (SS316) samples. This work was done in collaboration with pECM Systems Ltd® from Barnsley, UK. The interest of studying ECM on stainless steels (SS) resides on the fact that the application

of this process on SS typically results in various different surface finishes. Various studies [26], [27], [41], [42] have been undertaken in order to understand the behaviour of ECM on SS, however the process is not fully understood yet. SS are iron chromium alloys, typically with greater than 10 weight percentage (wt%) chromium. Chromium induces the formation of a protective oxide film that prevents further corrosion of the alloy [1], [27], giving the metal the special characteristic of corrosion resistance. This oxide film has low electrical conductivity; hence normal anodic dissolution often cannot proceed without oxide breakdown. Partial breakdown of the oxide film frequently occurs, which causes pits on the surface [43] or a non-uniform surface finish [27]. Therefore, for the experimental work in this thesis, the ECM machining parameters, such as interelectrode gap, voltage, electrolyte flow rate and electrolyte inlet temperature, were varied in order to evaluate their role, if any, on the achievement of a uniform breakdown of the oxide film. The experimental results are consistent with earlier experimental results [26], [27], [43] on the fact that the resulting surface finish is highly influenced by the ECM electrochemical parameters (overpotential and current density), and the characteristics of the electrolyte, such as flow rate and conductivity.

The complexity of experimentally controlling these parameters emphasises the need for the development of a computational model that allows the simulation the ECM process in full. For this purpose, the information extracted from the experimental tests was used to modify the previous 2D ECM simulation of the first part of this thesis, in order to build a more accurate model. Computer aided design (CAD) software was used to construct a 3D geometry, and the model was imported to COMSOL Multiphysics® to simulate the process, but this time in a 3D environment. This new simulation model includes fluid dynamics, heat transfer, mass transfer, electrodynamics and electrochemistry, and allows extracting enough information from the ECM process in order to predict the workpiece final shape and the surface finish of the samples. Moreover, the results achieved are a complement of previous studies [44]–[46] dedicated to investigate the effect of the ECM parameters on the material removal rate, surface finish and overcut, with the novelty that an accurate computational simulation of the ECM process, can be carry out *a priori* the experimental tests and allowing the extraction of enough information from the ECM process in order to predict the workpiece final shape and surface finish. Additionally, this simulation model considers the electrochemical effects on the process, and it can be applied to diverse other materials and electrolytes by just modifying the input ECM parameters.

### 1.2. *How the thesis is organized*

The present thesis is divided in four chapters:

In Chapter 1, the relevant theoretical background in machining processes, the principles of electrochemical machining and the basic finite element (FE) methodology are discussed. The objective of this chapter is to provide the necessary background knowledge in order to understand the concepts behind the results presented in Chapter 2.

In Chapter 2, an insight into the simulation of the ECM process is provided. A two-dimensional (2D) simulation of the ECM process using a finite element analysis (FEA) package is presented, followed by ECM experimental tests. The experimental work was developed on samples of SS316 due to their singular behaviour when they are electrochemically machined, i.e. the resulting surface finish of the samples is non-uniform or consistent. Therefore, a complete analysis of the ECM parameters effect on the resulting surface finish on the SS316 samples was undertaken and the results were used for enhancing the simulation. This chapter is closed by the introduction of a 3D ECM simulation model, which not only accurately predicts the final shape of the workpiece, but also the final surface finish on the SS316 samples.

In Chapter 3, the 3D ECM simulation model developed in Chapter 2 is applied for the simulation of two different cases of ECM on SS316 samples, case 1 being a reflective and shiny surface finish and case 2 a passivated one. Additionally, the model is applied for case 1 again but this time using a different electrolyte, NaCl instead of $NaNO_3$, case 3. And lastly, in case 4, the model is applied as a means for forecasting the optimal machining time and profile that can be achieved by ECM on the SS316 samples, since this is also one of the main requirements of the industrial collaborator. The aim of this chapter is to show the versatility of the ECM simulation model developed.

In Chapter 4, a general summary of the work carried out is presented and the main findings discussed. With consideration of these closing remarks, future work, in terms of the ECM research and computational simulation, is suggested.

## 1.3. *Literature review*

### 1.3.1. Machining Processes

Machining is any manufacturing process in which a tool shapes or sizes a workpiece by removing material from it. The manufacturing processes are governed by the growing advancement in all the aspects in the industry, e.g. materials development, processes, equipment and production control, and environmental sustainability.

In materials development, material composition, enhanced properties, manufacturing characteristics, reliability, service life, recyclability and cost are some of the development areas. In parallel, new materials with special characteristics, such as superconductivity, shape-memory and heat or deformation resistance are created every day [1]. Consequently this development had influenced the tool, mould, and die materials, improving the efficiency of the manufacturing processes, or pointing out the necessity of the development of new ones.

In terms of processes, equipment and production control, the efficiency of the manufacturing processes is having a major impact from the development of computers, controls and software. This technology is used for automation and inspection processes, and for material handling and product assembling. Moreover, the manufacturing companies are applying concepts of group technology, cellular manufacturing and flexible manufacturing, in addition to computational models and simulations for the design and manufacturing of products, resulting in the optimisation of process and production systems [1].

Environmental sustainability has been applied to many fields, including engineering, manufacturing and design. Specifically sustainability in manufacturing requires balancing between economic and environmental objectives, policies and practices. Some of the main focus areas are green manufacturing, life cycle factors and priorities in advancing manufacturing operations and processes [47]. The manufacturing processes that already exist have to be modified in order to comply with the new legislations and to reduce their environmental impact, and the new ones have to be designed in such a fashion that their environmental impact is minimal.

#### 1.3.1.1. Conventional machining processes

The machining process depends on the material to cut, the geometric characteristics of the piece, and the machining specifications and capabilities. Conventional machining processes of metals, e.g. turn, mill, drill, etc., [13], [48] are based on the same principle, a sharp tool of hard material is moved through a softer workpiece, part of which is consequently removed. The

harder and sharper the cutting tool is, the smaller the force required to make the cut. The friction between the workpiece and the tool causes temperature rise in both. The increased temperature usually results in the plastic deformation of the workpiece, which is not ideal for a machining process, and causes additional plastic deformation and wear of the tool [49], [50]. In extreme cases the integrity of the surface of the material is affected by this heat resulting in cracks and porosity that limit the performance of the piece [51].

Conventional machining is well known and widely used in industry, in order to succeed however, the tool must be harder than the workpiece material. Hence, the continuous development of new materials with improved characteristics, in terms of their toughness, hardness and elasticity, represents a limitation for the development of conventional machining tools that should be always a step ahead of these new enhanced materials.

#### 1.3.1.2. Non-conventional machining processes

The development of new machining processes is the answer to the need for accomplishing the manufacturing requirements of the new materials that otherwise would not be able to achieve or would not be economically viable by conventional machining processes [13], [52]. Non-conventional machining processes harness energy (mechanical, electrical, chemical or a combination of them) to remove the excess of material in the workpiece [48]. These processes have the advantage of being able to meet at least one of the following needs:

- machining of newly developed materials. Frequently, these materials have special properties (e.g. high resistance to fracture, hardness, heat resistance, etc.),
- machining of complex geometries, sometimes impossible to achieve by other manufacturing processes,
- avoid damages of the material, at the surface or internal, that usually occurs as a result of the stresses or heat produced in conventional machining processes.

These kind of processes are usually characterised by higher power consumption and lower material removal rates than the conventional machining processes. Non-conventional machining processes are classified according to the type of energy used to remove material: mechanical, electrical, thermal and chemical.

In mechanical processes, mechanical energy is applied in a different fashion than as the sharp-cutting tool used in the conventional machining. The typical way of applying the mechanical energy is for erosion on the work piece (e.g. ultrasonic machining, water jet cutting, etc.) [48].

In electrical processes, energy generated by electrical reactions is used to remove the material of the workpiece, usually involving chemical reactions as well (e.g. electroerosion, wire cutting, electrochemical machining, etc.) [48].

In thermal processes, thermal energy, heat, is applied in a small area of the work piece, resulting in the fusion or vaporisation of the material. Typically this thermal energy is generated by the conversion of electric energy into thermal energy (e.g. laser cutting, electrojet machining, etc.) [48].

In chemical processes, some acids and other substances are used to chemically attack the workpiece in order to remove material from its surface. The rest of the workpiece is protected by a mask, controlling the dissolution area (e.g. photochemical machining, etching, etc.) [48].

### 1.3.2. Electrochemical Machining

Electrochemical machining (ECM) is a non-conventional machining process, based on the localised anodic dissolution of any conductive material [13]. The workpiece (anode) and the tool (cathode), immersed in flowing electrolyte, are the electrodes of an electrolytic cell. When an electric potential is applied, metal ions from the anode travel towards the cathode. There is an inverse relation among the distance between the electrodes (interelectrode gap) and the quantity of ions dissolved, hence in ideal cases, this movement of metal ions from the workpiece leaves behind a negative imprint of the tool geometry [13], [14]. A high flow rate of electrolyte within the interelectrode gap flushes away the metal ions to prevent that they deposit at the tool surface [1], and at the same time mitigating the temperature rise of the system. Due to the fact that the material removal is only by electrochemical dissolution and that the process is contactless, ECM is not affected by the hardness, toughness or ductility of the workpiece. ECM can be used for drilling, grinding and profiling, where the cathode is the cutting tool [53].

Figure 1.3-1 shows a schematic of an electrochemical machining system. The ECM tool is generally made of brass, copper, bronze or stainless steel, and in the simplest case, its geometry is the negative shape of the expected workpiece. The electrolyte is a highly conductive inorganic salt solution, such as sodium chloride (NaCl) or sodium nitrate ($NaNO_3$) mixed with water. A DC power supply, in the range of 5-36 V, maintains the current density on the active machined surface around 1.5-8 A/mm$^2$ for industrial applications [1]; and a pulsed voltage, where the anodic dissolution occurs during the short pulse-on time and the dissolution products are flushed away during the pulse-off time, is usually used for high precision applications [54], [55].

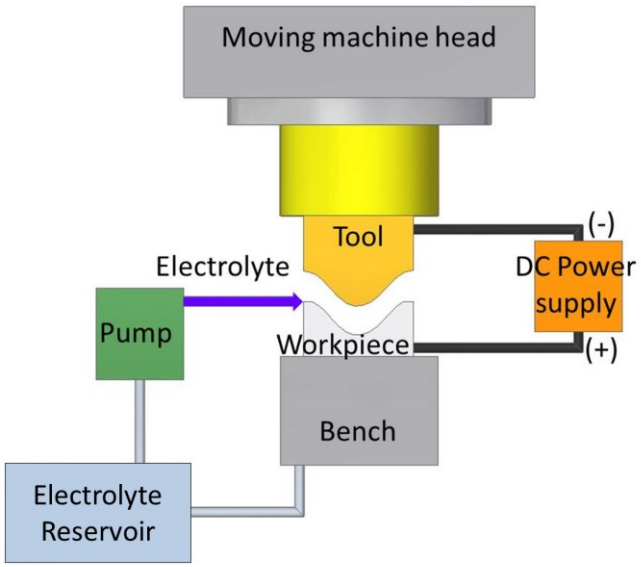


***Figure 1.3-1 Schematic of the electrochemical machining system.***

ECM is the result of a complex interaction of various physical and chemical phenomena, such as electrodynamics, mass transfer, heat transfer, fluid dynamics and electrochemistry, which occur in parallel and usually are dependent on each other [2]. Figure 1.3-2 shows these interactions in an illustrative fashion, highlighting the complexity of the process.

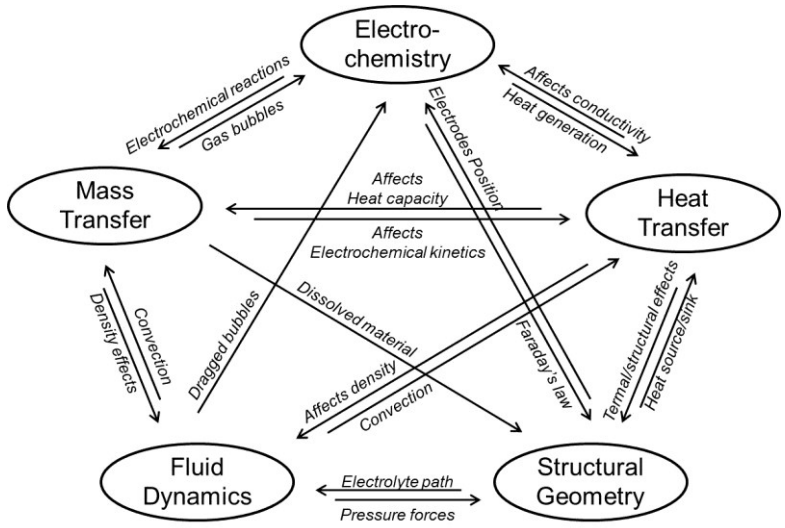


***Figure 1.3-2 Phenomena involved in ECM. Taken from [2].***

#### 1.3.2.1. The history of ECM

The concept of Electrochemical Machining (ECM) goes as far back as 1923, when Haring and Blum [56] studied a rectangular electrolytic cell with two cathodes at the small ends and an anode placed between them, named the Haring-Blum cell. This cell is still used to determine the macro-throwing power (ability of an electrolyte to deposit a film of uniform thickness across an electrode surface [57]) and is based on the phenomenon of electrolysis, which laws were established by Faraday in 1833 [13]. In 1929 Gusseff [15] registered the first patent on a "Method and apparatus for the electrolytic treatment of metals", where a process for dissolving metals electrochemically was presented. Then, in 1949 Faust [58] published a study on electropolishing. He defined electropolishing as the removal of the outermost skin of a metal by anodic dissolution in an acid or alkaline electrolyte. At that time, the process was not fully understood and only some basic recommendations for the electropolishing baths were given. These were the first steps toward the development of ECM.

E. Bishop [59], 1960, translated a book from A. Livshits about the novelty of a machining process where the necessity of the conventional conversion of electrical to mechanical energy was eliminated by using sparks for removing material, named electroerosion. The author believed that the metal removal was achieved dominantly by thermal effects. In 1968, De Barr and Oliver [49] presented a book explaining the basic theory for the electrochemical machining, the electrochemistry involved, the electrolytes selection, the tool parameters, and some of the ECM applications. Later on, in 1974, J. A. McGeough [60] also published a book about the principles of electrochemical machining. In it, studies of the diverse fields that are correlated in the ECM process, such as fluid dynamics, electrochemistry, and dynamics, kinematics and mechanical design of the machine components, were introduced. These books had become the basic texts for the electrochemical machining studies.

In 1959, ECM was developed as an industrial manufacturing option for shaping holes in metals by Anocut Engineering Company [16]. Later on, in 1961 Banerjee and Walker [25] presented a work about the electrolytic machining of iron threaded surfaces, where filaments formed on the edges of iron surfaces could be effectively removed by hydrochloric acid solutions, resulting in the formation of a highly active and smooth surface. In the same year Rolls-Royce plc implemented in UK the first ECM machine for the mass production of gas turbine blades [61]. By 1990 ECM was already employed for manufacturing of components in many industries, e.g. automotive (turbo charges and gears), offshore petroleum (turbine engine components and pumps), and medical engineering industries (surgical instruments and blades), as well by aerospace firms, which were its principal user for machining gas turbines, nozzles, valves, etc. [13], [62].

Since 1969, D. Landolt *et al.* have studied [63]–[66] the anodic dissolution of metals under electrochemical machining conditions. For this purpose a flow channel apparatus was designed to enable an optical study of the process by using glass walls and a high speed camera. Datta and Landolt [67] focus their studies on the surface quality of the metal after the ECM process and published a work about the topic in the Journal of the Electrochemical Society in 1975. Their results indicated that the onset of surface brightening was mass transfer controlled and coincided with the formation of a salt precipitation layer at the anode; in contrast with the studies presented by Bishop, who believed that ECM was just a thermal process. Later on Datta [68]–[71] continued with these studies and applied ECM for micromachining. His findings led to patenting a process for the planarization of surfaces via electrochemical metal removal [72].

ECM had found a variety of applications due to its capacity to reproduce an electrode shape in any metal regardless of their hardness. In 1976, the application of ECM was extended to special metals, such as titanium alloys, and the results were presented by J. Bannard [73] and J. Mathieu [74]. In 1999 The University of Edinburgh started the study of electrochemical machining in a collaboration between the departments of Chemistry and Mechanical Engineering; A. Mount, D. Clifton, P. S. Howarth, G. Alder, amongst others studied the electrochemistry on the systems and analysed the current density-voltage effects. Experimental validation of the ECM process on titanium, Inconel alloys [3], [75], and stainless steels [26], [27], [76] was also carried out. These studies gave an extended approach of the works developed by Bannard, and those developed at the end of the decade of the 80's, when Landolt *et al.*, published some works focusing on the electrochemical polishing of chromium alloys and stainless steels [42], [77], [78] using a rotating disc. Special attention has been directed to ECM on steels with high chromium content due to their wide applications in industry and their characteristic behaviour (oxidation resistance). Iron-chromium alloys, such as stainless steels, usually have a surface film formed by chromium that protects the metal from corrosion but also modifies the electrochemical machining process. Haisch *et al.*, 2001 [79] presented a work in this respect taking into account the role of microscopic heterogeneities of the steels, and later Mount *et al.*, 2001 [26], [27], [41] built a segmented tool for the further analysis of the ECM process. Their results described a change in the surface finish of the samples along the electrolyte flow and they found that this special behaviours was due to the change of the dissolution valence of the alloy. These results are in agreement with what was found later on by Lohrengel *et al*., 2003 [80] and Murkherjee, *et al*., 2008 [81].

Along the years, the parameters that affect ECM have been studied little by little in an attempt to understand better the process and forecast its results. In 1991 Ruszaj [82] carried out diverse experimental studies in the demonstration of the randomness of the phenomena and

the difficulty of a proper characterization of problem. Mukherjee *et al*., 2005 [81], [83] studied the effect of the overvoltage and the valence of the workpiece material on the material removal rate during ECM, and da Silva *et al.*, 2006 [84] studied the effects of modifying the feed rate, electrolyte type, electrolyte flow rate and voltage during the process. The accurate measurement of the parameters is also an important tool to understand the ECM process. For this purpose Clifton *et al.,* 2002 [76] developed an ultrasound technique to monitoring in-situ the ECM parameters such as the inter-electrode gap and the valence. Also, in this attempt of understanding the ECM variables, Muir *et al.*, 2007 [85] used the same methodology for collecting continuous, uninterrupted time-resolved data for the dissolution valence, interelectrode gap and overpotential, and Schneider *et al*., 2012 [86], [87] designed a system that could investigate in-situ the influence of the microstructure of the anode in the dissolution of the material.

Related to how ECM is applied, ECM was first applied for grinding in USA about 1953, where electrolyte was supplied between a grinding conductive wheel and a metal [49]. Electrochemical drilling was established in 1972 by the Central Asian Research Institute of Natural Gas [88]. This was followed by Chin and Tsang, 1978 [89], who published a work about how ECM behaves when using an electrolyte jet as electrode, in a process named erosion corrosion. Amalnik and McGeough, 1996 [90] focused their research on the design of features specifically for ECM, such as tools for the improvement of specifications and machine operation conditions. By the end of the 90's, the studies on the ECM process were focused on optimizing the accuracy of the process [91], [92]. These studies were mainly done by K. Rajurkar and his team, who published an extended review of the developments in Electrochemical Machining in 1999 [14], followed by a in depth review presented by Davynov in 2004 [34], where tool design, pulse current, micro-shaping, finishing, numerical control (CNC), environmental concerns, hybrid process and industrial applications were covered.

When the way of how the ECM process is carried out was modified, some great advantages could be achieved. For example, pulsed electrochemical machining (pECM) is a type of ECM, where high current densities (on the order of 100 $A/cm^2$) are used in a pulse mode rather than in direct mode [1]. Datta et al. in 1983 [31] developed a pECM system for applications in micromachining highlighting the environmental benefits and the reduction in machining time. This benefits were applied by Pavlinich in 2008 [93] in the manufacturing of gas turbine engine parts. Moreover, Zhang et al. in 2010 [94] noted that pECM improves anodic dissolution efficiency and achieve a more stable interelectrode gap. Elsewhere [95] investigations have indicated that pECM improves fatigue life over ECM and can eliminate the recast layer left after a EDM [43], [55], [94].

On the other hand, ECM has some disadvantages, some of them are presented in the macro-defects in the surface finish of the workpiece due to the electrolyte flow. Zaytsev, 2004 [96] published a work about this problem and proposed a vibrating electrode-tool as a solution to avoid it. With the objective of experimentally increasing the accuracy Jadhav *et al.*, 2007 [97] proposed the use a rotating electrode, and Kurita *et al.*, 2008 [98] develop a complex mechanical/electrochemical method for increase the accuracy in the mould machining process. Concerning finding the best balance of the process parameters Senthilkumar, 2011 [99] used a genetic algorithm-II (NSGA-II) to relate ECM parameters and optimize the process.

Another important application of ECM is micromachining. Hochen *et al.*, in 2003 [100] developed a work about the application of ECM with a flat-end cathode of 0.3 mm for the drilling of a workpiece. Hochen found that the most influential factor on the process was the electrolysis on/off time. Sen *et al.*, 2005 [101], [102] and Bhattacharyya, 2004 [103], [104] focus their research also on the micro-hole ECM drilling. The latter published a paper explaining the diversity of the problematic of the ECM process, but also recognizing the potential of its application in industry.

In order to overcome the difficulties related to tool-electrode design and dimensional accuracy in conventional ECM, Domanowski, 2000 [105] presented a work focused on the modelling of the process from the point of view of the shaping metal, named direct problem, and from the point of view of the tool design, named inverse problem. In the same year, Kozak and collaborators [106] from Warsaw University of Technology, Poland, developed and published a work about the design of a CAE-ECM system for electrochemical technology that could be used for process analysis, tool design and parameters selection.

In parallel with the experimental work, diverse numerical models of ECM have been developed. At the end of the 70's, the study of the ECM process, especially the search for a time dependent numerical solution, was one of the major research areas. Forsyth [19], [107] developed an ECM model in a two-dimensional environment using applied mathematics. In 1980 Sautebin *et al.* [108] presented a model of the ECM process and solved it by applying Finite Element (FE) method. Their results were verified experimentally with a laboratory apparatus using active dissolution of copper in $NaNO_3$. In general their results corresponded to those predicted theoretically; however the final roughness of the sample didn't agree with the simulation. Two years later in 1982, Prentice [109] published a version of this solution but using Finite Difference (FD) method instead. In an attempt of finding the most efficient way to manufacture metals for specific applications, some industries, as such as Philips DAP, developed a multiphysics modelling to ascertain the best balance of the process parameters [8], however

their validation is still in progress. A similar work with multiphysics modelling was developed by Hackert-Oschätzchen as part of his work with Jet-EMC in 2011 [2], [110], and with ECM of Aluminium matrix composites in 2014 [111].

#### 1.3.2.2. ECM advantages and disadvantages

ECM main advantage is its capability to machine complex shapes on hard metals; however it can be used to machine any conductive material. Its capability to machine complex shapes in a single operation results in reduction of the machining time and the associated cost. ECM is a contactless process and there is no tool wear so, unlike conventional machining methods, soft metals can be used as tools to form shapes on a harder workpiece. The absence of tool wear is as well a cost related advantage, because the need for a frequent tool replacement is avoided, and in consequence, prevents the long and costly tool-design process.

ECM leaves burr-free surfaces, causes no thermal damage of the part and the lack of tool forces prevents distortion of the part or stress damage [1]. ECM leaves behind a high quality surface finish (0.13 to 0.38 Ra) [112] and researches are still working on improving the surface quality left by ECM.

Additionally, ECM has higher metal removal rates, regardless the hardness of the workpiece [113], than the other non-conventional techniques. Table 1.3-1 presents a comparison of ECM with other machining processes: mechanical processes, electrodischarge machining (EDM), ultrasonic machining (USM), laser beam machining (LBM) and LIGA.

***Table 1.3-1 Comparison of the characteristics of machining processes according to*** [112], [114]***, where (+) Good, (o) Fair and (-) Poor.***

| Machining Process | Geometry complexity | Range of materials | Accu-racy | Proto-typing | Mass Production | Surface quality | Afforda-bility |
|---|---|---|---|---|---|---|---|
| Mechanical processes | + | o | + | + | o | o | + |
| ECM | + | o | - | - | o | + | o |
| EDM, USM | + | o | o | + | - | o | + |
| LBM | o | + | + | + | - | o | o |
| LIGA | - | - | o | - | + | + | - |

However the capital investment on the ECM equipment is significant and a huge amount of energy, approximately 100 times the energy used for conventional machining processes [115], is consumed during ECM, increasing the day-to-day cost of this technology. Additionally

particular attention has to be paid to the stability of the components of the machining system: tool frame, machining table, motion system, etc.

The operation conditions have to be constant and due the fact that the electrolyte heats up from the passage of current, precautions must be taken to avoid high electrolyte temperature which can cause changes in the electrolyte conductivity, producing undesirable effects on machining accuracy [13]. Moreover the electrolyte has to be carefully handled: it should be thoroughly filtered or treated to remove or extract the products of machining (in the case of a recirculating system) and its temperature should be ideally fixed before entering the machining equipment.

In general, ECM is not renowned for being an accurate process; this is because it is limited by the difficulty of predicting the final workpiece shape due the complexity of the process. And in some particular cases, the pieces produced by ECM need a secondary operation in order to recover some of the properties given by the conventional machining processes, e.g. fatigue strength [49].

The main disadvantage of ECM is the long and costly iterative method for the tool design. Although the tool shape is often considered simply the negative shape of the workpiece desired shape, the complexity of the process made almost impossible to forecast all the variations of the parameters during the process, which consequently affect the resulting workpiece. Several works in this extent have been carried out [11], [21], [30], [37], [46], [116], [117], however in the industry, time consuming and expensive empirical methods are still in use, making the overall ECM process uneconomical [114].

Additionally, there are some environmental concerns about this process. Solid machining products need to be disposed safely [113], and some of the soluble products in the electrolyte, that might be carcinogens (such as $Cr^{VI}$, which is not allowed legally in EU) are often disposed down the drainage system without treatment or filtering [113].

#### 1.3.2.3. Applications

The many advantages of ECM make it an attractive technique for the manufacturing industries. Provided a conductive material, the process will machine regardless of the material hardness, making it a powerful tool for the manufacturing of surperalloys [118].

ECM is generally used for smoothing surfaces, drilling holes, cutting and milling, and for shaping complex cavities in materials with special properties such as high-strength or high-stiffness. ECM can also be applied to remove fatigue cracks in steel structures [13]. Nowadays ECM

systems are available as computer numerical controlled (CNC) machining centres, with high production capabilities, high flexibility and maintenance of close dimensional tolerances [1].

Aerospace industry uses ECM particularly for mass production and surface quality control of turbine blades, jet-engine parts and nozzles [119], Figure 1.3-3(a). The forging industry uses it for the manufacturing of die cavities and small holes [1], Figure 1.3-3(b). Medical engineering industry is another big user of ECM, due to its capacity of machining titanium alloys (characterised for their biocompability, corrosion resistance and good mechanical properties). By using ECM, complex-shaped titanium implants can be machined [114].

Philips® applied ECM for the improvement of the production process of their shaver blades, Figure 1.3-3(c), and Rolls-Royce® did the same for their turbine blade manufacturing [120]. Another interesting application of ECM is its use for fabricating superhydrophobic surfaces on aluminium substrates that with other methods would be costly and time consuming [121].

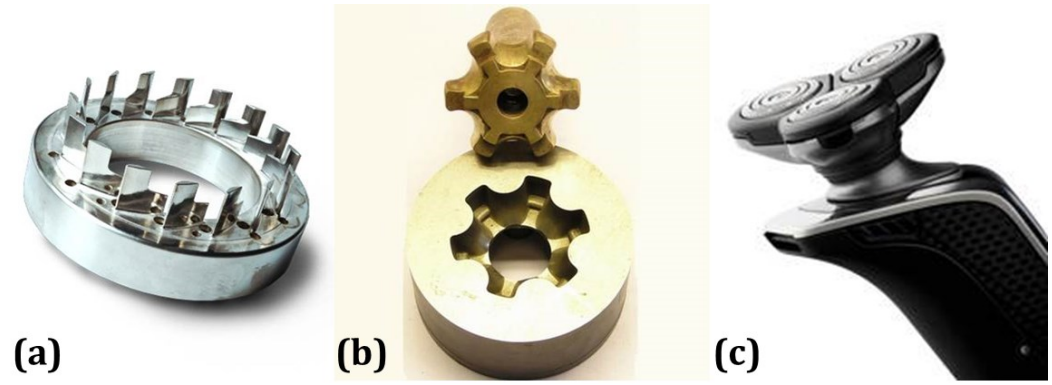


***Figure 1.3-3 Some examples of pieces fabricated with ECM: (a) turbocharger for cars and trucks*** [122]***, (b) moulds and dies for aircraft building*** [123]***, and (c) Philips® shaver*** [124]**.**

Though ECM is currently used in certain industries, it is not a widespread manufacturing process due to the lack of control of the process, the undesirable results that can be obtained, and the complex and iterative tool design process. Additionally, usually manufacturing companies tend to rely more on traditional known methods than to invest in new non-conventional methods, which use will require time in order to develop the needed knowledge and expertise for its correct application. This is one of the reasons why the present research work and simulation model of ECM is needed, the objective is to understand, forecast and control the outcomes from the process, promoting its use in industry.

### 1.3.3. Simulation of ECM, ideal case

Industrial practices in ECM have revealed some problems impeding the development and wider applications of the electrochemical machining process; one of them is the difficulty of predicting and controlling the final profile of complex workpiece shapes. Due to this, some numerical and computational simulations have been developed in order to solve this problem.

The first theoretical solution of the ECM potential equation with moving boundary conditions was presented in 1968 by J. M. Fitz-Gerald and J. A. McGeough [125]. The model proposed described the smoothing of surface irregularities on the anode surface. In 1972, McGeough [126] developed a quasi-steady model, based in the electric field between the electrodes in ECM. In 1977 Alkire and Bergh [18] developed a numerical calculation for predicting two dimensional (2D) shape changes at the cathode during electrodeposition. Their findings were applied later on the electro-dissolution of products from small cavities [38].

P. Forsyth, *et al*., 1978 [19], [107] derived a numerical procedure for calculating the solution of a 2D time dependent electrochemical machining problems. They used finite difference (FD) to solve it. In this work it is important to note the use of a finer mesh in the regions where a rapidly changing potential occurs. This adaptive mesh is still in use for the present solutions of the ECM problem.

Finite element (FE) numerical simulation was employed by Sautebin, *et al*. in 1980, for studying the rate of levelling a surface during anodic dissolution, and 1982 Prentice, *et al.* [109] addressed the same problem but solving it with FD method. In 1986 Narayanan, *et al.* [37] applied boundary element (BE) method for designing the ECM tool. In all cases, only the primary current distribution (neglecting electrodes kinetic and concentration-dependent effects) was solved.

In 1985 A. Lacey [127] developed a mathematical model where a constant overpotential at the workpiece surface was considered. The ECM problem was solved just for two-dimensional (2D) situations and evaluation was still needed. Another 2D electrochemical machining solution was published by T. Ozis in 1990 [128] and solved by using regula-falsi transformation.

By the end of the 1980's multiple attempts for the numerical solution of the ECM problem were presented, however, they were limited by computational capacity and the lack of full understanding of the ECM process. Therefore in 1990, A. Ruszaj [82] acknowledged the complex nature of the ECM process and developed a statistical investigation of the influence of some ECM parameters on the resulting workpiece shape. However, as many of the statistical

investigations, Ruszaj approach in limited for a very specific range of the process parameters, and it is not applicable for studying individual cases or where the qualitative results cannot be quantified.

In the last 20 years, with the development of the computational resources, the investigation of the electrochemical machining by numerical simulations has advanced further. H. Hardisty and A. R. Mileham [17], [39] worked in the development of a 2D ECM model based on a moving boundary problem, solved by finite difference (FED) method. In parallel, Kozak, *et al.*, [22], [105], [129], [130] built physical and mathematical models of the ECM process in an attempt for finding the optimal machining conditions and tool design that would lead to the workpiece profile expected. From here, multiple authors [11], [28], [105] had addressed the ECM process in two fashions: the direct problem, where the workpiece shape is predicted for a given tool shape, and the inverse problem, where the tool shape is predicted for a given workpiece. The latter is directly connected with the ECM-tool design. The inverse problem is more common in industrial applications and is more complicate to solve than direct problem [34].

Focusing on the direct problem, De Silva (2000) [131] developed an empirical model based on the characteristic relationships within the process parameters in order to increase the precision in ECM. Later on, in 2001 Temur, *et al*., [132], [133] modelled the electric field during the electrochemical dissolution of material. Temur was able to calculate the current density at each point on the workpiece for the whole machining process. The results of this work were compared with real part profiles and they showed good agreement for planar faces, error along the contour profile was around 0.15mm, but had some limitations when applied on spherical shapes.

Mount, *et al.,* 2003 [41], [134] focus their work on the two-dimensional simulation of the ECM process by applying the finite difference method, which allowed the simulation of the current density and workpiece geometry until the equilibrium gap was achieved. Their results were evaluated experimentally in [26], [27], [117] and small differences between the simulated and experimental data were observed. These discrepancies were attributed to variations in the dissolution valence of the metal during ECM.

It was not until 2004 that the simulation of the ECM process in a 3D environment was addressed. Davydov, *et al.* [34] and Purcar, *et al.* [23], [35], [40] worked on the development of a general numerical boundary element method for the ECM simulation in a 3D environment and the development of a user-friendly software for this purpose. This software could be integrated

with commercial computer aided design (CAD) packages; however, experimental validation was still missing.

Although diverse theoretical works carried out in order to solve the ECM direct problem; there are still discrepancies between the model and the benchmark experimental data, highlighting the need for a model that can integrate the physics and chemistry of ECM. In a first step for incorporating the physics in the ECM problem, Hourng and Chang (1993) [135] and Kozak (1998) [129] developed 2D mathematical simulation models of the ECM process accounting Ohmic heating and gas fraction effect on the electrolyte conductivity. And Deconinck, *et al*. (2010) [9], [10] focused their studies on the simulation of the effects that heat generated by electrode reactions have on the accuracy of the process. Most of these solutions were simplified into a two-dimensional ECM problem, or were carried out to shape solely a specific geometry, such as turbine blades [24], [136]–[138].

Recent complex ECM simulations have been developed including electrolyte flow in 2D [111] and in 3D [136], [139] virtual environments. Hackert-Oschätzchen, *et al*. (2014) presented a semi-coupled multiphysics model that included non-isothermal electrolyte flow in a 2D environment and their results were used as a frame for the simulation of the electrochemical material dissolution under the determinate inlet velocity and temperature. Similarly, Wang, *et al.*, (2014) [140] built a multiphysics model for ECM on an internal spiral hole based on finite element method (FEM) and solved with ANSYS®. This model forecasts the electrolyte velocity, temperature, conductivity and volume of $H_2$. A satisfactory agreement between the simulation results and the experimental ones was achieved, however the overpotential effects were not considered and the physics were considered unidimensional.

### 1.3.4. Towards the development of the ECM

The research and improvement on ECM is an on-going process. ECM is a complex process not fully characterised yet and there are some variables that still need to be addressed in order to forecast and control the process. For example, previous work had revealed that the current density efficiency can vary with electrolyte concentration and flow rate [67]; the overcut during ECM cannot be eliminated or completely predicted [141]; the electrolyte flow needs to be precise in order to avoid flow marks and patterns on the surface [142]; and the heat effect on the process, thus the conductivity of the electrolyte, cannot be fully controlled [10]. Therefore, further experimental research in the topic is needed. Moreover, the high interdependency of these parameters made evident the need for an accurate computational simulation of the ECM process. This simulation model should ideally include the different phenomena during the process, such as electrodynamics, fluid dynamics, heat transfer and electrochemistry.

Researchers are working on optimization of the process to improve surface quality for ECM, and to find new applications. An optimal ECM process is a vital step for increasing the use of this process in industry. Companies as Philips DAP® and Rolls Royce® are currently working on the development simulation models of ECM that allow them to use the process widely in their products [8]. Furthermore due to the complexity of the process, optimization models, such as Gray-Taguchi [143] and quality loss function [7], had been applied, but even though they have been demonstrated to be useful, their application is not yet commonly used.

Monitoring the ECM parameters has also been demonstrated to be an important tool to understand the ECM process. The development of more and more accurate systems to measure and observe the process in-situ is fundamental for the progress of ECM, as it was explained in section 1.3.2.1.

The application of ECM on special metals, such as stainless steels (SS) is up to now not entirely characterised. SS present an oxide film covering their surface which modifies the ECM behaviour. Consequently the resulting surface finish of the workpiece is affected and not entirely predictable. Hence, research in the area needs to be continued. More recently, ECM has also been applied on aluminium matrix composites [111] and hard exotic materials as Hasteloy and Nitinol [144]. Good results were achieved, opening this way a new development area, the research of ECM on more and more complex materials.

In modifying the fashion of how the process is carried out, some great advantages can be achieved, e.g. oscillating cathodes [142] or pulsed current [54]. For example, pulsed electrochemical machining (pECM) pulsed currents in order to eliminate the need for high electrolyte flow rates. Zhang in 2010 [94] noted that pECM improves anodic dissolution efficiency and achieve a more stable interelectrode gap. Elsewhere [95] investigations have indicated that pECM improves fatigue life over ECM. Moreover, pECM can eliminate the recast layer left after a EDM and results in a better surface finish [43], [55], [94]. Additionally, since 2008 Hackert-Oschätzchen [2], [110], [145] has been working on the development of Jet-ECM, and in 2014 Liu, *et al*. [146] presented the potential of producing complex microstructures using wire-ECM.

ECM can also be combined with other advanced machining processes, such as electrodischarge machining (EDM), laser-beam machining (LBM) or water-jet cutting (WJC). These new systems are called hybrid machining systems [1]. Since 2006 Kurita, *et al*. [98], [147] have been working

on a EDM/ECM/ECM-lapping complex machining. Hereafter, finding new application methods is also an area for improvement in the ECM technology.

ECM tool design continues to be of importance in ECM operations and is a research area which is continuously advancing [13]. New ECM-tool numerical solutions [30], and methods for two and three dimensional solutions are being developed until now [11], [129], [142], however their evaluation is still in progress.

In order to address some of these areas of development, in this thesis the application of the ECM technology in one special metal, SS316, was studied and a computational simulation model in two and three dimensional environments was developed.

### 1.4. *Aims and objectives of the thesis*

The aim of the work described in this thesis was to develop a methodology and an accurate simulation model for the electrochemical machining (ECM) process.

To this extent the following objectives have been achieved:

- development of a time-dependent simulation model of the ECM process in a two-dimensional (2D) environment, and validation of the simulation model through comparisons with published data, presented in Chapter 2, section 2.1.
- in collaboration with an industrial partner, experimental identification of crucial parameters on the ECM process and their role in the achievement of a determined surface finish was established, presented in Chapter 2, section 2.2.
- based on the 2D simulation model, experimental results and literature data, the development of a time-dependent simulation model of the ECM process in a three-dimensional (3D) environment, presented in Chapter 2, section 2.3.
- validation of the methodology and assessment of the applicability of the ECM simulation model through comparisons with experimental results, presented in Chapter 3.

The work described herein this thesis builds on the existing studies in ECM performed at the University of Edinburgh [27], [113], [114], [148]. Important experimental work in order to understand the ECM process, especially on stainless steels, was carried out and provided useful data for the inclusion of the overpotential behaviour in the ECM simulation model developed in in this thesis. D. Curry [118] gave the background for the development of the simulation model and his experimental results were used as a base for validation of this work. Limitations on software and memory usage at the time when the previous work was developed are now considered tractable and the work could be now extended, offering considerable practical benefits in reducing simulation time. The development of an accurate simulation model is essential for the spread of ECM and for new applications of this technology in industry.

By the end of this project, a 3D ECM simulation model is delivered and implemented in a real industrial problem, giving a step further in the advance of the ECM technology.

## 1.5. *Theoretical background*

### 1.5.1. Principles of ECM

Electrochemical Machining (ECM) is based on the removal of material from the workpiece atom by atom by a process named electrolysis. Electrolysis refers to the decomposition of a substance when an electric current is passed between two metal conductors, called electrodes, dipped into a liquid solution [149]. Such solution should be able to conduct electricity and is termed electrolyte. The complete system is referred as electrolytic cell and the electrodes are named cathode (negative polarity) and anode (positive polarity) respectively [60].

Some common applications of electrolysis are electroplating, where metal ions are deposited upon the surface of a cathodically polarized metal, and electropolishing, where the irregularities of a surface are eliminated by anodic dissolution. ECM is similar to electropolishing, an anodic dissolution process, but the rates of metal removal are considerably higher [60].

In ECM, when a potential difference (voltage) from an electric source is applied to the cell, electric current passes through the tool (cathode), the workpiece (anode) and the electrolyte, thus moving positive ions (atoms which have lost electrons) from the anode towards the cathode via the electrolyte. The movement of ions is accompanied by electrons flowing in the opposite direction to the positive current at the electrolyte [94].

The phenomena embodies Faraday's laws of electrolysis [13]:

i. the amount of any substance dissolved or deposited is directly related to the amount of electricity which has flowed,
ii. the amount of different substances deposited or dissolved by the same quantity of electricity are proportional to their chemical equivalent weights.

Hence, the combination of the two laws of electrolysis leads to the conclusion that the mass of material dissolved, $m$, is directly related to the current, $I$, passed in a time, $t$, and the characteristics of the workpiece material: molar mass, $M$, and valence, $z$. The two laws may be combined in equation 1.4-1 [60]:

$$m = \frac{MIt}{zF} \qquad \textbf{(1.5-1)}$$

, where $F$ is the constant known as Faraday's constant, which is the amount of electric charge necessary to liberate one gram-equivalent of one ion, $M/z$, during electrolysis. Its value is 96500 C/mol.

Usually not all the current is used to ionise the workpiece atoms during ECM. Some of the current can undertake undesirable electrochemical side reactions. Therefore an efficiency term, $\eta$, which can be described as the fraction of current applied to dissolve atoms in the overall process, is sometimes used.

$$m = \eta \frac{MIt}{zF} \qquad \textbf{(1.5-2)}$$

Some chemical reactions will take place at the electrodes during ECM, e.g. in the electrolyte will undergo ionic dissolution. Considering the machining of iron with 100% efficiency and using a neutral salt solution of sodium chloride (NaCl) as electrolyte, hydrogen ions will take away electrons at the cathode (tool) [114]:

$$2H_2O + 2e^- \rightarrow H_2^+ + 2(OH)^-$$

, similarly, metal ions will be dissolved at the anode (workpiece), assuming a valence of 2:

$$Fe \rightarrow Fe^{++} + 2e^-$$

The overall outcome of these electrochemical reactions must be hydroxyl ions combining with metal ions to precipitate as iron hydroxide (sludge). So the complete reaction is:

$$Fe + 2H_2O \rightarrow Fe(OH)_2 + H_2$$

If a metal alloy machined, additional reactions will take place during ECM, such as manganese and chromium dissolution when stainless steel is used.

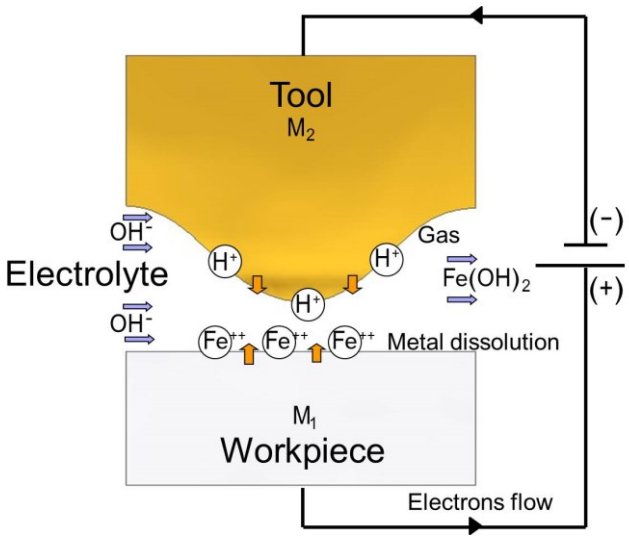


***Figure 1.5-1 Schematic of the electrochemical reactions at the tool and at the workpiece during ECM*** [13], [150]***.***

In this manner the workpiece is gradually machined and products, as iron hydroxide, get precipitated as sludge. Moreover there is no coating on the tool, only hydrogen gas evolves [151], as illustrated in Figure 1.5-1.

Some observations can be taken [60]:

- the anode metal dissolves electrochemically. The dissolution rate do not depends upon the hardness or other mechanical characteristics of the metal,
- the shape of the cathode (tool) remains unaltered. Only hydrogen gas is evolved at the cathode surface. This is the most relevant feature in ECM for metal shaping,
- the electrolyte flow is fast enough to avoid sludge accumulation within the interelectrode gap.
- the ECM products must be removed continuously from the electrolyte, usually by filtration, before it is recirculated.

From equation 1.4-1 the volumetric removal rate of anodic metal, $\dot{v}$, is given by [49]:

$$\dot{v} = \frac{MIt}{zF\rho_a} \qquad \textbf{(1.5-3)}$$

, where $\rho_a$ is the density of the anode metal.

Other characteristics that affect ECM are the electrolyte conductivity and the interelectrode gap. These parameters are associated with the current through Ohm's law, which states that the current, $I$, flowing in a conductor is directly related to the applied voltage, $V$.

$$V = RI \qquad \textbf{(1.5-4)}$$

, $R$ is the resistance of the conductor and is directly related to its length, $y$, and inversely related to its cross sectional area $A$.

$$R = \rho \frac{y}{A} \qquad \textbf{(1.5-5)}$$

, where $\rho$ is the specific resistance or the resistivity of the conductor. The conductor in ECM is the electrolyte. The reciprocal of the specific resistance is the specific conductivity of the electrolyte, $k_e$.

Relating equations 1.4-4 and 1.4-5, the average current density, $J$, is given by equation 1.4-6:

$$J = \frac{I}{A} = \frac{k_e V}{y} \qquad \textbf{(1.5-6)}$$

As the dissolution of the anode proceeds, the interelectrode gap along the electrodes length will gradually tend to a steady-state current value, usually maintained by mechanical movement of one electrode towards the other. The rate at which the metal is removed is approximately in inverse proportion to the distance between the electrodes. Under these conditions a shape, roughly complementary to that of the cathode, will be reproduced on the anode [13].

The accumulation of metallic and gaseous products of the ECM process within the interelectrode gap is undesirable. If the accumulation were left uncontrolled, this will lead to the reduction of the conductivity of the electrolyte and eventually a short circuit would occur between the two electrodes. To avoid this, the electrolyte is pumped through the interelectrode gap so these products are carried away. The movement in the electrolyte also helps to avoid overheating of the fluid, which can affect the electrolyte conductivity [13].

### 1.5.2. Basic governing equations for ECM

There are three basic equations needed for the numerical solution of the ECM process: Laplace's equation, Ohm's law and Faraday's law [60].

#### 1.5.2.1. Laplace's equation

In order to find the final shape of the workpiece in the direct problem, or the tool in the inverse problem, the "cos θ method" can be applied as explained in [49], [60]. This method however is limited to simple shapes or to shapes where the current flow lines are approximate parallel with each other. When more complex shapes are to be achieved, it is necessary to know the field distribution or potential, $\phi$, at any point within the electrolyte and on the electrodes surface, and in turn use it to determine the current density, $J$, during the process.

The field distribution is determined by Laplace's equation, for a two dimensional problem [49]:

$$\frac{\partial^2 \phi}{\partial x^2} + \frac{\partial^2 \phi}{\partial y^2} = 0 \qquad \textbf{(1.5-7)}$$

, and for a three dimensional problem:

$$\frac{\partial^2 \phi}{\partial x^2} + \frac{\partial^2 \phi}{\partial y^2} + \frac{\partial^2 \phi}{\partial z^2} = 0 \qquad \textbf{(1.5-8)}$$

For the electric current, $I$ [49]:

$$\frac{\partial^2 I}{\partial x^2} + \frac{\partial^2 I}{\partial y^2} = 0 \qquad \textbf{(1.5-9)}$$

, and

$$\frac{\partial^2 I}{\partial x^2} + \frac{\partial^2 I}{\partial y^2} + \frac{\partial^2 I}{\partial z^2} = 0 \qquad \textbf{(1.5-10)}$$

for two dimensional and three dimensional problems respectively.

The solution of equations (1.4-7)-(1.4-10) will allow the determination of the instantaneous current density at the workpiece surface using equation 1.4-6 [49].

Some assumptions have to be made in order to solve Laplace's equation:

- the workpiece shape and the material removal rate remains constant for a time interval $\partial t$,
- a constant voltage, $V$, is applied between the electrodes.

In a non-ideal ECM, $\phi$ during the process is given by the difference between the voltage applied, $V$, and the overpotential, $V_0$, at the electrodes, $(V - V_0)$.

#### 1.5.2.2. Ohm's law

Electric current, $I$, is the flow of electric charge (moving electrons) within a conductor. It can also be carried by the ions in an electrolyte, or by ions and electrons such as in plasma [152]. Ohm's law describes the flow of electric current, $I$, through the interelectrode gap, and states that $I$ is directly related to the applied voltage $V$ [153]:

$$I = \frac{1}{R} V \qquad \textbf{(1.5-11)}$$

In ECM the electrolytes are the conductors of the electricity, so $R$ is related to the electrolyte conductivity, $k_e$, according to equation 1.4-5. In other words, Ohm's law can be applied in the form [60]:

$$J = k_e \phi \qquad \textbf{(1.5-12)}$$

, where $k_e$ is the bulk electrolyte conductivity, and $\phi$ is the electric field within the interelectrode gap. The current density, $J$, is the electric current, $I$, per unit area of cross section, $A$, and can be found from solving Laplace's equation in section 1.5.2.1.

If the diffusion layer, a thin layer of electrolyte adjacent to the electrode, presents a thickness and a potential drop across it sufficiently small, $k_e$ can be assumed to be constant and have its bulk value everywhere [60].

#### 1.5.2.3. Faraday's law

In ECM, material is removed from the workpiece due the passage of current through the electrolytic cell. The rate at which the material is removed is given by Faraday's laws [49], [60] given above.

The combination of these two laws indicate that the mass of the material removed or deposited, $m$, at the anode is related to current, $I$, time, $t$, and the anode material characteristics, as it can be observed in equation 1.4-1 in section 1.4.1.

#### 1.5.2.4. Potential boundary conditions

Additionally, it is important to highlight the boundary conditions for the potential at the electrodes and the conditions under which Laplace's equation, Ohm's law and Faraday's laws are applied.

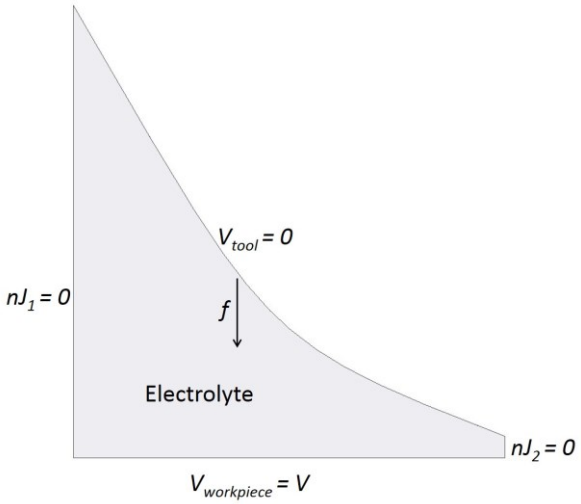


***Figure 1.5-2 Electrolyte model from*** [17] ***showing an example of the boundary conditions used in ECM simulations.***

For example, in a model as the illustrated in Figure 1.5-2, if the electrode surfaces are equipotential, the boundary conditions are [24], [134]:

$$\phi_{anode} = V \qquad \textbf{(1.5-13)}$$

$$\phi_{cathode} = 0 \qquad \textbf{(1.5-14)}$$

$$nJ_{1,2} = 0 \qquad \textbf{(1.5-15)}$$

, where $\phi_{anode}$and $\phi_{cathode}$are the electric potential at workpiece and tool respectively. And $nJ_{1,2}$ is the normal current density assumed at the side boundaries of the model.

The reactions at both electrodes cause a current density-dependent overpotential. This means that there is a thin layer at the surface of the electrodes across which there is a jump in the potential [127]; therefore at the cathode:

$$\phi_{cathode} = f(J) \qquad \textbf{(1.5-16)}$$

And at the anode

$$\phi_{anode} = V - g(J) \qquad \textbf{(1.5-17)}$$

, where $f(J)$ and $g(J)$ are function of the cathodic and anodic current density respectively [60]. In this thesis, the parametrisation of this functions is addressed.

### 1.5.3.ECM parameters

#### 1.5.3.1. Electrolyte characteristics

Electrolyte is a solution able to conduct electricity. It must have high electrical conductivity, low toxicity and low corrosiveness. The electrolyte has three main functions in ECM [154]:

i. to carry the current between the electrodes,
ii. to remove the products from the machining,
iii. to dissipate the heat produced for the electrochemical reactions.

The electrolytes most commonly used are sodium chloride (NaCl) and sodium nitrate ($NaNO_3$). Sodium chloride is characterised as being more corrosive but has a stable conductivity over a broad pH range [155]. On the other hand sodium nitrate is much less corrosive, but promotes the formation of an oxide layer at the workpiece surface, reducing the efficiency of ECM [155]. The reactions within the electrolytic cell require higher voltage when using strong passivating electrolyte like $NaNO_3$ [156].

Mineral water and other aqueous solutions of inorganic chloride and nitrate salts have also been used as electrolytes. Citric acid has been used mainly to eliminate the smutting (small marks left at the electrode) problem. Moreover, these solutions are completely biodegradable

eliminating this way one of the main environmental concerns about electrolyte disposal of the ECM process [12], [141].

Electrolyte conductivity. The conductivity of the electrolyte is determined by the type and number of the ions present in the electrolyte and defines the cell resistance. The properties of the electrolyte solution also influence the interelectrode reactions. In ECM, the resistance of the conductor, $R$ in equation 1.4-4, is calculated from the electrolytic conductivity, $k_e$, the cross section area of the interelectrode gap, $A$, and the separation $y$, between the electrodes (interelectrode gap).

Water is the most usual solvent for electrolytes due to its special characteristics [157]:

i. water molecules are able to H bond with neighbours and this leads to highly structured solvent,
ii. it ionises itself to a small extent, so always contains a low concentration of $OH^-$ and $H^+$,
iii. it tends to interact electrostatically with charged species and is able to solvate most ions, hence maintaining high conductivities.

At low concentrations it is useful to compare the conductivity of different electrolytes by reference to its concentration. Concentration is often calculated from either the weight of the solute per unit weight (w/w) or weight per unit volume (w/v) of solution. At high electrolyte concentrations, the electrolytic conductance is not proportional to the concentration [157].

The electrical conductivity of the electrolyte increase with temperature and with concentration up to the limit of solubility of the salt, where then it decreases [60].

Electrolytes can be classified into acidic, neutral or alkaline types. This classification is usually defined by the pH of the electrolyte, which is the negative logarithm of the hydrogen ion concentration. The water is said to be neutral, with a pH of 7. If the pH is less than 7, the solution is considered acidic and if the pH value exceeds 7, the solution is considered alkaline. Neutral electrolytes (e.g. NaCl, $NaNO_3$) are the most commonly used in ECM [126].

For many metals alkaline electrolytes are not suitable because of the formation of adherent insoluble anodic products, preventing or restricting the dissolution of the workpiece. Acidic electrolytes are highly corrosive, good for ECM, but present a comparatively difficult disposal problem upon exhaustion [49].

#### 1.5.3.2. Electrolyte flow

ECM products, solid ions and bubbles, must be removed at a sufficient velocity in order to maintain a stable ECM process. Unless there is a violent agitation of the solution, there will be a concentration or depletion of ions near the surface of the electrodes. Additionally, when current is passed through a conductor, i.e. electrodes and electrolyte, the conductor is heated by Joule heating. Heating of the electrolyte produces changes in the conductivity of the electrolyte, and could also lead to boiling with cause irregular current flow, thus generating irregular metal removal [49].

These effects can be minimised by flowing the electrolyte through the interelectrode gap with a sufficiently high velocity. At high flow rates, the solid dissolution products are removed, thus ion depletion is considered negligible, and Joule heating is minimised or, in some cases, neglected.

The electrolyte flow between the electrodes can be visualised as the flow of a liquid within a channel, the interelectrode gap, which is limited by the tool and the workpiece. The flow within the interelectrode gap can be laminar, turbulent or transitional depending on its velocity. The Reynolds number $\mathrm{Re}$, is a dimensionless parameter related to the interelectrode gap geometry and the electrolyte velocity, and describes the regime of the electrolyte flow [158].

$$\mathrm{Re} = \frac{Ul}{v} \qquad \textit{(1.5-18)}$$

, where $U$ is the velocity at the centre of the channel, $l$ is the characteristic length (width of the interelectrode gap) of the channel, and $v$ is the kinematic viscosity of the electrolyte. For $\mathrm{Re} < 2300$ the flow is smooth and laminar, and for $\mathrm{Re} > 4000$ the flow is turbulent. Once $\mathrm{Re} > 2300$ is reached, the flow pattern through the channel exhibits irregular fluctuations superimposed upon the main electrolyte flow stream [158].

High flow rates and high pressures normally used in ECM would make unlikely that the flow during the process remain laminar, nonetheless a complete theoretical description of the electrolyte flow and ECM settings under turbulent conditions is still not possible [113], therefore as a first approximation, a simplified ECM model is usually used where the electrolyte flow is considered laminar.

Moreover, the entrance length, $l_e$, required to establish the turbulent flow is typically $l_e = 4.4l\,\mathrm{Re}^{1/6}$ [159], which typically will occur within the end of the systems used in this work. Therefore, it is expected that at the entrance of the system, the flow exhibits a different hydrodynamic regime [113].

#### 1.5.3.3. Interelectrode gap

The space between the tool (cathode) and the workpiece (anode) is called interelectrode gap. In the simplest case, the copying accuracy of the tool shape by the workpiece is determined by the interelectrode gap; therefore ECM looks forward the achievement of a uniform and stable distance between the electrodes, usually between 0.15 and 1 mm. Additionally, the interelectrode gap has influence in:

- the electrolyte flow velocity, which in turn affects the temperature, the cathodic bubble distribution, and in consequence the electrolyte conductivity,
- the electrical field, which is determined by the tool and workpiece profile,
- the anodic overpotential and current efficiency, which are affected by the current density distribution [160].

#### 1.5.3.4. Electrode potentials

When a metal is placed in an electrolyte solution, i.e. in an electrolytic cell, an equilibrium potential usually becomes established between the metal and the solution. This potential arises from the transfer of ions among them. The equilibrium potential is reached when an electrical double layer is formed. Double layer is the name given to a pair of ion layers, whose charge are equal and opposite, formed at the interface between the metal and the electrolyte, one at the metal surface and one at the solution adjacent to the metal [60].

The overpotential, $V_0$, is the voltage needed, over the electrode equilibrium potential, for a given current to start flowing through the double layer [161]. The use of an externally applied potential difference between the electrodes is needed to make this current flow across the electrolytic cell. The direction the potential difference will govern the current direction. This current promotes the movement of ions between the surface of the electrode and the electrolyte (metal dissolution). A higher current will lead to a greater the working voltage (difference between the voltage applied and overpotential), hence to a greater metal removal.

$V_0$ is commonly assumed to be invariant during ECM [114], however previous work [85], [118], [134] have demonstrated the importance of the variability of $V_0$. Moreover, the potential applied has to also overcome the following resistances or potential drops, Figure 1.5-3, that are normally in electrochemical reactions: activation overpotential, concentration overpotential and ohmic resistance overpotential [60], [162].

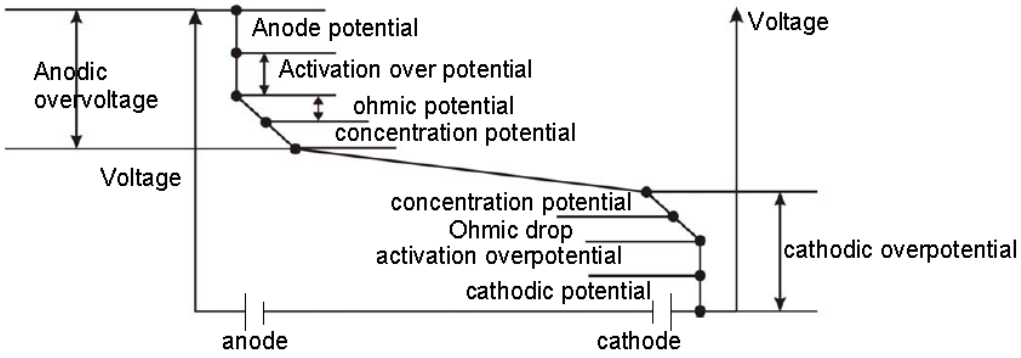


***Figure 1.5-3 Total potential drop in an ECM cell. Image taken from*** [162]

i) Activation overpotential

If a potential difference is applied across the cell to induce anodic dissolution, the electrode potential is altered from its equilibrium value by an activation overpotential, $n_a$, in order to start the ion migration. ECM is a highly irreversible process, i.e. the rate of the ion transfer is lower than the rate of the mass transport. Numerically this means that $n_a$ probably exceeds 0.05 V.

ii) Concentration overpotential

As dissolution proceeds, the movement of ions is controlled by three processes:

- migration, movement under the influence of the electric field,
- convection, bodily movement forced by the agitation of the electrolyte,
- diffusion, movement due to ion concentration gradients in the solution.

When the rate of metal dissolution is greater than the rate at which the metal ions can diffuse away from the electrode, a condition is reached in which an ionic concentration gradient exists over a thin layer of electrolyte adjacent to the electrode. This layer is called diffusion layer. A change in the electrode overpotential occurs due to this concentration gradient, and the

numerical difference between the previous and this new value is said to be the concentration overpotential $n_c$ [60]. The thickness, $d$, of the diffusion layer increases in the electrolyte flow downstream direction, and decreases with increasing velocity. A method for estimating the average diffusion layer thickness was developed by [163], [164], where $d$ is related to the average Nusselt number $Nu$.

iii) Ohmic resistance overpotential

Resistance overpotential, $n_r$, is the potential drop that occurs when a thin layer of electrolyte or a thin film layer (e.g. oxide film) is formed on the electrode surface. Its magnitude depends on the current flowing in the cell, and on the nature and conductivity of the electrolyte and of this thin layer. For a small volume of electrolyte, the resistance overpotential is inversely related to the electrolyte concentration. There is a clearly connection between the resistance and the activation overpotential. In practical cases, the presence of the former is usually noticed by the need for increasing the voltage required to maintain the reaction [60].

#### 1.5.3.5. Tool characteristics

One of the main advantages of ECM is the possibility of using a soft metal as a tool, as it is a contactless process and no tool wear takes place. The tool is generally made of brass, copper, bronze or stainless steel.

The design of the tool determines the current density distribution and, hence, the shape of the feature being machined, which is in theory a perfect negative image of the workpiece desired. This advantage however, is limited by the complexity of the tool design process. The cathode design mainly deals with the determination of a tool shape which will produce a workpiece with prescribed dimensions and accuracy.

Difficulties in designing ECM tools come from a lack of adequate understanding of ECM phenomena, thus the tool shape design is still done empirically and iteratively in practice [14]. However, there are some basic considerations that must be considered for the tool geometry design [46]:

i) high peaks or deep valleys should be avoided. High peaks restrict the electrolyte flow and increase the possibility of electric field concentration, resulting in sparks. Deep valleys retain small amounts of electrolyte, which results in impressions of the eddy currents,

ii) sharp edges, close to 90°, prevent a good flow of the electrolyte, causing stray machining and oxidation marks,
iii) electrolyte flow slots through which the electrolyte exits the array tool-workpiece are needed to avoid marks at the workpiece surface,
iv) surface finish quality of the tool should be heeded, because the workpiece will mirror the tool imperfections, and
v) insulation is required to prevent overcut, e.g. for drilling by ECM, the sides of the tool should be insulated in order to limit the material dissolution to the direction of the tool movement (depth).

#### 1.5.3.6. Tool feed rate

The tool feed rate is the velocity at which the tool approaches to the workpiece. The material removal rate is function of this tool feed rate. As the tool advances towards work, the interelectrode gap decreases and the current increases, thus more metal is removed. The tool movement slide must be stable and is usually controlled by a hydraulic cylinder.

#### 1.5.3.7. Workpiece material

As it has been explained, one of the main advantages of ECM is its capability to machine any conductive material, regardless its mechanical properties, such as hardness, toughness, and ductility, but considering their atomic, physical, chemical and electrical properties.

From equation 1.4-1, the characteristics of the workpiece material needed are molar mass, $M$, and valence, $z$, however, other characteristics as density, $\rho_a$, and chemical composition, also play an important role in the ECM behaviour.

Passivation is defined as a phenomenon in which a metal or alloy exhibits a high corrosion resistance due to formation of a protective film oxide on the metal surface under oxidizing conditions, i.e. ECM [165]. Conditions, such as electrolyte pH and electrode potential, lead to passivation in many metals. Examples of passive metals are chromium, aluminium, iron (in some environments), nickel, titanium and many of their alloys. Stainless steels (iron alloy with high chromium (Cr) content) are highly resistant to corrosion in a rather wide variety of atmospheres as a result of the passivation phenomenon. Cr content is characterised by formatting a very stable, thin corrosion resistant surface film [60], [165] at its surface.

During anodic dissolution, a curve of anodic potential against current density can be obtained, named polarisation curves. A simple characteristic polarisation curve is illustrated in Figure 1.5-4. For anodic potentials in the range AB in Figure 1.5-4, the metal is said to be in the “active”

state and dissolves by the removal of cations from the crystal planes. Since the rates of dissolution depend on the geometry of the tool and workpiece, the metal surface dissolves locally [60], [166] copying the tool profile.

When the anode potential becomes greater than B in Figure 1.5-4, a solid oxide film may form at the anode surface, which causes the reaction rate to be reduced; for example to the level CD in Figure 1.5-4. The metal is then said to have become "passive". When the oxide films are present, dissolution takes place in random manner over the metal surface (it is now controlled by the film and not by the geometry of the crystal plane). Since the atoms are removed in a random fashion, the metal surface becomes polished. For oxide films with good electric conductivity and for appropriate conditions of potential, the oxidation of solution ions may take place in preference to, or in addition to, polishing or passivation of the workpiece.

If a passive film is present on a metal and the metal is exposed to a solution containing an appropriate concentration of aggressive anions, those anions will penetrate into the film, thus the protective anodic film is damaged or may break it down completely. This condition is represented by DE in Figure 1.5-4 and is called "transpassive region". If the break is not uniform, the areas of penetration permit greater local current flow than elsewhere over the electrode where the film is unbroken. Such local current flow can lead to the formation of pitting on the electrode surface. Pitting is most likely to occur at weak points of the oxide film (e.g. at grain boundaries). The potential at which the oxide film is disrupted is the "critical breakdown potential" [60], [166].

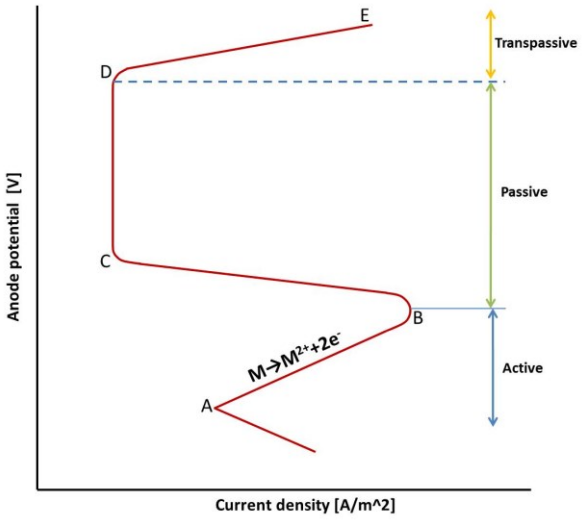


***Figure 1.5-4 Schematic polarisation curve for a metal that displays an active-passive transition*** [60]**.**

Valence is the number of electrons at which a given atom generally bonds or the number of bonds that an atom forms [167]. The workpiece valence is required to describe the electrochemical dissolution and calculating the material removal rate according to Faraday's law. Determining the accurate dissolution valence of the workpiece is difficult to achieve, because it depends on the electrolyte used, the electrolyte concentration, the electrolyte and electrode temperature, and the presence or not of an oxide film or bubbles during the ECM process. Additionally, an element may behave differently in a metal alloy, or the corrosion potential of the metal may not be stable [94]. All these factors will affect the actual value of the valence during ECM, thus changing the characteristics of the ECM process and the results achieved.

## 1.6. *Simulation methodology*

### 1.6.1. Introduction

Computer simulation has become an essential tool in science and engineering. When used in manufacturing engineering, its primary purpose is to create a faster and a more accurate process, components and tooling with more precise dimensions, and the reduction of energy consumption and costs involved [168]. Computational simulation is a translation of real-world physical and chemical laws into their virtual form [169], with the objective of using a digital environment where the process can be developed with optimised parameters, and the resulting error can be forecast and corrected before the implementation of the process in the real-world.

Problem solving by modelling and simulation is an iterative and interactive process which can involve cyclical and evolutionary procedures [170]. Today a broad spectrum of options for simulation is available, from basic programing languages to various high-level packages implementing advanced methods [169]. Recent development of computer aided design (CAD) and finite element (FE) packages has provided the necessary virtual environment to simulate the ECM process, thus giving a 3D visualisation of the process and the results for analysis.

In this section only the basic methodology for simulating the ECM process is presented. (application and results are showed in Chapter 2). For this methodology, first, the ECM modelling and its corresponding simplification is carried out. Then the main assumptions taken and constraints of the simplified model are explained, followed by their implementation in the simulation. Afterwards, the results are extracted and multiple display options are presented. At the end of this section, some of the problems encountered during the simulation process are presented in order to propose correction actions to enhance the simulation methodology.

### 1.6.2. Finite element method, packages and characteristics

The Finite Element Method (FEM) is a numerical technique where a continuum system is divided into small elements. Constitutive relations of the physics governing the problem can be defined for each element and assembled back to reach a system of equations whose solutions give the behaviour of the total system. Due to this partitioning, the solution is an approximation of the real one, but accurate enough to be valid [171], [172].

Alkire et al. [18] was the first in using FEM for the calculating the shape changes at the cathode during electrodeposition. Hardisty *et al*. [17], [39] and Purcar et al. [23], [35] investigated the applicability of FEM to the simulation in 2D and 3D, respectively, of the ECM process. Their results showed excellent agreement between the computer predictions and theory, however

experimental validation was still needed. Moreover recent works [44], [110], [124] where FEM was used in a multiphysics 2D environment demonstrated that FEM is a useful tool for complementing analytic and experimental techniques.

The development of new technologies in CAD systems, such as SolidWorks®, SolidEdge®, and Inventor®, and FEM packages, such as ANSYS®, ABAQUS®, and COMSOL Multiphysics®, have provided the opportunity to develop models where some of the different physical and chemical phenomena during the ECM process, such as electrodynamics, fluid dynamics, heat transfer and electrochemistry, can be integrated in the simulation. Due to the complexity of the ECM process however, most of these solution are simplified to a two-dimensional (2D) problem. Simulation models of the ECM process in a three dimensional environment are still under development. These models are mainly applied for the manufacture of turbine blades, due to their complexity of machining by conventional methods [24], [136], [137].

Commercial CAD software, SolidEdge®, and FE package, COMSOL Multiphysics®, were used in the present work, in order to avoid lengthy finite element (FE) development times and to make use of the graphics facilities available. COMSOL Multiphysics® was chosen for this work because it is user friendly and because of its capability to allow the development of a fully coupled model using electric currents, electrolyte flow, moving boundaries and Joule heating.

This simulation model aims to extend the understanding of the ECM process and broaden the application of ECM in industry by providing an accurate tool for the forecast of the process outcomes. The model is divided into five sections: system analysis, model generation, model set up, computer simulation, and analysis of results.

### 1.6.3. System analysis

#### 1.6.3.1. Modelling aims

In order to establish the aims of the simulation, the system of interest must first be analysed, i.e. if the simulation is required to predict, control, explain or design the process, hence what information should be expected from the results.

For example, the working principle of ECM is anodic dissolution in which the workpiece is the anode and the tool the cathode of an electrolytic cell. Electrolyte is flowing in the gap between the electrodes (interelectrode gap) and the electric current conduction is achieved by the movement of the ions through it. The positive ions from the anode flow through the electrolyte towards the cathode, leaving behind an imprint of approximately the negative shape of the tool.

The electrolyte flushes away the metal ions before they reach the cathode. Figure 1.6-1 illustrate a schematic of the ECM system.

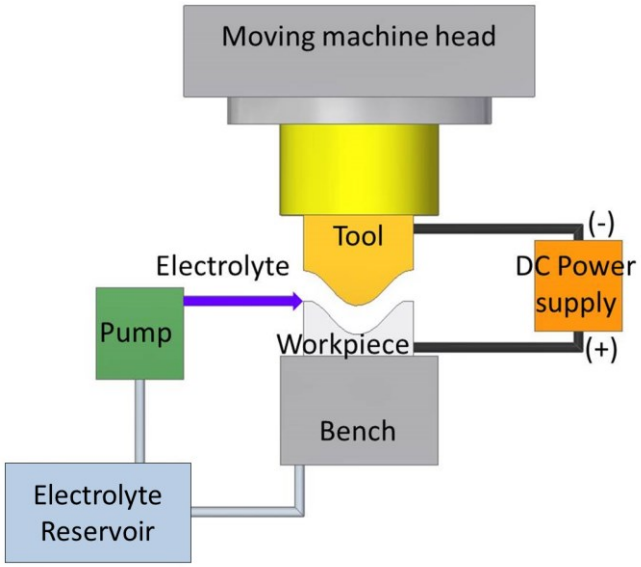


***Figure 1.6-1 Schematic of an ECM system.***

For the ECM problem, the main aim of the simulation is to forecast the behaviour of the process, and the results can be divided into three categories:

i. determination of the final surface profile. This is dependent on which electrode, workpiece or tool, is to be predicted,
ii. optimization of the machining parameters,
iii. enhancement in the accuracy of the workpiece surface finish.

#### 1.6.3.2. Framework

The framework provides the modeller with a means to construct a mental image of the problem. As proposed by Page [173], the framework can give a perspective of the problem according with:

i. the time at which things happen,
ii. a prediction of when the things will be happening,
iii. a sequence of actions

Figure 1.6-1 presents the complete ECM system. The workpiece is placed on the bench of the ECM machine, and the tool is held by the moving machine head. Both, tool and workpiece, are

connected to the DC power supply by conductive clamps. Electrolyte is pumped into the system and within the interelectrode gap. The tool-workpiece array is positioned in such a fashion that the electrolyte can flow out from the system to be collected into the electrolyte reservoir.

#### 1.6.3.3. Simplifications

Matko *et al*. [174] argue that modelling deals primarily with the relationships between the actual processes and the model, and simulation deals with the relationships between the model and the computer simulation technology. Thus, the simplifications done in the translation from the real-world to the virtual one usually are the main factors determining the accuracy of the resulting simulation.

Building simulations may be considered artful as there are many physical, engineering and numerical assumptions that have significant influences on the results. Neither the computer nor the model can completely replace human decisions, intuition and experience, that still play a significant role in determining the validity and usefulness of the model [174].

In the present work, there was no need for modelling all the components in the ECM system illustrated in Figure 1.6-1. The function of each of the parts can be introduced in the model as input, constraint, boundary condition or assumption, depending on its effect on the area of interest: the interelectrode gap. Therefore the first and maybe most important simplification for the ECM process simulation is that only the interelectrode gap will be modelled. The tool and the workpiece will be the boundaries of the model which in turn will be filled with flowing electrolyte. The pump and the electrolyte collection will be represented by the "electrolyte flow rate", and the DC Power supply by the electric constraints applied to the model. Figure 1.6-2 depicts an example of this simplification.

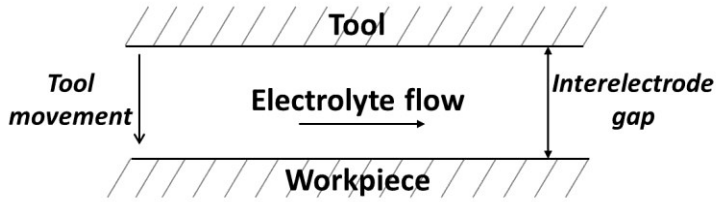


***Figure 1.6-2 Simplified schematic of an ECM system.***

### 1.6.4. Model generation

Depending on the goals of the simulation, available input data and computational resources, there is the need for simplifying the geometry and the applied physics [2]. For the ECM process simulation, the tool and workpiece geometries must be provided by the modeller. And the

software allows the user to adjust specific variables such as material properties, initial conditions, constraints, boundary conditions, etc.

The geometry defined for the present work describes the shape of the interelectrode gap. The tool is the top boundary and the workpiece is the bottom boundary of the model. The required profiles for this work were constructed using SolidEdge®, however any computer aided design (CAD) software could be used. Figure 1.6-3 presents an example of an initial ECM system in a 2D environment. For the ECM simulation, only the space between the tool and the workpiece (interelectrode gap), uniformly filled with electrolyte, will be simulated.

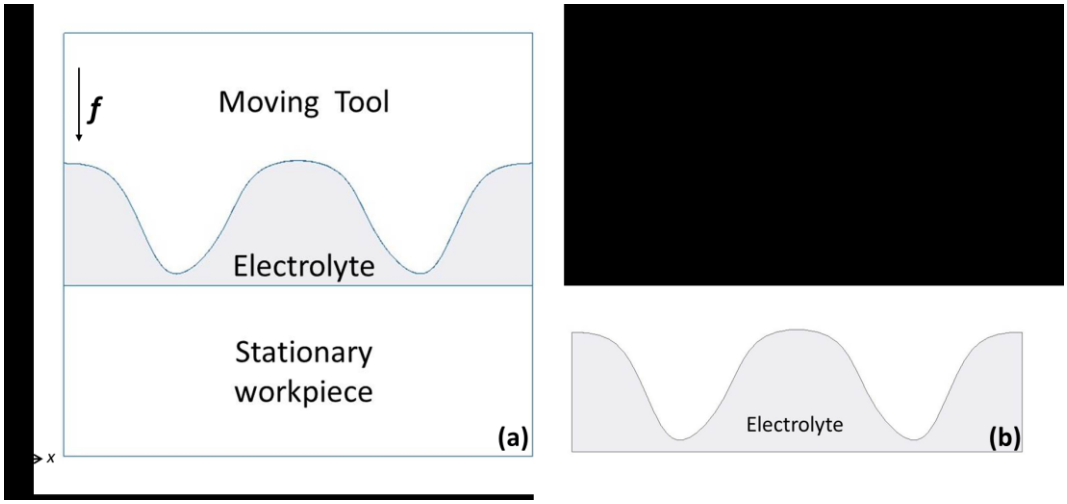


***Figure 1.6-3 Model of the ECM system. (a) Tool, electrolyte and workpiece in a 2D environment, (b) Electrolyte. Model used for the ECM simulation according with*** [118]***.***

One of the advantages for developing a computational simulation model is the possibility of only simulating one section of the system, where all the physics can be applied regardless of the size and position of the section in the system. Figure 1.6-3(b) displays the final electrolyte model used for the simulation, which was imported into COMSOL Multiphysics®. All the parameters, e.g. dimensions, orientation, etc., specified in the CAD software are also imported to the FE package.

### 1.6.5. Model set up

#### 1.6.5.1. Governing equations for the ECM simulation

Good simulation practices include to know the equations involved in the problem and to have an idea of the results expected. For the work carried out in this thesis, the ECM basic theory presented in section 1.4 was required. Table 1.6-1 presents some of the equations used for the simulation of ECM (to be explained in sections 2.3).

***Table 1.6-1 Equations used in ECM on SS316 simulation model.***

| | Value | Name |
|---|---|---|
| K1 | A1/(zn1*F1*Rho1) | Electrochemical constant |
| dx | x-X | x-displacement |
| dy | y-Y | y-displacement |

, where $A_1$ is the molar mass, $z_{n1}$ the valence, $Rho_1$ the density of the workpiece and $F_1$ is Faraday's constant. Note that the notation used in the table is the actual one used for introducing the equations in the FE package.

Additionally, each of the physics applied to the model, e.g. fluid dynamics and Joule heating, have their own default equations associated, that are already included in COMSOL Multiphysics®. These equations need to be set in order to use them into the model.

#### 1.6.5.2. Initial conditions, loads and constraints

The initial conditions, loads and constraints in the model represent the setup conditions, limits or special relationships defining the model. They can be applied on a point, edge, area or volume. The choice of the correct ones is maybe the most difficult part of the computational simulation. It is important to remember that the simplification of the model and its translation to a virtual environment should respect the real behaviour of the system as far as possible; therefore the function of each part of the system should be introduced as one of these initial condition, loads or constraints, but also as a boundary condition or assumption. An over or under constrained model can provide essentially useless information, and if the correct constraints are applied in the wrong places, the results can be just as bad [175].

***Workpiece material***

For the ECM simulation, the workpiece material properties should be defined, e.g. molar mass, valence, and density. Table 1.6-2 below presents an example the values and nomenclature used in the simulation. Again note that the notation used in the table is the actual one used for introducing the equations in the FE package.

***Table 1.6-2. SS316 properties used for the ECM simulation model, data taken from*** [176]***.***

| | Value | Name |
|---|---|---|
| zn1 | 3.5 | Valence Stainless Steel 316 (shiny surface finish [27]) |
| A1 | 56.2e-3[kg/mol] | Molecular mass of WP SS316 |
| Rho1 | 7870[kg/(m^3)] | Density of the WP SS316 |

Some materials are already contained in COMSOL Multiphysics®, and can be chosen from the material browser library or the characteristics of a special material can be added manually by the user.

***Electrolyte characteristics***

The type of electrolyte and its characteristics has to be introduced as a constraint for the ECM process simulation. Electrolyte temperature, $T_e$, and its electrical conductivity, $k_e$, are the properties of interest for the simulation. The electrolyte electrical conductivity and density are temperature dependent; hence, the initial temperature, $T_e$, is introduced in the equations (1.6-3) and (1.6-4) linearized from [177]:

$$k_e = M_k T_e + B_k \qquad \textbf{(1.6-1)}$$

$$Rho_e = M_{Rho} T_e + B_{Rho} \qquad \textbf{(1.6-2)}$$

, where $k_e$ is the electrolyte conductivity, $M_k$ is the gradient of the conductivity equation, $B_k$ is the *y*-intercept of the conductivity equation, $Rho_{Ele}$ is the density of the electrolyte, $M_{Rho}$ is the gradient of the density equation, $B_{Rho}$ is the *y*-intercept of the density equation, and $T_e$ is inlet electrolyte temperature. The values for equation (1.6-3) and (1.6-4) were extracted from experimental published values from [177]. Table 1.6-3 presents the nomenclature, and some values and equations used for this work.

***Table 1.6-3 $NaNO_3$ Electrolyte characteristics for the ECM simulation model.***

| | **Value** | **Name** |
|---|---|---|
| T | Te | Inlet electrolyte temperature |
| Mk | 0.336[S/(K*m)] | Gradient Conductivity $NaNO_3$ |
| Bk | 82.964[S/m] | y-intercept Conductivity $NaNO_3$ |
| Sig1 | (Mk*Te)-Bk | Conductivity $NaNO_3$ |
| MRho | -0.6357[kg/(K*m^3)] | Gradient Rho $NaNO_3$ |
| BRho | 1371.5[kg/m^3] | y-intercept Rho $NaNO_3$ |
| rho | (MRho*Te)+BRho | Density of $NaNO_3$ |

***Tool feed rate***

The too feed rate, $f$, is the velocity at which the tool moves towards the workpiece during the simulation. For the present example, the tool feed rate is also added as a parameter for the simulation.

***Electrodes voltage***

The reference voltage, $V = 0$ V, is at the tool and an overpotential, $V_0$, is assumed to be generated at the workpiece surface during the ECM process. The potential difference applied, $V_1$, to the system has to be provided by the user as a constraint and can be added as a global definition of the model. The voltage is assumed to be uniform during all the simulation and the overvoltage is dependent on the current density during the process, as indicated in equation (1.6-3).

$$J = k_e(V_1 - V_0) \qquad \textbf{(1.6-3)}$$

Additionally, the overpotential behaviour was determined by experimental data, and this information was added to the model from [118].

### 1.6.5.3. Physics application

COMSOL Multiphysics® has the capability to allow the development of simulations using coupled multiphysics phenomena. This FE package is integrated by multiple modules that can solve common physic phenomenon such as structural analysis, fluid flow, pressure, electric currents, heat transfer, Joule heating, etc., and couple them into a single solution. Some of the physics applied to this example model are presented below.

***Moving boundaries***

For the simulation of the movement of the tool and the dissolution of the workpiece, and therefore the deformation of the interelectrode gap, an Arbitrary Lagrangian-Eulerian (ALE) formulation was used. In ALE formulation, the FE mesh is neither fixed spatially (Eulerian formulation) nor attached to the workpiece material (Lagrangian formulation); the mesh follows the material flow and the problem is solved for displacement in a Lagrangian step, while the mesh is repositioned and the problem is solved for velocities in an Eulerian step. The idea is to use the Eulerian approach for modelling the area around the tool, which moves with a uniform velocity, and avoid severe element distortion. And the Lagrangian approach is used for the unconstrained flow of material at the free boundaries, hence for shaping the workpiece surface where the dissolution of material occurs [171].

The model is developed in a global coordinate system, allowing free deformation of all the system. The mesh attached to the static tool is fixed, thus $v_x$, $v_y$ and $v_z$ = 0 m/s, with respect to the global coordinate system. The mesh attached to the workpiece moves in relation to the boundary system, and according to Faraday's laws [13] in equations (1.6-1) and (1.6-2). The mesh attached to the walls is fixed in direction $x$, then $v_x$ =0 m/s, and it can be free in $y$ or $z$, thus $v_y$ and $v_z$ are established by the user with respect to the global coordinate system. Figure 1.6-4 depicts an example of a moving mesh boundary conditions for an 2D ECM simulation model with static tool (top boundary), and planar and static workpiece (bottom boundary) attached to a moving boundary to simulate the material dissolution

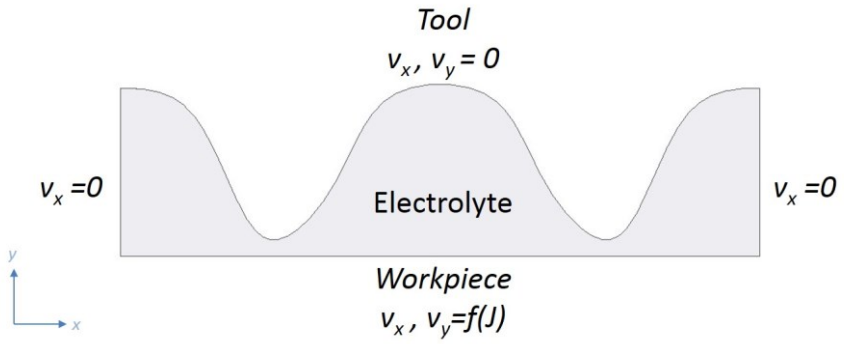


***Figure 1.6-4 Moving mesh boundary conditions for a 2D ECM simulation model with static tool (top boundary), and planar and static workpiece (bottom boundary) attached to a moving boundary to simulate the material dissolution.***

***Electric currents***

The electrode surfaces are equipotentials, where the boundary conditions are:

$$V_{tool} = 0 \qquad \textbf{(1.6-4)}$$

$$V_{WP} = V_1 \qquad \textbf{(1.6-5)}$$

$$n\vec{J}_{1,2} = 0 \qquad \textbf{(1.6-6)}$$

, where $V_{tool}$ is the electric potential at the cathode (tool), $V_{WP}$ is the electric potential at the anode (workpiece), $V_1$ is the voltage applied to the system, and $n\vec{J}_{1,2}$ is the normal current density at the sides of the model.

### 1.6.6. Computer simulation

#### 1.6.6.1. Meshing

For the FE analysis, a continuous region is divided into discrete regions called elements. The process is called meshing. The element type of the mesh can be chosen. The element shape depends on the geometry of the problem, and will affect the accuracy of the results and the computational time and resources used. The elements can be a line, an area or a volume, and according to the two dimensional or the three dimensional geometries, their shape can be: triangular or tetrahedral, rectangular or prism, or quadrilateral or hexahedral [178]. Each corner of the shape is called node, and the number of nodes determine the number of equations to solve by FEM.

For the simulation of the ECM process, the initial designed mesh usually cannot hold its original shape and it is distorted due to the dissolution of material. The distortion causes premature convergence and numerical errors. To handle this problem, new meshes must be generated at intermediate stages during the simulation. This is called adaptive meshing [171]. There are mainly three types of adaptive meshing. One adaptive mesh procedure is the re-meshing technique and includes the generation of a completely new FE mesh. The second technique is called refinement which involves increasing the local mesh density by reducing the local element size. The last adaptive mesh technique is called smoothing and includes the reallocation of the nodes to provide better element shapes. The adaptive mesh procedures decreases solution errors during calculation, therefore increasing the accuracy of the simulation [171].

The mesh module of COMSOL Multiphysics® was used for the present work. The element size could be established, i.e. maximum element size of $1.5 \times 10^{-3}$ m and minimum element size of $1.0 \times 10^{-4}$ m for model developed. The maximum element growth rate was 1.3. This change in size and growth rate be can modified using the simple input interface of the FEA package. Figure 1.6-5 presents an example of a mesh developed in this work based in previous work [118]. A denser (finer) mesh is evident in the areas with high curvature. The element shape was triangular.

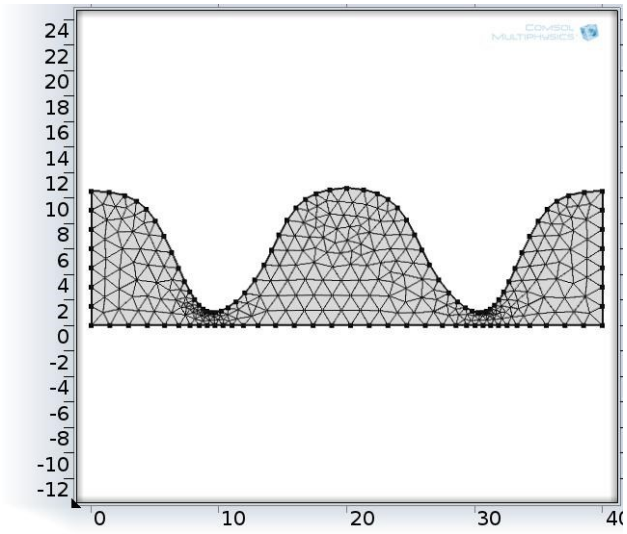


***Figure 1.6-5 Refinement adaptive meshed model according to*** [118]***. Triangular mesh, 1.0x10$^{-4}$ m minimum element size, 1.5x10$^{-3}$ max element size.***

#### 1.6.6.2. Simulation steps

COMSOL Multiphysics® can solve various physical phenomena in a process called 'coupling'. Model coupling integrates the global definitions (parameters and variables), so once they are established at the beginning of the simulation, they are considered for all the physics applied [169]. On the other hand, for a correct coupling, the study has to follow a sequence. This sequence will depend on the physics applied and the interaction between them. It is the responsibility of the user to establish this sequence.

#### 1.6.6.3. Simulation time

The length of the simulation is given by the machining time. Therefore an exit condition, the same as the actual machining time, was established for the present example.

### 1.6.7. Analysis of results

In addition to the full numerical results, graphical views offer the user and the non-technical community a useful overview of the simulation. Therefore, the latest FE packages are able to present the results of a simulation in a graphical-based environment, reducing communication problems between the modeller and the client.

#### 1.6.7.1. Verification and validation

Although much effort is taken to eliminate possible errors, different approaches to the same problem, e.g. set up, mesh chosen, element type, etc., can produce variation of results. Moreover, due to the fact that the computational simulation process is a result of the translation of a problem from the real world to a virtual environment, followed by the simplification of the

model and that several assumptions made, the results should always be verified to ensure that they are reasonable. This can be done mathematically, usually done for only one or two cases, if possible, or due to the complexity of some of the problems, by comparison of the simulation results with previous published results as done in Chapter 2 of the present thesis; or by comparison with experimental data as done in Chapter 3.

#### 1.6.7.2. Documentation

A good documentation of the methodology used for the FE analysis of a problem is needed in order to reproduce it and to present the solutions to the client. This thesis is an example of this documentation. Additionally, some FE packages have the option of creating a report of the analysis. A good documentation should comprise comprehensive information about the model, including the physics, settings and variables, and sometimes the underlying equations of the simulation.

#### 1.6.7.3. Implementation and applications

After the simulation, the next step is the implementation of the results in the real world. Ultimately the modeller should use his knowledge and experience to evaluate the results and determine if they are applicable or not. FEM is only a tool for the simulation of a process and at its best only an estimate of the solution of the problem. It helps the understanding of the process and the forecast of actual results; however it cannot entirely substitute experimental tests. ECM is one example of the importance of a computational simulation in engineering and science; due to its complexity, other methods for the prediction of it have not been as successful.

### 1.6.8. Conclusions

The present methodology for the simulation of the ECM process by FEM using SolidEdge® and COMSOL Multiphysics® can be divided in five sections: system analysis, model generation, model set up, computer simulation and analysis of results. The system analysis establishes the aims of the simulation, hence identifying the area of interest and making the necessary simplifications for the construction of a clear model that includes all the information of the system. Then, in the model generation step, this information is used to build the geometry of the problem in a virtual environment and to adapt it for the computational simulation. Equations, initial conditions, loads, constraints and physics will be set on the model set up step. The aim is to mirror the real behaviour of the problem in a virtual environment. Once the model is properly defined, the computational simulation can be carried out. To this extent, the model should be first divided in small elements (meshing), and then, a solution sequence of the physics involved should be followed. This sequence must be based on the relationships within

the phenomena. The results should be analysed in order to evaluate their accuracy and applicability in the real world. Additionally a good documentation of the steps followed and the outcome of the simulation should be kept. The present section is an example of this documentation, where the specifics of the problem will be indicated, and it is a useful tool towards the development of a simulation model repeatable and the achievement of consistent results.

# *Chapter 2*

## *ECM simulation model and its application in SS316 samples*

*Wisdom is knowing what to do next,*
*skill is knowing how to do it, and virtue is doing it.*
*-David Starr Jordan*

## 2.1. *Simulation of ECM in a 2D environment*

### 2.1.1. Introduction

As discussed in Chapter 1, electrochemical machining (ECM) can be a complicated and often expensive manufacturing process. Traditional ECM techniques involve a serial of trial-and-error processes in order to ascertain the optimal parameters for a specific job and machine configuration. This approach is long and costly, and therefore, it is one of the main limitations for the use of ECM in industry. In an effort to solve this problem, computational simulation techniques can be used for the understanding and forecast of the ECM behaviour. By performing the machining virtually, the results could be predicted, and errors prevented and solved without the experimental testing. This simulations have the objective of reducing the time and cost of the ECM set-up.

In this section a computational simulation of the ECM process in a two-dimensional (2D) environment is developed. In the first part, the theory for a 2D model of ECM is introduced; then, this theory is applied to develop a computational simulation of the process. The study of the ECM mechanism is complicated because the dissolution occurs at different rates at each point of the workpiece surface profile and it depends on the local current density, which changes continuously as the machining proceeds [17]. Various authors had attempted to model ECM by applying the boundary element method [22], [35]–[37], the finite difference method [23], [41], [129], and the finite element method [39], [40], [134]. However these studies were limited by the complexity of setting up the problem or technological limitations at the time they were performed. Therefore, computational technology advancement in recent years is one of the main reasons driving the further development of the ECM research and hence, the development of the simulation model in this thesis.

For this model, a tool with fixed geometry is used to shape a static workpiece. The workpiece dissolution obeys Faraday's laws, but it also depends on the interaction of various physical and chemical phenomena, e.g. heat transfer, mass transfer, fluid dynamics and electrochemistry [2]. The ECM computational simulation developed in this work is based on finite element method (FEM), and a commercial computer aided design (CAD) software, SolidEdge®, and a finite element analysis (FEA) package, COMSOL Multiphysics®, are used. One of the advantages of this new simulation model over the previous work is the ability to provide information of the ECM behaviour at any time during the simulation, before and after reaching the steady state, such as current density, electric field distribution, difference potential, etc. Moreover, by incorporating as many physical and chemical parameters as possible, should ensure that the final profile of the workpiece can be accurately predicted. The simulation results were then compared with

published works in order to validate them. A good agreement between the results obtained and the published theoretical and benchmark experimental results was achieved. However some improvement can still be done in order to enhance the accuracy of the results.

### 2.1.2. ECM theory for two dimensional (2D) problem

The first step for the work presented in this section is to provide the essential theoretical background for the ECM process modelling. For the case when a tool with fixed-geometry shapes a workpiece parallel to the tool, the solution was developed using existing solutions [17], [39], [179]. One of the simplest methods commonly used for the study of the ECM process is to consider a static workpiece at the bottom of the system, and a moving tool approaching to it from the top with a vertical and uniform velocity , $f$ .

For an ideal case, a simplification of the mathematical problem is done. The area of interest for the study is only the space between the electrodes (interelectrode gap), hence the profile constructed is an enclosed box where the lower boundary is the workpiece, the upper boundary is the tool, and the lateral boundaries are considered isolated. The interelectrode gap is assumed to be filled with a uniform concentrated electrolyte. See Figure 2.1-1.

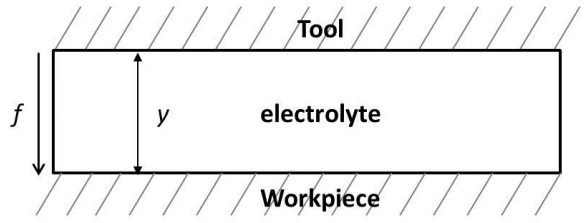


***Figure 2.1-1 Diagram for 2D ECM model. The tool and the workpiece are the top and bottom boundary respectively, and the space between them is the interelectrode gap.***

There are two ways of addressing the simulation of ECM, which are called direct and inverse problem. For the direct problem, a tool with fixed geometry is used to shape a workpiece. The dissolution of the workpiece surface obeys ECM theory, copying iteratively the shape of the tool. The simulation is terminated when the solution reach an equilibrium interelectrode gap value and the final workpiece geometry is a negative profile of the tool shape [28], [34].

For the tool design, known as inverse problem [28], [34], the workpiece geometry remains fixed and the tool shape is iteratively changed until it can produce the expected workpiece profile. In industrial practice, previous experimental experience is employed to propose the first approximation to the tool shape; however arriving to the final tool geometry may require a long

series of iterations [17]. This second problem mainly deals with a time consuming iterative task, however this is the most frequent problem encountered in industry.

The formulation of the ECM process depends on the scheme of the problem. For the direct problem the tool shape and trajectory must be specified [34], [60], while for the inverse problem it is necessary to additionally determine the working surface of the tool. In both cases the ECM machining parameters, e.g. workpiece material, voltage applied, $V_1$ (V), tool feed rate $f$ (m/s), etc., should be chosen by the user. In the present work, a direct problem approach, i.e. given the tool profile, the generated workpiece surface needs to be determined, was considered.

When a constant voltage, $V_1$ (V), is applied between the electrodes, electric current, $I$ (A), crosses the interelectrode gap, $y$ (m), carrying metal ions from the workpiece surface towards the tool. According to Faraday's laws [17], the amount of any substance dissolved or deposited is directly related to the amount of current, $I$ that has flowed [60]. The basic equation for the material dissolved, $m$ (kg), assuming an efficiency of 100%, is given by equation 2.1-1:

$$m = CIt \qquad \textbf{(2.1-1)}$$

, where $C$ is given by equation 2.1-2:

$$C = \frac{M}{zF} \qquad \textbf{(2.1-2)}$$

, being $M$ (kg/mol) the molar mass and $z$ (1) the valence of the workpiece material, and $F$ the Faraday's constant (96 500 C/mol).

As a consequence of this dissolution, the workpiece surface is deformed. If the workpiece profile is broken into a number of points evenly distributed along its length (nodes), each of these nodes moves with a velocity, $v$ (m/s), according to equation 2.1-3 [2]:

$$v = \frac{C}{\rho_a} J = C' J \qquad \textbf{(2.1-3)}$$

$$C' = \frac{C}{\rho_a} \qquad \textbf{(2.1-4)}$$

, where $\rho_a$ is the density of the workpiece material and $J$ (A/m$^2$) is the current density at the node and is given by Ohm's law:

$$J = \frac{k_e}{y}(V_1 - V_0) \qquad \textbf{(2.1-5)}$$

$k_e$ (S/m) is the electric electrolyte conductivity, $y$ (m) is the interelectrode gap for flat electrodes. When a reference voltage, $V = 0$ V, is assumed at the tool, on the workpiece $V_1$ (V) is the voltage applied and an overpotential, $V_0$, is generated at the surface during the ECM process.

From equations (2.1-1)-(2.1-5), it can be observed that $m$ depends on the current density, the characteristics of the electrolyte and the workpiece material. In the analysis presented here, the electrolyte flow is not considered and $k_e$, is assumed constant throughout the ECM operation. Additionally, all the current is assumed to be used for removing metal form the anode, i.e. the current efficiency $\eta$ =100%.

When the geometry is more complex, the distribution of the electric potential changes and is based on the solution of the Laplace equation that describes the potential in an electric field as in equation 2.1-5 [134]:

$$\frac{d^2\phi}{dx^2} + \frac{d^2\phi}{dy^2} = 0 \qquad \textbf{(2.1-6)}$$

If the tool has a constant $f$ (m/s), the velocity at which $y$ (m) changes can be expressed by equation 2.1-6:

$$\frac{dy}{dt} = v - f \qquad \textbf{(2.1-7)}$$

When the dissolution rate of the workpiece (velocity of dissolution), $v$, equals to the feed rate of the tool, $f$, $y$ does not change with the time anymore. This means $y$ is at an equilibrium value, $y_e$, which depends on $C'$, $k_e$, $V_1$, and $V_0$, and it is given by equation 2.1-7 [17]:

$$y_e = \frac{C' k_e (V_1 - V_0)}{f} \qquad \textbf{(2.1-8)}$$

In the ideal cases a well mix, steady and uniform electrolyte is assumed, hence its conductivity remains constant.

The voltage applied and the feed rate can be controlled by the ECM operator; however, maintenance of a constant conductivity in the electrolyte and a well control of the overpotential are almost impossible [134]. These are the principal difficulties to overcome in the prediction of the final shape of the workpiece.

### 2.1.3. Computational model for the simulation of ECM in a 2D environment

The main objective of ECM is achieving the required geometry of the workpiece. Ideally, as the electrochemical dissolution proceeds, the profile of the workpiece changes until a negative reproduction of the tool is obtained.

A computer simulation of the ECM process will help to find the evolution in time and the final shape of the workpiece for given conditions of machining. Finite Element Method (FEM) has demonstrated to be a useful tool for complementing analytical and experimental techniques [172], hence it is used for the present work. In order to avoid time consuming programing, the simulation was developed with the commercial FEA package, COMSOL Multiphysics®. This software comprises a user friendly interface and can handle the diverse physics involved in ECM and couple them into a single solution.

For the development of the computational simulation of ECM, it is necessary to specify the model input parameters, which depend on the type of ECM problem. If a direct problem is to be solved, these parameters include electrolyte characteristics, workpiece material properties, and machining parameters, e.g. feed rate, voltage, overpotential, etc.; while for an inverse problem, an initial approximate shape of the tool is also desirable. In the simulation presented here, a direct problem approach is used.

In this section, two cases of the direct problem for the simulation of ECM in a 2D environment are developed for benchmarking the simulation model. The first replicates Hardisty *et al*. [17] work , and the second Curry, D. [118] work. The later one was developed at the University of Edinburgh ECM group and it is the main background reference for the research developed in this thesis.

### 2.1.4. 2D ECM model: case 1

#### 2.1.4.1. System analysis

The first step was to construct the model of the problem. ECM is developed in a system conformed by a tool of a fix profile and a planar workpiece. The tool is hold on the top by a moving machining head, and moves down towards the workpiece surface, parallel to the $y$ axis and with a steady feed rate $f$. The workpiece is supported by the machine bench and it is static. Both, the tool and the workpiece are connected to a DC power supply by conductive clamps. The interelectrode gap is filled uniformly by the electrolyte.

As explained above, for computational optimization, there is no need for modelling all the components of the ECM system, but only the area of interest: the interelectrode gap. Based on Hardisty *et al*. [17], a parabolic shaped tool was used to shape the stationary workpiece. Figure 2.1-2 depicts the interelectrode gap model with the upper and lower boundaries defining the tool and the workpiece profile respectively. The model has a length of 2 mm and the minimum $y$ between the tool and the workpiece is 0.5 mm.

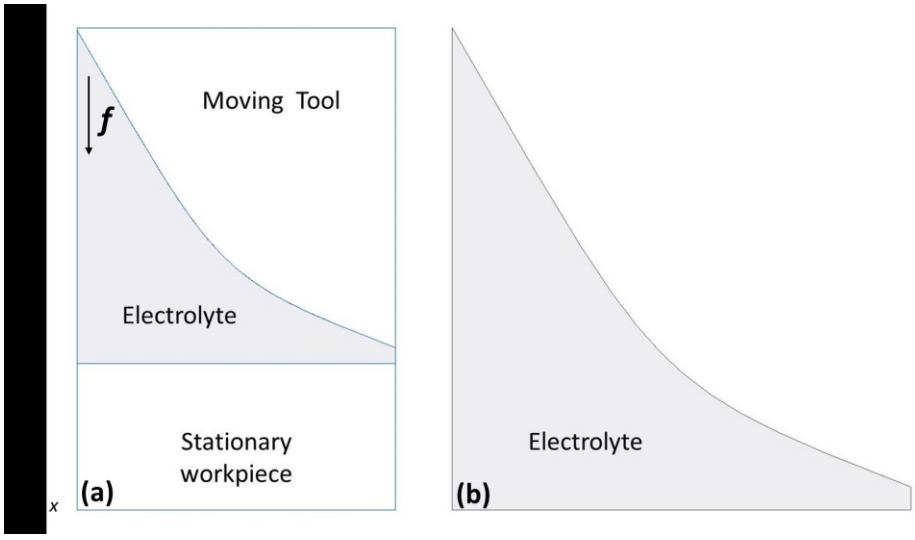


***Figure 2.1-2 CAD model used for the simulation of the ECM process in a 2D environment from*** [17]***. (a) Complete system: tool, electrolyte, and workpiece. (b) Electrolyte geometry used for the ECM simulation.***

#### 2.1.4.2. Model generation

A two-dimensional model of the system at time zero was built using a computer aided design (CAD) software, SolidEdge®. The tool was set as the upper boundary of the model and a flat horizontal profile was set as the workpiece at bottom boundary. The lateral boundaries were straight lines representing open boundaries. A moving boundary was attached to tool and the

workpiece profiles. These moving boundaries would reproduce the movement of the tool and the dissolution of the workpiece. The interelectrode initial profile can be observed in Figure 2.1-2(b).

#### 2.1.4.3. Model set up

As mention above, a moving mesh was attached to the surface of the electrodes. For the direct problem, where the tool shape and the machining parameters are known, the mesh attached to the surface of the cathode moves at a known velocity, and the mesh attached to the anode moves according to the equations for the dissolution rate of material, equation 2.1-6. This dissolution is defined by the relationship between the conductivity properties of the electrolyte, interelectrode gap and current density at each node of the moving mesh [60], [134]. The electrolyte properties were set in accordance to typical experimental data [17], [134].

Upon running the simulation, the ECM boundary conditions had to be provided. The main parameters to consider are the workpiece material specifications, *i.e. M, z,* $\rho_a$, the input machining parameters, *i.e.* $V_1$, $V_0$, $f$, and electrolyte characteristics, *i.e.* $T_e$, $Q$, $k_e$. These values were set according to the literature benchmark data [17] used to validate our work. Figure 2.1-3 presents the boundary conditions used for the ECM simulation.

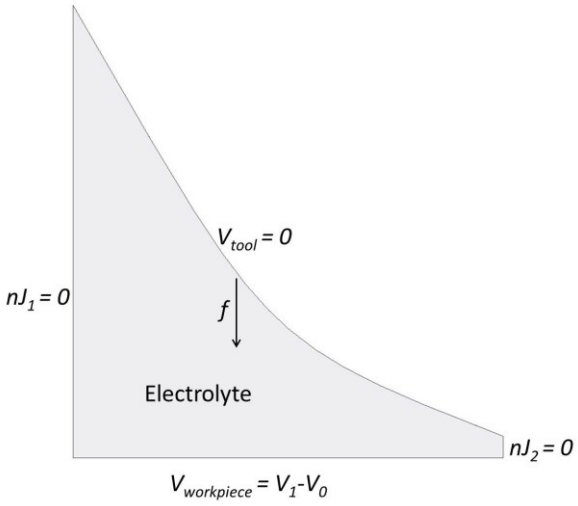


***Figure 2.1-3 Electrolyte model from*** [17] ***showing the boundary conditions used in the ECM simulation.***

***Workpiece material***

The workpiece material selected was a flat surface of Inconel 718. Molar mass $M$ = 59.79 g/mol; valence $z$ = 2.7; and density $\rho_a$ = 8228 kg/m$^3$ [180].

***Electrolyte***

The ECM process was considered to be performed using an electrolyte with a conductivity $k_e$ = 16 S/m. This is in agreement of using Sodium Chloride (NaCl) as electrolyte at 15 [°C]. In Figure 2.1-4 the density, $\rho_e$, and the conductivity, $k_e$, of NaCl in relation of the temperature are presented. As a first approach, no flow of the electrolyte is considered, but it is assumed that the electrolyte covers uniformly the electrode gap.

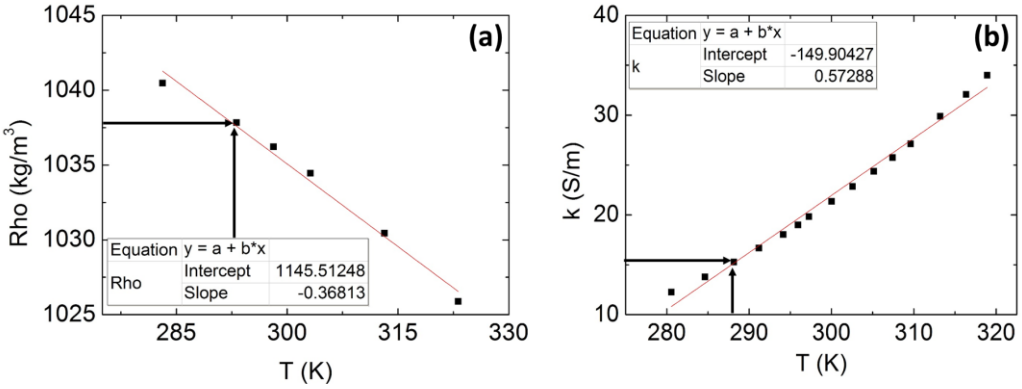


***Figure 2.1-4 Density (a) and conductivity (b) of NaCl in relation with the temperature*** [181], [182]***. Linear fitting (red line) and their corresponding equations are presented.***

***Table 2.1-1 Variables for the 2D ECM simulation***

| | Name | Value |
|---|---|---|
| $\eta$ | Current efficiency | 100 % |
| $M$ | Molar mass of the workpiece | 59.79 g/mol |
| $z$ | Valence of the workpiece | 2.7 |
| $\rho_a$ | Density of the workpiece | 8228 kg/m$^3$ |
| $F$ | Faraday's Constant | 96500 C/mol |
| $k_e$ | Conductivity of electrolyte | 16 S/m |
| $V_1$ | Voltage between electrodes | 10 V |
| $V_0$ | Constant overvoltage | 0 |
| $f$ | Tool feed rate | 0.0145 mm/s |

***Machining parameters***

The machining parameters were a constant $V_1$ applied between the electrodes, and $V_0$, also assumed constant during the whole simulation, at the workpiece surface. The lateral

boundaries were considered insulated, $nJ = 0$. The tool moved with a constant velocity, $f$, towards the workpiece, and the initial $y$, in the narrower part was maximum 0.5 mm. Table 2.1-1 present a summary of the variables applied to the ECM simulation model according to [17].

#### 2.1.4.4. Computer simulation

***Meshing***

FEM needs that the problem is divided in small elements, a process called meshing, and for the present work this was done with the mesh module of the FE package. The initial mesh generated usually cannot hold its original shape due to the distortion of the workpiece profile; therefore an adaptive mesh should be used. The adaptive mesh used for this problem was the remeshing technique, where a complete new mesh is created in each step. An advantage of using COMSOL Multiphysics® is that the program is able to automatically regenerate the mesh after it is deformed. This remeshing gives more accurate results, but it consumes more time and computational resources. Figure 2.1-5 display the meshed interelectrode gap (filled with electrolyte) where the modified mesh can be readily identified.

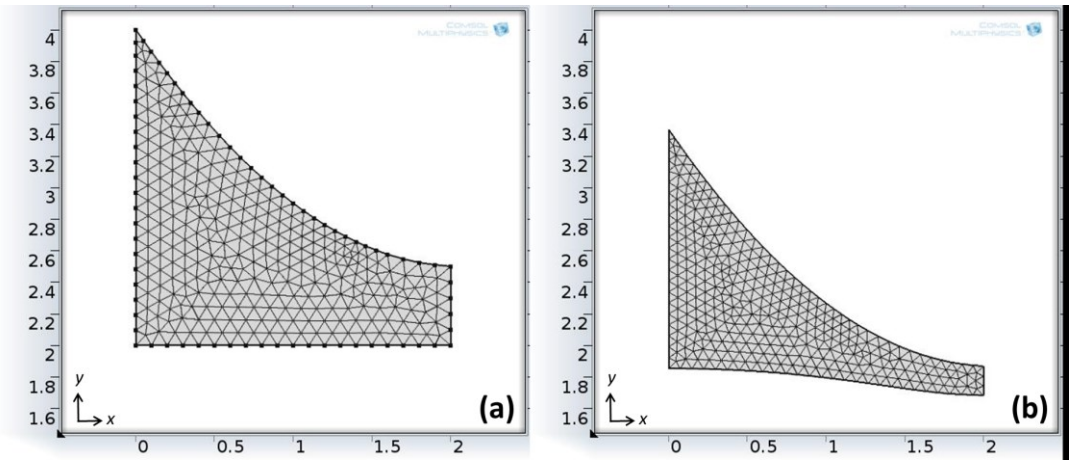


***Figure 2.1-5 Example of the adaptive mesh at (a) t = 0 s, and (b) t =60 s. using the automatic remeshing of COMSOL Multiphysics®.***

***Simulation time***

The length of the simulation was given by the machining time. Therefore an exit condition before the steady state is reached, $t$ = 60 s, was established for the present example.

#### 2.1.4.5. Analysis of results

To validate that the data of the simulation model developed were accurate, the simulation results were compared with previous work in ECM. Hardisty *et al.* [17] also applied FEM for the

time-dependent computational investigation of the ECM process, therefore his work was duplicated in the first part of the this work. Figure 2.1-3 presents the model setup for the present simulation. The parameters $V_1$ =10 V, $f$ = 0.0145 mm/s and $k$ = 16 S/m were applied, in agreement with Hardisty *et al*. work. The model had a length of 2 mm and the minimum $y$ between the tool and the workpiece was 0.5 mm. Figure 2.1-6 displays how the workpiece profile was changing with the time in an attempt of copying the shape of the tool.

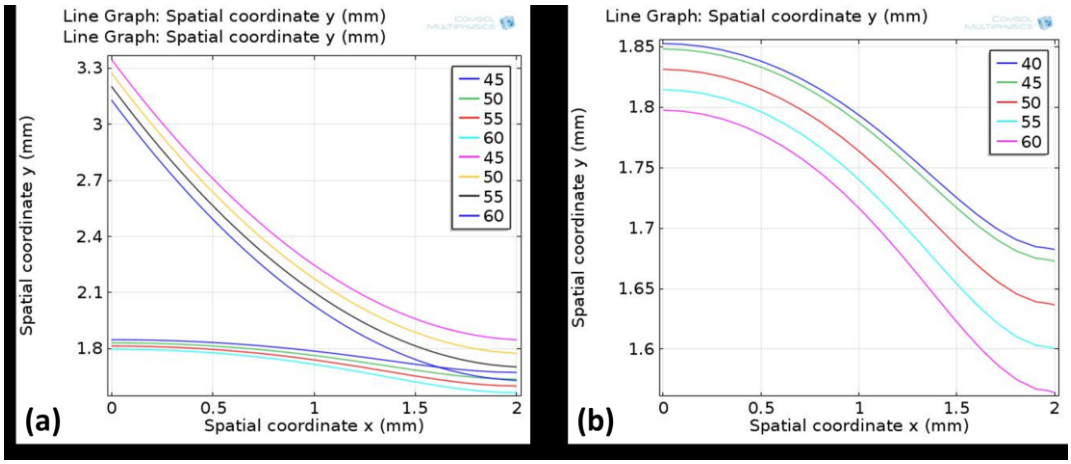


***Figure 2.1-6 Results of simulation using COMSOL Multiphysics, according to*** [17]***, from t = 45 s to t = 60 s. (a) Top set of lines (pink, yellow, black and blue) indicate the position of the tool. Bottom set of lines (blue, green, red and turquoise) indicate the workpiece profiles. (b) Close view of the workpiece profile.***

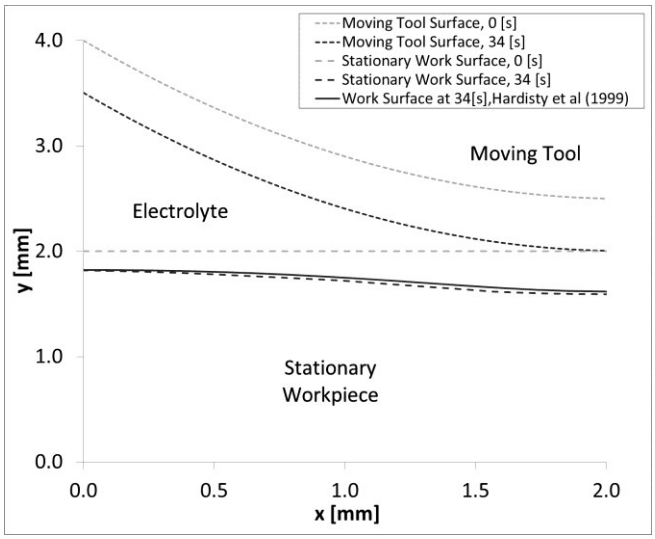


***Figure 2.1-7 Tool and stationary workpiece surface profiles at 0 and 34 [s], and in comparison with Hardisty et al.*** [17] ***profile. Top set of lines are the tool position, and bottom set of lines are the workpiece profiles. (- -) Simulation results. (–) Hardisty et al. profile at 34 s.***

Figure 2.1-7 shows a comparison between the simulation results and Hardisty *et al.* [17] work at $t$ = 0 s and $t$ 34 s. Although there was not an exact agreement between the results achieved with the model developed and the literature ones, the maximum difference was of 0.027 mm which is less than 7% of the maximum profile deformation. This disparity could be due to a different mesh used, the mesh element type selected or the assumptions made for some of the parameters used in the simulation model here.

At $t$ = 50 s, the simulation was stopped, the mesh was regenerated, and the process was then restarted up to 90 s. Ideally the mesh should be regenerated for each iteration, but this would compromise the computational capacity, hence it was decided that the simulation would run until 50 s before remeshing the gap

Figure 2.1-8 depicts the profile of the model at this time. The workpiece reproduces the tool profile at the right side of the system; however, the left side could not fully copy the profile. As explained before, the dissolution of material is inversely related to the interelectrode gap. As the initial geometry of the workpiece was a straight line; the right side of the workpiece was much closer to the tool than the left side, thus more dissolution was expected on the right side than on the left one. It can be observed that in the right bottom sides of Figure 2.1-8 there is a small peak in the geometry. A plausible explanation for this behaviour might be the isolated boundaries assumed for the model.

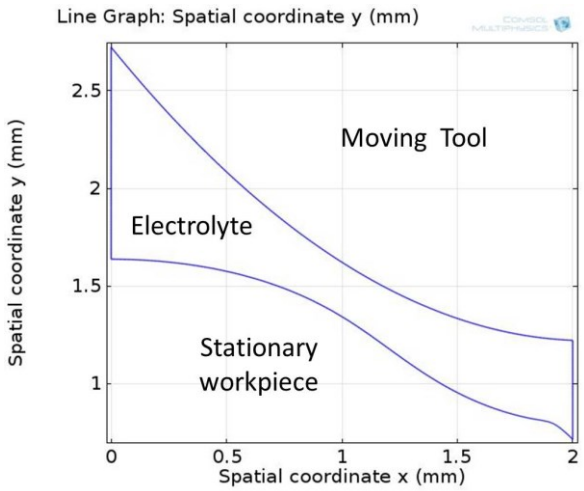


***Figure 2.1-8 Profile of the workpiece from Figure 2.1-7 at t=90 s. Top line is the tool profile and bottom line is the workpiece profile.***

The use of COMSOL Multiphysics® for the ECM simulation allows the monitoring of the process continuously before reaching steady state and the display of the final workpiece profile.

Additionally, the user is able to select the exit condition during the simulation: the selection of a maximum machining time. Despite of some of these data could not be verified with Hardisty *et al.* [17] work, this ECM simulation model can provide additional data from the process, such as current density, electric potential distribution and surface profiles, during and at the end of the simulation.

### 2.1.5. 2D ECM model: case 2

For the second case, the simulation model developed by Curry, D. [118] was duplicated. Curry*'s* work was selected for this purpose due to the availability of data, and in consequence, the feasibility of comparing and validating the simulation results with theoretical and experimental ones.

Curry developed a time-dependent simulation of the ECM process based on moving boundary finite element techniques and used MATLAB and FEMLAB FEA solver 3.0 to construct the simulation model. MATLAB was used for the ECM material removal calculations and geometry manipulation, and FEMLAB was applied for handling the meshing of geometries and solution of Laplace's equation. By the time when this work was developed, FEMLAB was not capable of automating moving boundary problems.

The model developed by Curry, D. comprised only the interelectrode gap, being the tool and the workpiece the top and bottom boundaries respectively, and connected laterally by two vertical lines, Figure 2.1-9. The simulation process was divided in three sections: preprocessing, processing, and post-processing. In the preprocessing step, the ECM parameters (workpiece, tool feed rate, starting gap, electrolyte conductivity, voltage and simulation time) and the geometry of the model were set. The geometry used in his model was developed in a CAD software and then imported to FEMLAB. The moving boundary, attached to the tool and the workpiece, was defined manually into the FEA package and this information was exported from FEMLAB to MATLAB.

In the processing step, the meshing and finite element method (FEM) was developed. An adaptive mesh was used, and the mesh and simulation results, such as voltage and current density, were stored to be then exported to MATLAB. In MATLAB, the material removal was calculated, and the movement of the moving boundaries could be determined. Using this information, a new geometry of the interelectrode gap was generated and imported back into FEMLAB in order to carry out a second iteration of the ECM process. The simulation stopped when the machining time was achieved or when the current density during ECM reached a stable state.

In the post-processing step, the data stored was analyzed and information about the ECM behavior was displayed. The information that could be extracted from this ECM simulation model contained: final geometry, current density and material removed.

As it can be observed, the ECM simulation developed by Curry, is still a long and iterative process. It requires manual manipulation of the data and the use and interaction of three different software, with their respective loss of information, *i.e.* accumulative errors, in each translation. To this extent, the work developed in this thesis is a continuation of Curry's work, in an attempt of building a more user friendly ECM simulation model, which additionally provides further information about the process, and deliver more accurate results.

#### 2.1.5.1. System analysis

Similar to what was done for the Hardisty *et al.*[17] model, the ECM system presented in Curry's work is simplified and only the interelectrode gap was modelled. A two-dimensional model of the system at $t$ =0 s was built using a CAD software, SolidEdge®. Figure 2.1-9 depicts this interelectrode gap model, where the upper and lower boundaries were the tool and the workpiece profile respectively. Electrical parameters, such as $V_1$ and $V_0$, were applied on the workpiece and tool surfaces. The lateral boundaries were considered insulated. And the tool moved down towards the workpiece surface, parallel to the $y$ axis and with steady $f$ .

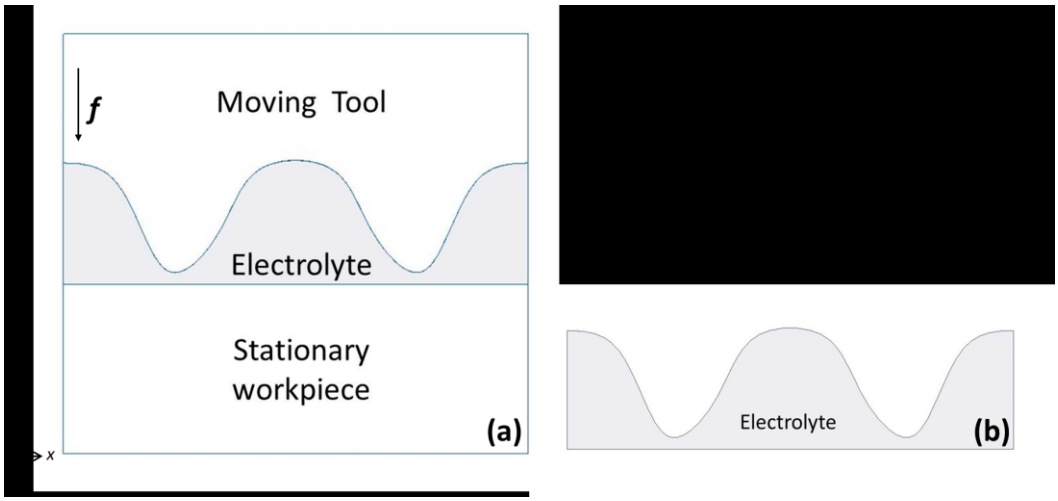


***Figure 2.1-9 CAD model used for the simulation of the ECM process in a 2D environment from [118]. (a) Complete system: tool, electrolyte, and workpiece. (b) Electrolyte geometry used for the ECM simulation.***

#### 2.1.5.2. Model generation

A CAD software, SolidEdge®, was used to develop the initial profile of the tool and workpiece. The tool was set as the upper boundary of the model and a flat horizontal profile was set as the workpiece and bottom boundary. A moving boundary was attached to the tool and the workpiece profiles, and these moving boundaries would reproduce the movement of the tool and the dissolution of the workpiece. The interelectrode initial profile can be observed in Figure

2.2-9 (b). The profile used for the tool in this simulation was based on a double cosine curve derived from the equation 2.1-9 and designed by *Alder et al.* [21]:

$$z = 5\cos\left(\frac{4\pi x}{40}\right) - 1.25\cos\left(\frac{8\pi x}{40}\right) \qquad \textbf{(2.1-9)}$$

#### 2.1.5.3. Model set up

A moving mesh for the simulation model was attached to the surface of the electrodes. The mesh attached to the surface of the cathode moved at a known velocity $f$, and the mesh attached to the anode moved according to the equations for the electrochemical dissolution of material, equation 2.1-6. The electrolyte properties were set in accordance to typical experimental data [17], [134]. The ECM boundary conditions and the main ECM parameters, i.e. workpiece material, machining parameters ($V_1$, $V_0$, and $f$) were provided. These values were set according to Curry, D. [134]: $V_1$ = 16 V, $V_0$ = 3 V, $f$ = 0.5 mm/min and $k$ = 16 S/m. The model had a length of 40 mm and the minimum gap between the tool and the workpiece was 1 mm. Figure 2.1-10 presents the boundary conditions used for the ECM simulation.

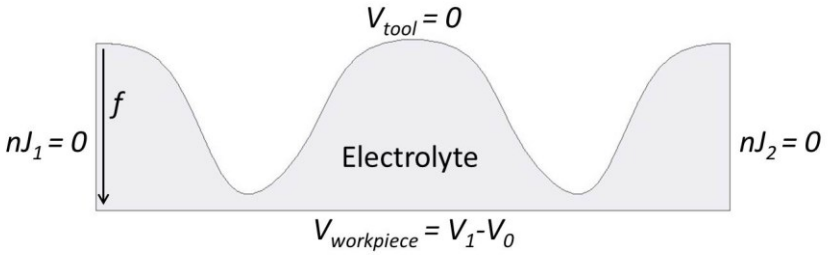


***Figure 2.1-10 Electrolyte model from*** [118] ***showing the boundary conditions used in the ECM simulation.***

Equations describing how the conductivity and the density of the electrolyte are affected by the temperature can also be considered, Figure 2.1-4 from [181], [182]. At this stage of the work however, the electrolyte was considered isothermal, uniform and static.

***Workpiece material***

A flat surface of Inconel 718 was selected for the simulation: $M$ = 59.79 g/mol; $z$ = 2.7; and $\rho_a$ = 8228 kg/m$^3$ [180].

***Machining parameters***

A constant $V_1$ was applied between the electrodes. $V_0$ was assumed to be constant during the simulation. The lateral boundaries were considered to be insulated $nJ = 0$. The tool moved with a constant $f$ towards the workpiece, and the initial $y$, in the narrower part, was 1 mm.

***Electrolyte***

The ECM process was considered to be performed using an electrolyte with a conductivity $k_e$ = 16 S/m. This is in agreement of using Sodium Chloride (NaCl) as electrolyte. In Figure 2.1-4 the properties of NaCl are given. No flow of the electrolyte was considered.

Table 2.1-2 present a summary of the variables applied to the ECM simulation model according to [118].

***Table 2.1-2 Variables for the ECM simulation***

| | Name | Value |
|---|---|---|
| $\eta$ | Current efficiency | 100 % |
| $M$ | Molar mass of the workpiece | 59.79 g/mol |
| $z$ | Valence of the workpiece | 2.7 |
| $\rho_a$ | Density of the workpiece | 8228 kg/m$^3$ |
| $F$ | Faraday's Constant | 96500 C/mol |
| $k_e$ | Conductivity of electrolyte | 16 S/m |
| $V_1$ | Voltage between electrodes | 16 V |
| $V_0$ | Overvoltage | 3 V |
| $f$ | Tool feed rate | 0.5 mm/s |

#### 2.1.5.4. Computer simulation

***Meshing***

The meshing was built with the mesh module of the FE package. The initial mesh generated usually cannot hold its original shape due to the distortion of the workpiece profile; therefore an adaptive mesh was used. The adaptive mesh used in this second case was the refinement technique, where the mesh density is increased locally in areas with high curvature or of special interest for the analysis by reducing the local element size. An advantage of using COMSOL Multiphysics® is that the program is able to automatically generate this mesh. This gives more accurate results, but also consumes more time and computational resources. Figure 2.1-11

displays the meshed interelectrode gap (filled with electrolyte) where the density and size of the elements can be readily identified to become denser with the curvature. A triangular mesh was used.

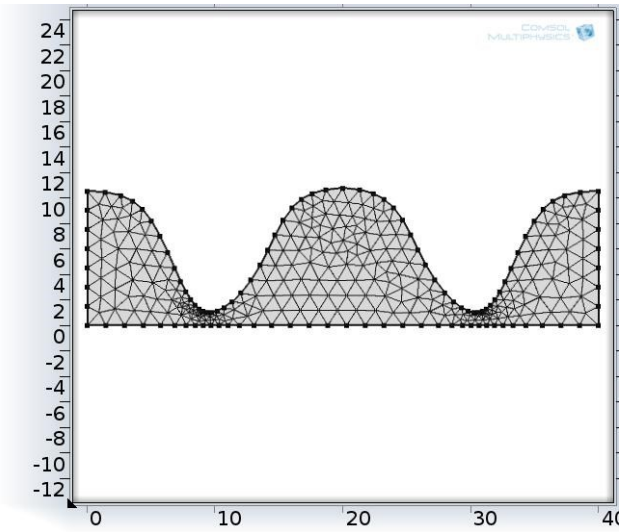


***Figure 2.1-11 Example of the adaptive mesh at (a) t = 0 s, using the automatic adaptive mesh of COMSOL Multiphysics®. Minimum element size 1.5x10$^{-4}$ mm and maximum element size 0.1 mm.***

***Simulation time***

The length of the simulation was given by the machining time. Therefore an exit condition before the equilibrium was reached, $t$ = 600 s, was established for the present example.

### 2.1.5.5. Analysis of results

The simulation results were then compared with Curry, D. [118] work. Figure 2.1-10 shows the model setup for this simulation. The parameters $V_1$ =16 V, $V_0$ = 3 V, $f$ = 0.5 mm/min and $k$ = 16 S/mm were applied accordingly with Curry's work. The model had a length of 40 mm and the minimum $y$ between the tool and the workpiece was 1 mm. The workpiece surface moved with time in an attempt of copying the shape of the tool. For this case, the simulation was stopped at $t$ = 600 [s]. The workpiece shape in some intermediate steps during the simulation and the final shape are presented in Figure 2.1-12. As mentioned before, one of the advantages of the model developed in this work is that values can be easily read at any point during the machining time.

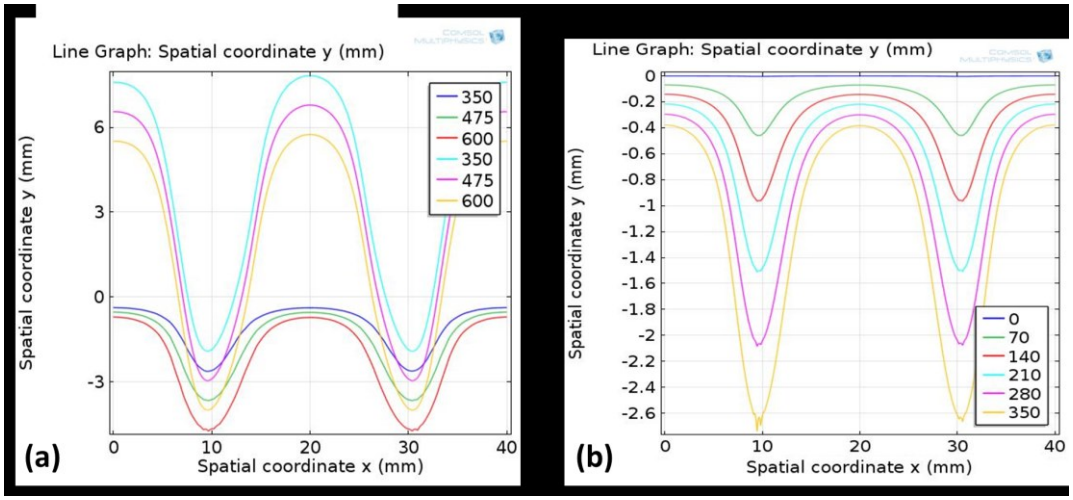


***Figure 2.1-12 Results of simulation using COMSOL Multiphysics®, according to*** [118]***. (a) Top set of lines (turquoise, pink, and yellow) are the profile of the tool from t = 350 s to t = 600 s. Bottom set of lines (blue, green, and red) are the workpiece profiles from t = 350 s to t = 600 s. (b) Close view of the workpiece profile from t = 0 s to t = 350 s.***

As in case 1, a comparison between the simulation results and Curry's ones was carried out at $t$ = 230 s and $t$ 480 s. Figure 2.1-13 shows this comparison. A good agreement can be observed between the results in the *y* axis, however in the *x* axis the curves tend to be wider than Curry's data. This behaviour is more evident at 480 s than at 230 s, so this discrepancy is assumed to be due to the lateral dissolution of the material which was not considered in Curry's work.

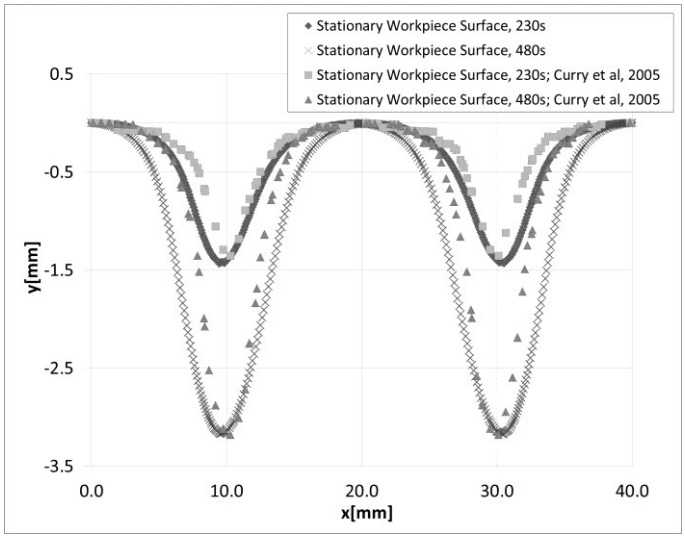


***Figure 2.1-13 Stationary workpiece profile at t = 230s and t = 480s. Values set to zero for an easier comparison. Simulation results (rhomboids and crosses), Curry's*** [118] ***results (squares and triangles).***

One of the main advantages of the simulation model developed here is that it can be used for extracting more accurate information from the ECM. Below some of the additional information extracted from the ECM simulation is presented The same working parameters used by Curry, *D.* [134] were applied. This information will help to understand better the process.

***Electric field,*** $E$

The electric field is generated by the electric charge that crosses the interelectrode gap. The electric field distribution during the ECM process gives an idea of how the dissolution of the material is going to behave. The dissolution will be higher in the sections where the interelectrode gap is smaller. This is because the path that the current has to cross is shorter, hence the resistance is smaller. Knowing that the electric field is inversely related to this distance, the electric field distribution will show shorter and more uniform lines in the areas where the current density is higher, small gaps, and longer and less uniform lines for larger gaps.

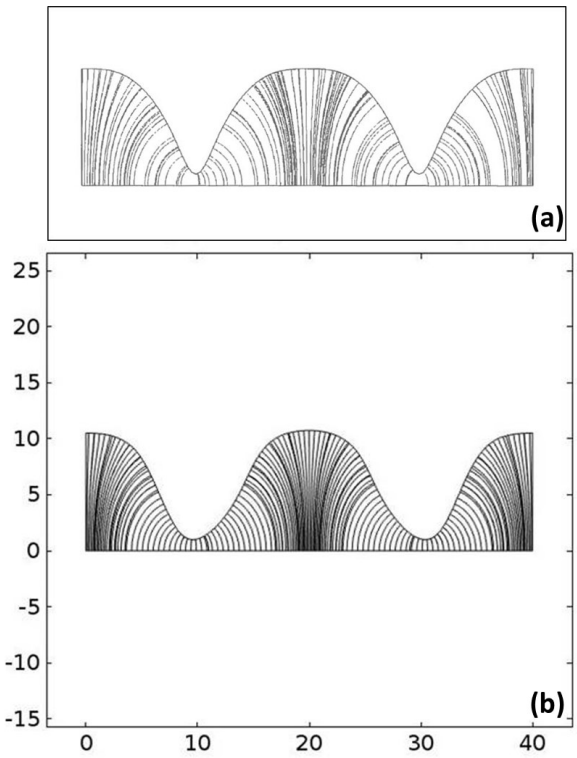


***Figure 2.1-14 Diagram illustrating the electric field using a stream-lined representation at t=0 s. Figure (a) taken from*** [118]***. (b) Simulation results using COMSOL Multiphysics, according to*** [118]***.***

The electric field lines within the interelectrode gap at $t$ = 0 s are presented in Figure 2.1-14 and are based on the solution of the Laplace field equation 2.1-5. A qualitative comparison

between Curry, D. [134] results and this thesis work can be observed in Figure 2.1-14, (a) and (b) respectively. The field distribution in both cases coincides, and agrees with the results expected. When the electric field lines are uniform along to the surface, the current density is considered to be constant.

Figure 2.1-15 presents the electric field at t=370 s. At equilibrium, the electric field should be the same in all points of the gap and the electric field lines parallel, hence the current density stable. This can be observed in the lower parts of the curve where the tool profile was correctly imprinted in the workpiece surface. However the electric field lines were deformed and concentrated on the centre and outside extremes of the profile, where the imprint was not accurate enough.

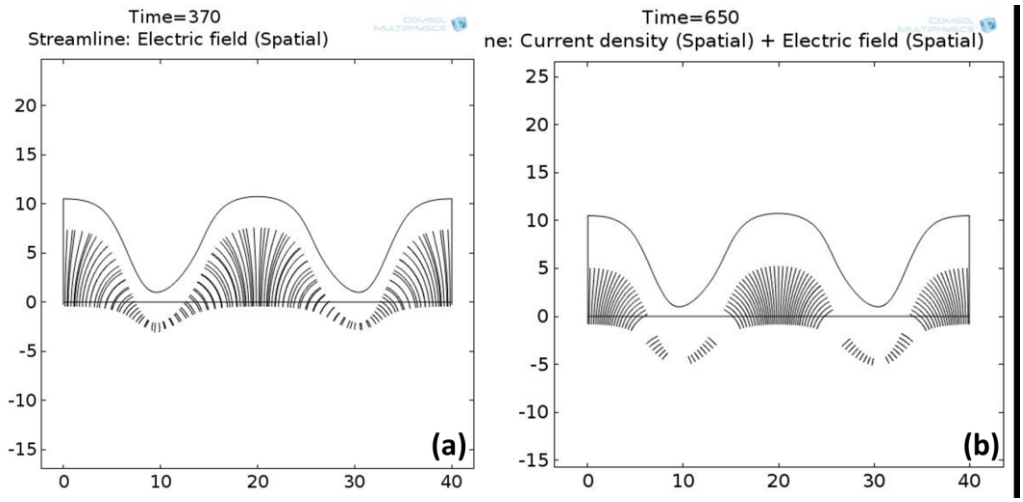


***Figure 2.1-15 Simulation results using COMSOL Multiphysics, according to*** [118]***. Electric field using a stream-lined representation, t=370 s and t=650 s.***

#### *Current density, $J$*

During the ECM process, current density, $J$, is highly related to the dissolution of the workpiece. High current density should be used for a high machining rate, however it should not be too high to produce excessive heat in the system, thus causing electrical breakdown. Figure 2.1-16 displays $J$ at the workpiece surface. The output has the form of a spline line where the maximum values are in the points where the tool and the work piece are closer to each other. COMSOL Multiphysics® allows plotting $J$ at different values during the process, it can be observed that $J$ changed with time and approached equilibrium at the end of the simulation, as expected from [27], [41]. From the results, it can be seen $J$ stabilized at 3.2x10$^5$ A/m$^2$, and 500 s. Figure 2.1-16 (b) shows the change in time of $J$ at the workpiece surface. It

can be observed that current density stabilises at 500 s. Afterwards, the current density goes beyond the equilibrium and increases until short circuit after 600 s.

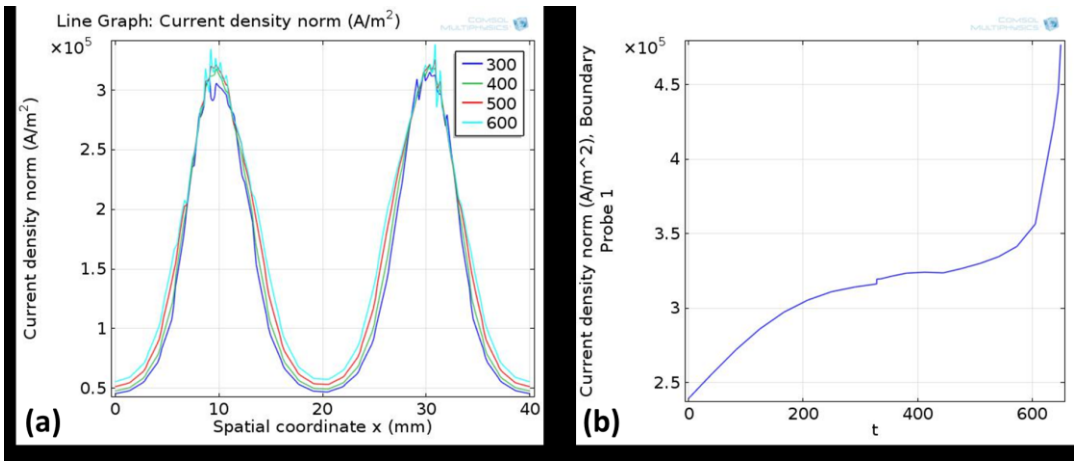


***Figure 2.1-16. Simulation results using COMSOL Multiphysics, according to*** [118]***. (a) Sample graph showing the spline function of the current density along the workpiece at 300, 400, 500 and 600 s. (b) Current density at the workpiece in relation with time.***

***Material removal,*** $m$

The material removed, $m$, from the workpiece surface by the ECM process can be calculated from equation 2.1-1. $m$ is dependent on the current density, the workpiece material characteristics and machined time. Figure 2.1-17 presents the material removed from the workpiece in mm. The effect of the material removal can be observed on the profile deformation of the moving boundary attached to the workpiece surface. See Figure 2.1-12 and Figure 2.1-13. As expected, there was a higher removal of material in the areas where the tool was closer to the workpiece.

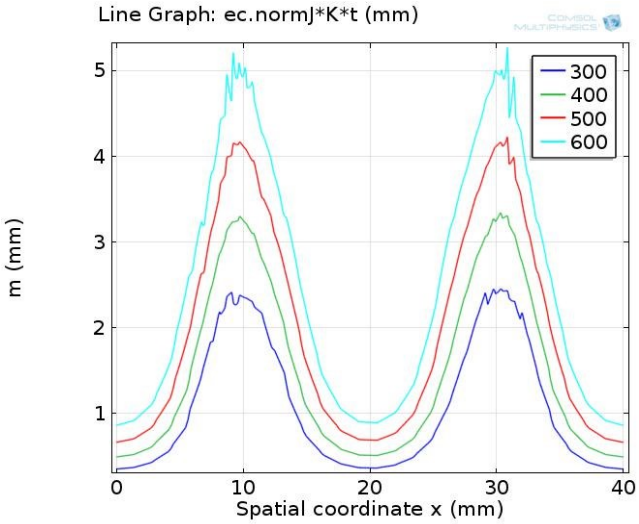


***Figure 2.1-17 Simulation results using COMSOL Multiphysics, according to*** [118]***. (a) Sample graph showing the material removed (in mm) from the workpiece at 300, 400, 500 and 600 s.***

Further analysis and experimental validation is still needed, however until now, the ECM simulation model in a 2D environment developed in this section agrees with theory and previous work. Hence this model is the first step to help the reduction in time and cost of ECM applied in industry.

### 2.1.6. Conclusions

The development of a 2D simulation model of ECM is the response for the need for understanding, controlling and predicting the process. An accurate simulation model will promote the use of ECM in the industry and extend its application. Various authors had developed 2D ECM simulation models before; however they were limited by the technology available at the moment when the studies were carried out. This thesis is a continuation of their work.

This section presents an enhanced simulation model for the simulation of the ECM process in a 2D environment. The use of COMSOL Multiphysics® for this computational model allows obtaining information at any time during the simulation of ECM, such as electric field, current density, electric potential distribution and the workpiece shape deformation. The results obtained in this section are in agreement with those available in the literature results from [17] and [134] used as benchmark to validate this ECM simulation model. Moreover, this methodology allows the accurate prediction of the workpiece final shape after the ECM process.

Additionally, this model provides an easier and convenient way to set up the parameters used in the ECM process. An accurate simulation of the ECM process will save time and resources for its application in the research and industry, and can offer a tool for its further study and development. The next step consists of applying an electrolyte in movement, experimental validation of the ECM simulation results, and developing a simulation of the ECM process in a three-dimensional (3D) environment.

## 2.2. *ECM on stainless steel 316 samples*

### 2.2.1. Introduction

In this section, experimental work applying electrochemical machining (ECM) on stainless steel 316 (SS316) samples is presented. This work was done using samples and machining information provided by pECM Systems Ltd® from Barnsley, UK. The interest of studying ECM on stainless steels (SS), characterised by its high corrosion resistance and multiple pharmaceutical and medical applications [176], resides on the fact that typically this process generates various different surface finish. Additionally, pECM Systems Ltd® required that the parameters affecting this surface finish were identified. The results of this work will be included in the development of a non-ideal simulation of the ECM process.

Some studies [26], [27], [41], [42] had been undertaken in order to understand the behaviour of ECM on SS, however the process is not fully understood yet. An electrochemically polished surface is usually associated with the random removal of atoms from the anode (workpiece), whose surface has become covered with a protective oxide film that prevents further corrosion [27]. This oxide film however, has low electrical conductivity and prevents the normal anodic dissolution; hence ECM cannot proceed without breakdown of the film. Partial breakdown of the oxide film often occurs, which causes pitting [43] or a non-uniform surface finish [41]. The objective of the present work was the achievement of a homogeneous breakdown of the oxide film, thus generating a uniform reflective and bright surface finish on the SS316 samples.

In the first part of this section, the experimental ECM set up and sample preparation is explained. ECM was applied on SS316 pipes of 1.5" diameter and 17 cm length varying the machining parameters such as voltage, interelectrode gap, inlet electrolyte temperature, and electrolyte flow rate. Each experiment lasted 10 s. The surface finish resulting from the ECM tests was not uniform across the samples, thus they were divided in four categories: passivated at the entrance – reflective and bright at the exit, reflective and bright, reflective and dark, and passivated. Afterwards, a revision of the ECM parameters applied on these tests was carried out in order to evaluate their influence, if any, on the resulting surface finish.

Results indicated that overvoltage, which is dependent on the interelectrode gap and the voltage applied, was one of the main parameters affecting the surface finish; additionally there was a strong relationship between the resulting surface finish and the electrolyte flow as expected from [27], [79]. The interelectrode gap and the inlet electrolyte temperature also affected the resulting surface finish but their influence was not so evident. Finally, the variation

in the electrolyte temperature during the process was found to have a great impact on the uniformity of the surface finish along the sample.

The results presented in this section could be used as a tool for tailoring the surface finish of a SS316 sample for specific applications, reducing manufacturing costs and duration of the ECM process. Moreover, this analysis and subsequent further development could be applied with other metal alloys and it is an important step towards the understanding of the ECM process.

### 2.2.2. Properties of Stainless Steel

Stainless Steels (SS) are iron-based alloys containing a minimum chromium content of 10.5% weight percentage (wt%) [114] and characterised mainly by their corrosion resistance, high strength and ductility. Other typical alloying elements are nickel, molybdenum, copper, titanium, silicon, manganese, niobium, aluminium, nitrogen and sulphur[1]. In the presence of oxygen (air), chromium induces the development of a chemical bond between the metal and the oxygen, forming a thin, hard adherent oxide film that protects the metal from corrosion (passivation). The oxide film has the ability to heal itself, meaning that no matter how much of the surface is removed, the steel is still corrosion resistant. The higher the carbon (C) content, the lower the corrosion resistance of the stainless steels. The reason is that carbon combines with the chromium and forms chromium carbides, which lower the passivity of the steel. The chromium carbides introduce a second phase in the metal which promotes galvanic corrosion [1].

Besides corrosion resistant, stainless steels are:

- aesthetic: they can be polished to a satin or mirror finish,
- more resistant to dry corrosion. Dry corrosion occurs at high temperatures and causes the steel to oxidise or scale up,
- ideal for food storage. There is no coating to break down contaminating the liquids or the food.

Stainless steels are generally categorised in terms of their chromium content [27]:

i. Austenitic steels (series 200 and 300), composed of chromium (Cr), nickel (Ni) and manganese (Mn) in iron (Fe). Excellent corrosion resistance and non-magnetic.
ii. Ferrous steels (series 400), with high chromium content, up to 27%. Magnetic and good corrosion resistance, but lower ductility.

iii. Martensitic steels (series 400 and 500), do not contain Ni and have Cr content up to 18%. Moderate corrosion resistance but high strength, hardness, and fatigue resistance.

iv. Precipitation-hardening (PH) steels, contain chromium and nickel (17% Cr, 4% Ni), along with copper, aluminium, titanium or molybdenum. Good corrosion resistance and ductility, and high strength at elevated temperatures.

v. Duplex structure steels, mixture of austenite and ferrite grades. Good strength and higher resistance to corrosion.

Typical SS applications are in the chemical, food-processing and oil industries, kitchen products, health care and surgical equipment, and automotive trim [1]. Additionally, SS are a growing market due to their application in architecture [183]. As an example, Figure 2.1-1 shows the different SS that should be used for the rebars accordingly with the chlorides concentration and pH in the building concrete in order to avoid corrosion.

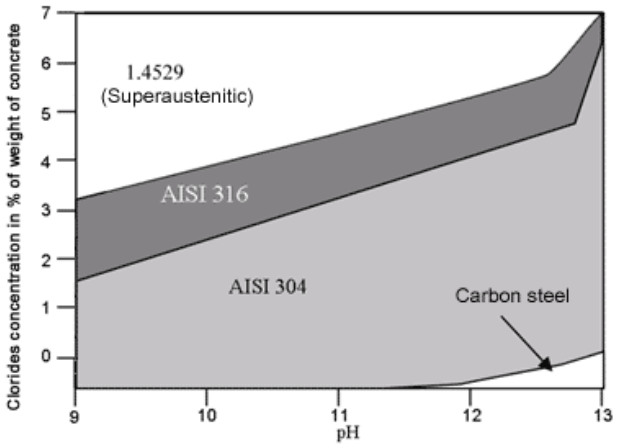


***Figure 2.2-1 Different steels that can be used safely in building depending on chlorides concentration and pH of the concrete. Image taken from*** [184]**.**

#### 2.2.2.1. The Passivated Oxide Film in Stainless Steel

From experimental work [27], [79], it is know that a solid surface film forms on the SS substrate surface during high rate anodic dissolution, i.e. during ECM. The schematic of SS passivation mechanism is depicted in Figure 2.2-2. Some studies have been done to address the structure of this oxide film [27], [79], [185], however not much is known about it and the complex mechanism of its dissolution. Moreover there are even contradictory theories about this metal passivity [185]. The adhesion of this surface film depends on the type of the electrolyte used for ECM. The use of NaCl as electrolyte leads to a surface film of loosely bound particles which can be easy removed from the metal surface. When $NaNO_3$ is used as electrolyte, the film is strongly

attached to the surface [79]. Studies ex-situ for the first case and in-situ for the second one demonstrated that the film is formed mainly by Fe, Cr and C, suggesting that the film originates from the chromium carbides in the steel matrix. The $NaNO_3$ samples showed less concentration of Cr than the NaCl samples [186]. The oxide films on SS are generally considered to have duplex character, an inner rich Cr region and an outer rich Fe region. The Cr in the inner region maintains the passivity of SS. Passivity refers to the lack of reaction of the underlying metal with the atmosphere. If the oxide film is damaged, the Cr will repassivate the metal [114] as illustrated in Figure 2.2-2.

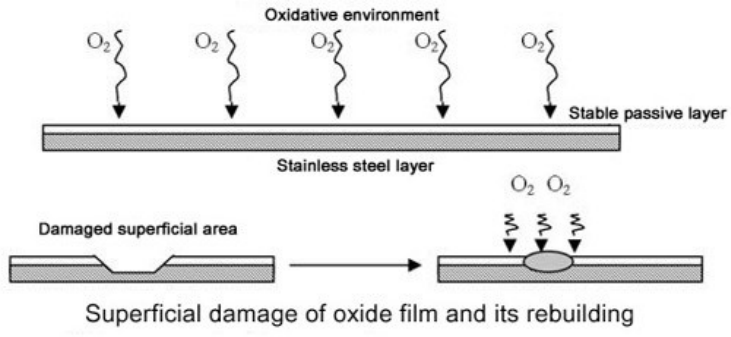


***Figure 2.2-2 Schematic illustrating stainless steel passivation mechanism. Image taken from*** [184]**.**

### 2.2.3. Experimental set up

#### 2.2.3.1. Electrochemical machining (ECM) system setup

Figure 2.2-3 shows the ECM array consisting of a cylindrical solid tool and a SS316 pipe provided by pECM Systems Ltd® (workpiece) placed vertically and concentric to each other on the bedplate of the ECM machine. ECM was applied on the internal face of the pipe, hence the tool is left without insulation so the machining takes places along the full length of the pipe. The tool was held by the machine head and the workpiece was fixed to the bedplate by a non-conductive vise. Both, tool and pipe were connected to a DC power supply by conductive clamps. The electrolyte was pumped into the system and flows from the top and between the pipe and the tool. The system was positioned in such a fashion that the electrolyte could exit the array and be collected in the electrolyte reservoir.

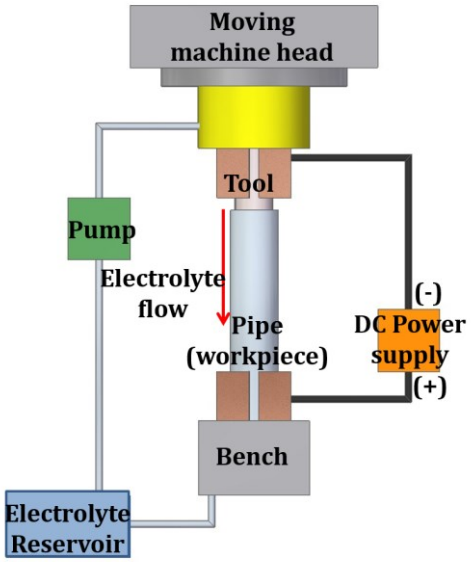


***Figure 2.2-3 Electrochemical machine setup diagram (SolidEdge®).***

#### 2.2.3.2. Sample preparation

The pipes machined were commercial stainless steel 316 (SS316) pipes of 17 cm length and 3.81 cm diameter, which were manufactured by rolling and welding. ECM was applied to the internal face of the pipes, which surface finish prior to processing was dark, opaque and uniform along the pipe. The welding process left behind a weld-flash along the interior face of the pipe. The exterior of the pipe was not treated.

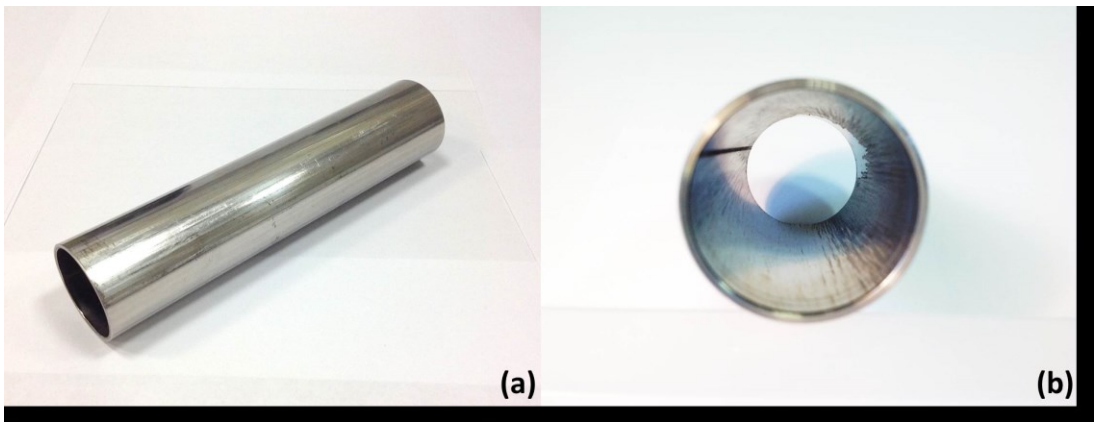


***Figure 2.2-4 Commercial SS316 pipes machined by ECM. (a) SS316 pipe. (b) Internal face view of the SS316 pipe after ECM. The weld-flash is visible on the left side, and flow marks are evident on the right side of the pipe.***

Upon running the ECM process, some parameters were provided. The main parameters to consider were the workpiece material specifications and the electrolyte characteristics. Table 2.2-1 presents the parameters considered for this ECM tests.

***Table 2.2-1 Parameters established for ECM on SS316 pipes.***

| | Name | Value |
|---|---|---|
| $M$ | Molar mass of the workpiece | 56.2 g/mol |
| $z$ | Valence of the workpiece | 3.6 |
| $\rho_a$ | Density of the workpiece | 7870 kg/m$^3$ |
| $F$ | Faraday's Constant | 96500 C/mol |
| | Electrolyte type | $NaNO_3$ |

#### 2.2.3.3. Electrolyte

The primary function of the electrolyte in the ECM process is to provide ions to carry electric current within the interelectrode gap. Therefore, the electrolyte should be able to initiate and sustain the dissolution at the anode; keeping the simultaneous cathodic deposition of metal as low as possible [49]. The ECM reactions induce progressive change in the electrolyte along the flow path length, such as temperature change, flow variation, and hydrogen bubble generation [134]. This typically causes changes in the related properties and hence in the ECM process along the flow path [27].

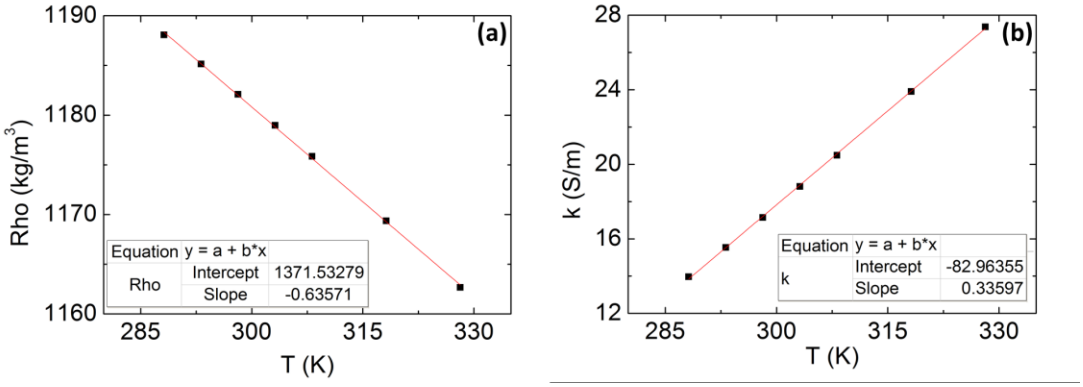


***Figure 2.2-5 Density (a) and conductivity (b) of $NaNO_3$ in relation with the temperature*** [177] ***at 22% mass percent. Fitting line (red line) and equation describing the density and behaviour are presented.***

For this work, ECM was performed using $NaNO_3$ as electrolyte. Figure 2.2-5 presents the density, $\rho_e$, and conductivity, $k_e$, of $NaNO_3$ in relation with the temperature [16]. This

information is needed in order to parametrise the electrolyte behaviour under the changes in temperature during ECM. This parametrisation will be included in the 3D simulation model developed in section 2.3.

Additionally, the electrolyte flow has two more functions: it sweeps away the metal ions (ECM products) dissolved from the anode before they can reach the cathode, and simultaneously controls the temperature of the system. Therefore a high electrolyte flow is needed to be pumped through the interelectrode gap in order to prevent boiling by Joule heating and to effectively flush away the products of the electrode reactions. These products may be solutions, gas (bubbles) or solids [187], which accumulated can result in sparking between the electrodes or between the electrodes and the dissolution products.

#### 2.2.3.4. ECM Tool

The tool was a solid cylinder of SS with the same length as the workpiece, and diameter as that of the interior diameter of the pipe (workpiece) but undersized radially by 2, 4 or 8 mm. The tool was static, i.e. $f = 0$ m/s.

### 2.2.4. Machining parameters

ECM input machining parameters are the parameters that the user could vary for each test, these machining parameters were: interelectrode gap, $y$, voltage, $V_1$, electrolyte flow rate, $Q$, and electrolyte inlet temperature, $T_e$. The dimensions of the tool give the size of the interelectrode gap. Electrical clips were connected to the array providing DC current under a constant voltage of 18, 24 and 36 V (possible voltage losses in the system were not considered). The electrolyte used was Sodium Nitrate ($NaNO_3$) with specific gravity (S.G.) of 1.15. Figure 2.2-5 shows the density and the conductivity of the electrolyte as a function of the temperature. Electrolyte flow rate was set at 10, 25, 40 and 60 l/min. The electrochemical cell was configured in a way to recirculate the electrolyte. The inlet electrolyte temperature was considered constant; however the machining was developed in two different days, so the ambient temperature changed, thus the electrolyte inlet temperature, $T_e$, from 7 to 15.3 °C. The electric current during the process was measured and recorded using the accompanying data acquisition software, provided by pEMC systems Ltd®. Each test lasted 10 seconds. Table 2.2-2 presents a summary of the variables used in the ECM process.

***Table 2.2-2 Variables used for ECM on SS316 experimental tests.***

| | Name | Value |
|---|---|---|
| $y$ | Interelectrode gap | 2, 4, 8 mm |
| $V_1$ | Voltage | 18, 24, 36 V |
| $Q$ | Electrolyte flow rate | 10, 25, 40, 60 l/min |
| $T_e$ | Inlet electrolyte temperature | 7, 15.3 °C |

### 2.2.5. Results and discussion

The surface finish of the samples results from the specular or non-specular reflection of light from the crystal faces electrochemically dissolved at different rates during the ECM process [13]. An electrochemically polished surface is usually associated with the random removal of atoms from the anode (workpiece). The chromium in SS induces the formation of a protective film of oxide on the material surface [27]. This protective film needs to be broken by the ECM process in order to dissolve the material. A partial breakdown of this film is a common problem during ECM and results in non-uniform surface finish of the workpiece [26], [41], [43].

***Table 2.2-3 Surface finish classification of the SS316 pipes machined by ECM.***

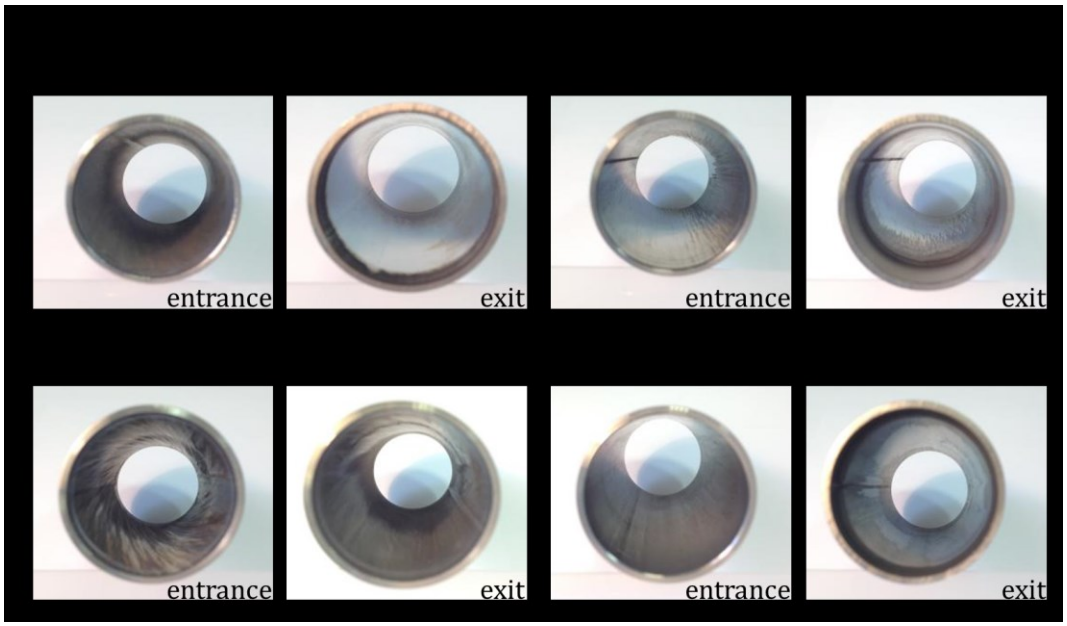


Table 2.2-3 summarises the resulting surface finish qualities of the SS samples after ECM. The samples were divided in four categories according to their surface finish quality: passivated entrance – reflective and bright exit, reflective and bright, reflective and dark, and passivated.

***Table 2.2-4 Images of the SS326 samples using optical microscopy with magnification 20x, 50x and 100x, on the first, second and third row respectively.***

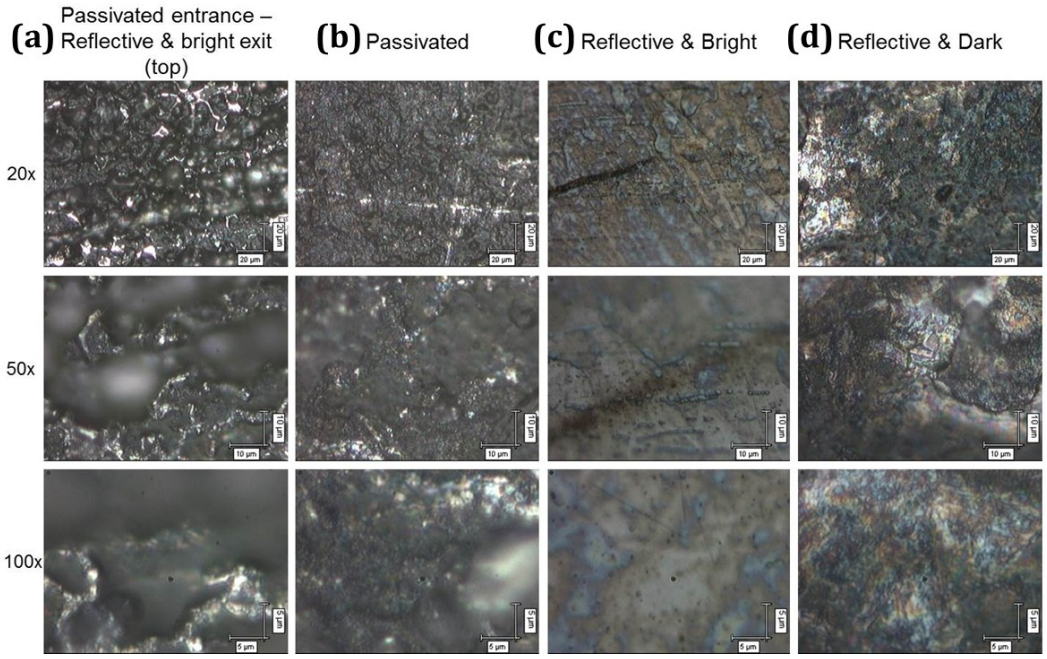


**Passivated entrance – reflective and bright exit**

Table 2.2-3(a) presents a typical sample with a passivated surface finish at the entrance and a reflective and bright surface finish at the exit. An average roughness in the top part of the sample (passivated entrance) of 2.303 μm was measured with a profilometer Mitutoyo® and this high roughness is evident in the images of Table 2.2-4(a), being the black sections the oxide film, and the small white sections the metal matrix. The out-of-focus patches are result of heterogeneous heights of the film.

Globules can be observed in the images of Table 2.2-4(a) and previous work [186] had demonstrated that the globules are ferrous oxide complexes. Moreover Sazou, 2009 [188] observed that this surface finish is achieved when the time of machining in relation with the machining parameters is not enough to strip away the oxide film from the metal surface. The machining time in the tests carried out for this thesis lasted 10 s, hence this is a plausible explanation for the resulting surface finish.

A small ring of passivated surface at the exit of the pipe is visible; this passivation is due to the accumulation of the electrolyte in this area forming a small pool before it can exit the array. The weld-flash is also visible but just at the entrance of the pipe.

**Passivated**

Table 2.2-3(b) shows a typical sample with passivated surface finish. Average roughness of 540nm was measured with a profilometer Mitutoyo®. The microscope images of the samples are presented in Table 2.2-4(b). An almost uniform dark oxide film covering the metal surface was observed with only small sections of the matrix visible in white.

The film layer present in this samples was easily loose, and previous studies [186], [188] found that this film is formed mainly by iron, chromium and carbon. However, it has not been possible to precisely characterise the composition and structure of the solid dissolution products. Some studies [113] suggest that in this film the carbon content is high and by accumulating it on the surface, the metal is difficult to oxidise and therefore difficult to be machined electrochemically. The non-uniformity in height of the film is still evident by the out-of-focus sections at of the images; this difference however is smaller than the exhibited by the passivated entrance – reflective and bright exit samples, Table 2.2-4(a).

The sample presented in Table 2.2-3(b) exhibits evident flow marks. This was characteristic of the 8 mm gap, and this behaviour of the electrolyte flow in an annulus system has been observed before in fluid dynamics studies [189].

**Reflective and Bright**

A typical reflective and bright sample is presented in Table 2.2-3(c). The microscope images of these samples are showed in Table 2.2-4(c). An average roughness of 116 nm was measured with a profilometer Mitutoyo® and 265 nm with an optoelectronic microscope ZYGO®. These values are higher than the expected for a reflective and bright electrochemical machined surface; this variation however is believed to be due to the curvature of the samples, which made difficult the roughness measurement.

The microscopy images reveals a uniform surface, covered by an oxide film. Wagner, 2002 [186] found that this is a carbide-rich film and it is characteristic of ECM with $NaNO_3$. The enrichment of carbide particles indicates that the passivated film does not allow a preferential removal of carbides. This randomness in the dissolution of the material surface leads to the mirror-type surface [13].

A small ring of passivated surface at the exit of the pipe is visible similarly to the passivated entrance - reflective and bright exit samples; this passivation is also due to the accumulation of the electrolyte in this area forming a small pool before it can exit the array. The weld-flash is visible as well in all the length of the pipe, and some flow marks can also be observed.

**Reflective and Dark**

A typical example of the samples with reflective and dark surface finish is presented in Table 2.2-3(d). Average roughness of 308 nm was measured with a profilometer Mitutoyo® and 426 nm using the optoelectronic microscope ZYGO®. Similar to the results obtained for the Reflective and Bright samples, this roughness is higher than the expected due to the curvature of the samples.

In Table 2.2-4(d) typical optical microscopy images of these reflective and dark samples are presented. A non-uniform oxide film can be observed where fragments of the oxide film are clearly defined. This film is firmly attached to the surface metal due to the use of $NaNO_3$ as electrolyte, as demonstrated in previous work [186]. This oxide film was studied in-situ by Wagner, *et al*. [186], who found that the film, formed by carbides and oxides, hinders the $Fe^{n+}$ diffusion. Sazou, 2002 [188] found a sudden increase of the electric potential in the areas where the oxide film is present, leading to local areas being dissolved to a different grade.

The same small ring of passivated surface at the exit of the pipe is visible at the exit of the samples, and the weld-flash is barely visible in all the length of the pipe. No flow marks can be observed.

Visual similarity between the passivated surface (Table 2.2-4(b)) and the reflective and dark surface (Table 2.2-4(d)) can be observed; this is due to the presence of the oxide film in both cases with the difference that in the first case this film is loose and in the second, the film is firmly attached to the surface of the metal.

In order to understand the behaviour of ECM on the SS316 samples, some ECM parameters, such as current density, $J$, overpotential, $V_0$, and temperature difference, $\delta T$, were compared among the samples. These parameters are in turn dependent on the controlled input parameters (voltage, gap, electrolyte inlet temperature, and electrolyte flow rate). The aim is to identify their influence, if any, on the resulting surface finish of the sample. By properly adjusting the process parameters, the achievement of a reflective and bright surface finish is expected.

#### 2.2.5.1. Overpotential, $V_0$

Metal dissolution in ECM is accomplished by the application of an external potential difference between the electrodes. The potential needed to ensure a continuous discharge of metal ions between the electrode and the electrolyte is known as overpotential, $V_0$. This notion is widely

applied to the qualitative characteristic of the electrode electrochemical activity, namely low overpotential means high activity, and high overpotential means low activity (assuming that the process is developed in a fixed current density and solution composition) [161]. The results of this work also prove the importance of $V_0$ in the resulting surface finish of the SS316 samples. Previous work [26], [41] found that a bright and reflective surface finish is achieved when $V_0$ is in the range of 9.7 and 12.4 V. Results from this work provided a wider range of 9.1 – 15.0 V. See Figure 2.2-6.

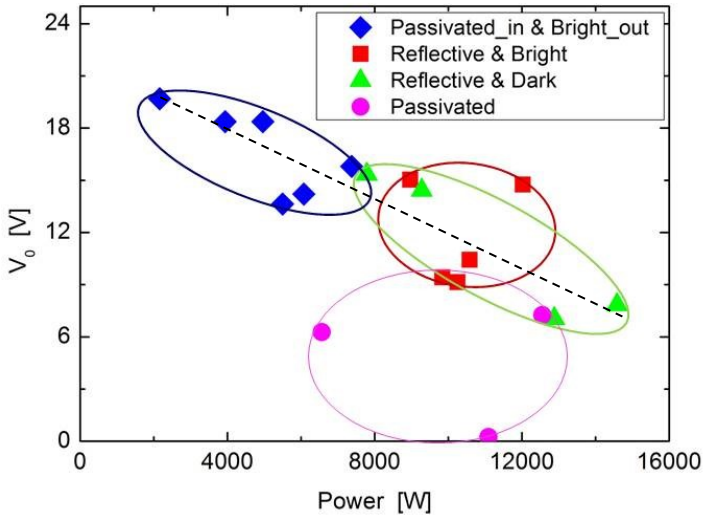


***Figure 2.2-6 Power, $P$, and overpotential, $V_0$, in relation with the surface finish: passivated entrance – reflective and bright exit (blue rhomboids), reflective and bright (red squares), reflective and dark (green triangles), and passivated (pink circles).***

The relationship between the power (function of the voltage and current applied) and the overpotential during the ECM process is presented in Figure 2.2-6. As mentioned in [118], the power applied to the system was inversely related to the overpotential at the workpiece. Samples that present a more uniform reflective surface finish (squares and triangles in Figure 2.2-6) are obtained when the power was over 7KW and the overpotential was limited between 7 and 15 V. In the samples with a variable surface finish (rhomboids), passivated surface at the entrance and a reflective and bright surface at the exit, the overpotential was over 14 V and the power is below 7 KW. This is consistent with previous work [27] where these areas of different surface finish were related to a variation of the dissolution valence of SS316. Under the same machining conditions, this variation in valence is reflected on the overpotential during the ECM process. Hence, low valence is related to a higher voltage needed to drive the workpiece

dissolution reaction and a rise of $V_0$ [27]. If the voltage applied is not enough for maintaining a steady ion migration through the oxide film, a non-uniform surface finish is attained. When the overpotential was below 7 V, the surface finish was passivated (circles in Figure 2.2-6). In these cases the potential between the electrodes is too high, so even though the oxide film was broken, the metal dissolution was uncontrolled [73].

#### 2.2.5.2. Current density, $J$

Current density can be explained simply as the quantity of electric current that flows on a unit of area during ECM. McGeough in 2005 [13] noted that when the current density $J$ was raised, the surface finish on the workpiece becomes smoother. Lozano-Morales in 2009 [43] found the same behaviour when ECM was applied on samples of niobium.

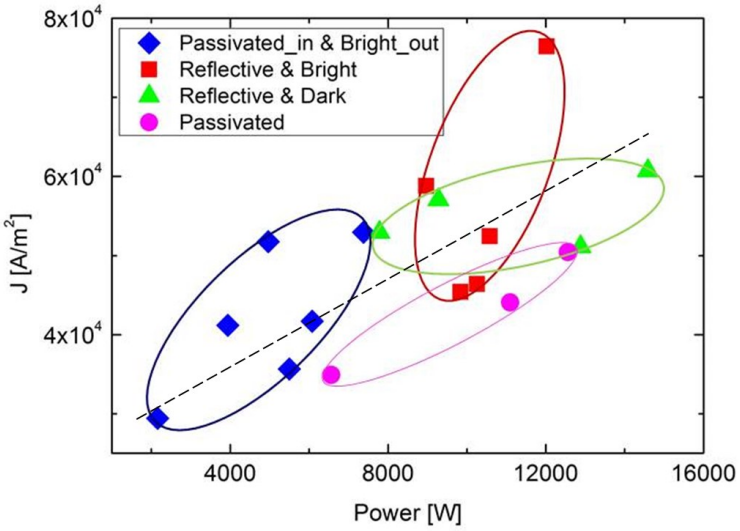


***Figure 2.2-7 Current density, $J$, and Power, $P$, in relation with the surface finish: passivated entrance – reflective and bright exit (blue rhomboids), reflective and bright (red squares), reflective and dark (green triangles), and passivated (pink circles).***

Figure 2.2-7 presents the influence of $J$ on the resulting surface finish. For $J$ over 4.5 A/cm$^2$, and $P$ over 7 KW a reflective surface was achieved (squares and triangles in Figure 2.2-7). However, when the current density or the power during ECM dropped below those values, there was not enough energy to break uniformly the oxide film, hence a passivated or non-uniform surface finish was obtained. Moreover, there is a relationship between the overvoltage and the current density. $V_0$ can be used to prove changes in the electrochemical reaction at the electrode surface [114] and this will affect the surface finish of the sample. Figure 2.2-8

presents this relationship. It can be observed that if $V_0$ increases, more energy is needed to drive the reactions at the sample surface. If this energy is not enough to maintain a stable migration of ions from the workpiece, a non-uniform surface finish is attained (blue rhomboids in Figure 2.2-8).

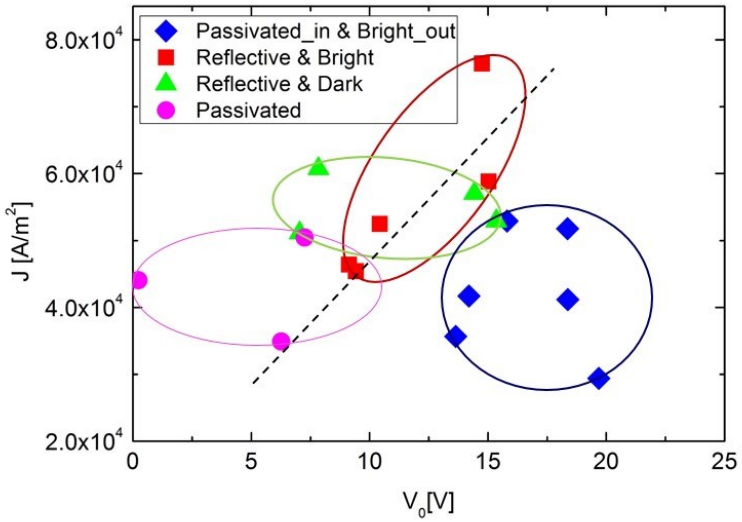


***Figure 2.2-8 Current density, $J$, and overpotential, $V_0$, in relation with the surface finish: passivated entrance – reflective and bright exit (blue rhomboids), reflective and bright (red squares), reflective and dark (green triangles), and passivated (pink circles).***

In practice, not all the current density is used for the removal of material, which can affect the results presented here. Metal dissolution due to high valence or side reactions, such as oxide precipitation, may exist and affect the current density efficiency. Moreover, the electrolyte conductivity plays a crucial role in $J$. Furthermore $k_e$, in turn, is dependent on the temperature, electrolyte flow rate, electrolyte concentration, etc. [94], thus affecting the overall outcome.

#### 2.2.5.3. Electrolyte flow rate, $Q$

The role of the electrolyte flow rate is twofold: it flushes away the metal ions (ECM products) dissolved from the anode before they can reach the cathode and, at the same time, it mitigates the temperature increase of the system. The accumulation of the machining products could lead to a shortcut of the system, and the increase of the temperature affects the conductivity of the electrolyte [13]. Similar to the power supply, there is an impact of the flow rate in the overpotential during the process and it is presented in Figure 2.2-9.

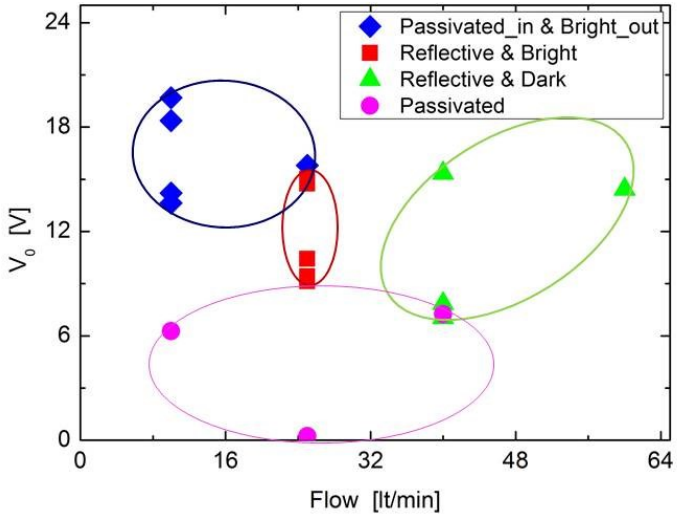


***Figure 2.2-9 Electrolyte flow rate, $Q$, and overpotential, $V_0$, in relation with the surface finish: passivated entrance – reflective and bright exit (blue rhomboids), reflective and bright (red squares), reflective and dark (green triangles), and passivated (pink circles).***

Figure 2.2-9 demonstrates the influence of the electrolyte flow rate on the surface finish. Low flow rates (<20 l/min) resulted in a passivated or a non-uniform surface finish along the sample. This might be due to the fact that the ECM products, e.g. sludge or bubbles, and the heat generated during the ECM process were not well dissipated. Usually the change in temperature results in a change in the conductivity of the electrolyte, thus affecting the resulting surface finish. McGeough [13] stated that the surface was smoother when the electrolyte velocity was increased, however if the flow rate was too high (>40 l/min) the process resulted in a dark surface (triangles in Figure 2.2-9). From previous work [79], it is known that this dark surface is a film consisting mainly of Fe, C and small traces of Cr. This film is strongly attached to the workpiece surface and limits the current efficiency [60] during ECM. Results show that the flow rate which was associated with a reflective and bright surface finish was approximately 25 l/min (squares in Figure 2.2-9).

Wagner, T. [186] in 2002 gave a plausible explanation for the effect of the electrolyte flow rate on the surface finish. A very thin and compact film is assumed to exist on the SS substrate before ECM. During ECM, the electric current breaks this film, and local electrolyte flow turbulence will ideally remove the surface film particles (oxides, chromium carbides and reaction products). If the turbulence in the electrolyte flow cannot remove the oxide-film lose particles, $Fe^{n+}$-diffusion through this surface layer is possible and the current density efficiency

decreases drastically. Hence, in order to break the film, higher current density is needed. Figure 2.2-10 illustrates this mechanism.

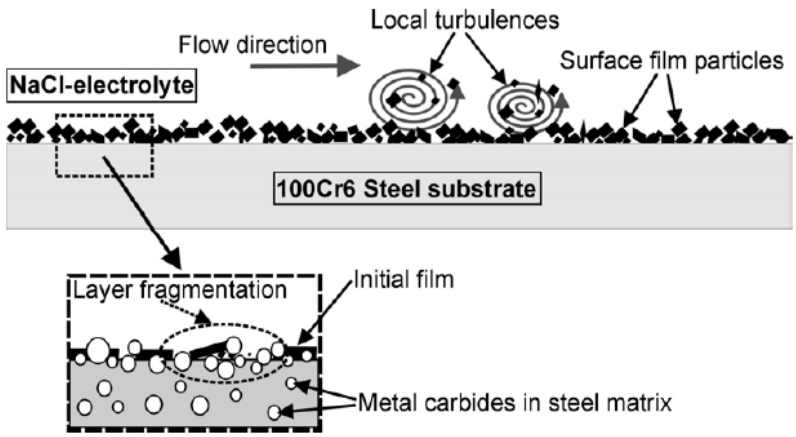


***Figure 2.2-10 Basic principle of anodic metal dissolution using NaCl-electrolytes on 100Cr6 steel. The surface film (black) lose particles can be removed by local turbulences in the flowing electrolyte. Image taken from*** [186]***.***

It is important to highlight that high flow rate also favours removal of metal and nitrate ions from the electrode surface, inhibiting metal nitrate ions precipitation and promoting barrier oxide formation (re-passivation). On the other hand, low flow rates favours metal nitrate ions precipitation and pitting grow [41]. Furthermore it would be worth to consider the duration of the ECM process; Mileham, 1982 [190] and Mount, 2001 [26] found that at short times (<50s) and high electrolyte flow, a progressive growth of the dull, pitted surface occurred and spread upstream from the downstream end of the workpiece; this is in agreement with the findings of this work.

#### 2.2.5.4. Interelectrode gap, $y$

The space between the electrodes, into where the electrolyte flows, is named interelectrode gap, and was demonstrated to be another important parameter determining the resulting surface finish of the sample. Results show that a big gap (≈8 mm) usually was associated with a passivated surface finish. This is due to the fact that the interelectrode gap is related inversely to the current density of the ECM process [2]; when $J$ was reduced, i.e. by increasing the gap, there was not enough energy during the process to break the oxide film uniformly [2]. Figure 2.2-11 shows the relationship between the surface finish, the electrolyte flow and interelectrode gap. From fluid dynamics, it is known that the velocity of the flow increases when the interelectrode gap is smaller. It is important to note that when this electrolyte velocity is too low, the resulting surface finish is non-uniform (blue rhomboids in Figure

2.2-11), making evident that the current density was not enough to maintain an steady ion migration through the oxide film and that the turbulence in the fluid flow was not enough for flushing away the ECM products.

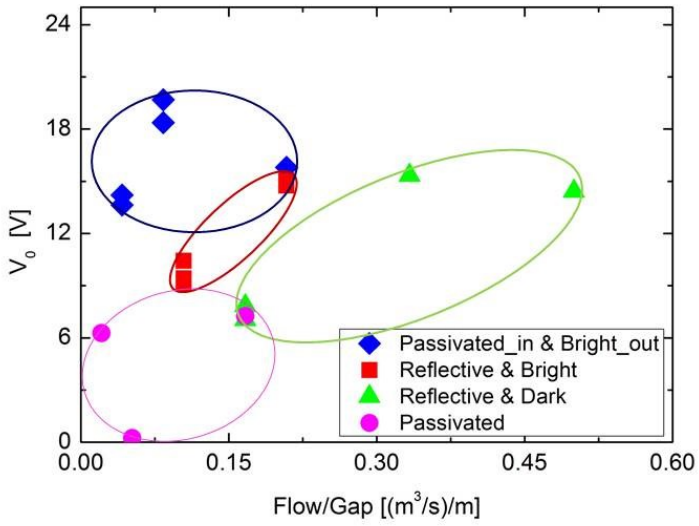


***Figure 2.2-11 Electrolyte flow rate, $Q$, inter electrode gap, $y$, and overpotential, $V_0$, in relation with the surface finish: passivated entrance – reflective and bright exit (blue rhomboids), reflective and bright (red squares), reflective and dark (green triangles), and passivated (pink circles).***

#### 2.2.5.5. Temperature difference, $\delta T$

Deconinck in 2010 [10] established how the electrochemical reactions rates depend strongly on the electrolyte temperature, which in turn depends on the electrolyte flow rate, interelectrode gap and potential applied. Moreover it is known that the electric conductivity is directly related to the temperature of the electrolyte [9], [20]. When the conductivity varies, the electrochemical reactions during ECM are affected, thus changing the resulting surface finish on the sample.

Experimental tests did not reveal a clear effect of the electrolyte inlet temperature, $T_e$, on the resulting surface finish; however some samples were found to have two different surface finish along their length following the flow path of the electrolyte. This non-uniform surface finish was usually characterised by a passivated section at the entrance and a reflective and bright at the exit.

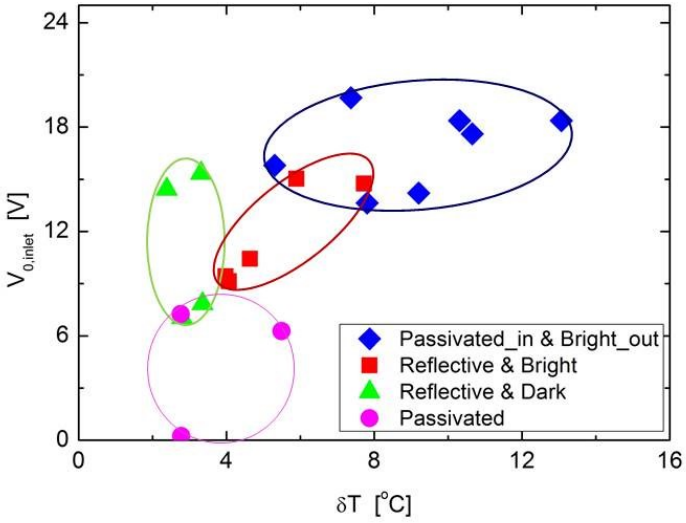


***Figure 2.2-12 Temperature difference, $\delta T$, between the electrolyte inlet and outlet temperature, and overpotential, $V_0$, in relation with the surface finish: passivated entrance – reflective and bright exit (blue rhomboids), reflective and bright (red squares), reflective and dark (green triangles), and passivated (pink circles).***

It was observed that when the electrolyte flowed between the tool and the pipe during ECM, the electrolyte temperature increases along the length of the sample, i.e. the electrolyte enters at a temperature $T_e$ and starts heating up until a temperature $T_{out}$ ($T_e < T_{out}$). This behaviour is attributed to Joule Heating [10]. The change in temperature, $\delta T$, (where $\delta T$ = $T_{out}$ - $T_e$) modifies the electrolyte conductivity, $k_e$, thus changing the surface finish. For this study, the electrolyte inlet temperature for each sample was measured in situ, and the electrolyte outlet temperature was calculated based on the ECM parameters used. Figure 2.2-12 shows $\delta T$ and their relationship with the resulting surface finish. The samples that present two different surface finish (rhomboids in Figure 2.2-12) are the ones whose $\delta T$ was higher. This difference was usually the result of a low electrolyte flow rate, which was not enough (<25 l/min) to dissipate the heat of the ECM process. Additionally, it can be observed that a uniform surface finish was achieved when $\delta T$ was small (<8 °C). (squares, triangles and circles in Figure 2.2-12).

#### 2.2.5.6. Valence, $z$

Valence, $z$, has also been demonstrated to influence the surface finish on SS during the ECM process. Mount, *et al.* [41] in their studies of ECM on SS found that when the average dissolution

valence was high, $z$ = 3.5 ±0.1, the resulting surface was reflective and bright. This surface fish is characteristic of iron and chromium dissolving in their high valence states (as Fe(III), $z_{Fe}$ =3, and Cr(VI), $z_{Cr}$ =6) [41]; however, if $z$ was lower, 2.5 ±0.1, the surface finish was passivated. As in has been seen previously [26], [27], the decrease in dissolution valence corresponds with a progressive change in the electrode surface, i.e. from a smooth bright surface to a passivated one. In this work the valence during the ECM process was not measured, so these findings could not be verified for our samples.

### 2.2.6.Conclusions

This section presents an experimental analysis of the parameters that influence the surface finish of SS316 samples machined with ECM. The machining parameters, voltage, gap, flow rate, and inlet electrolyte temperature, were varied in turn, and the samples were divided according to the resulting surface finish.

Results highlight a strong relationship between surface finish and overpotential during ECM. The overpotential is dependent on the current density and the characteristics of the electrolyte (flow rate, conductivity and inlet temperature). Overpotential between 9 and 15 V was necessary to obtain the desirable reflective and bright surface finish; if the overpotential was lower, a passivated surface usually was obtained. The variation in the electrolyte temperature during the process was found to have a great impact on the uniformity of the surface finish along the sample. A non-uniform surface finish along the length of some samples was characteristic of a low electrolyte flow rate, and hence deficient heat dissipation. Additionally, the interelectrode gap also affected the resulting surface finish but its influence was not so evident. A big interelectrode gap (8 mm) however, usually resulted in a passivated surface finish. Current density during the ECM process also demonstrated to have a strong influence in the resulting surface finish; $J$ higher than 4.5 A/cm$^2$ was generally needed to obtain a reflective surface finish. Furthermore, it is important to remember that $J$ is related to the interelectrode gap, and the temperature and conductivity of the electrolyte. In summary, $V_0$ between 9 and 15 V, $J$ over 4.5x10$^4$ A/m$^2$, $Q$ equal to 25 l/min, and $P$ higher than 7 KW, were required to obtain a bright and reflective surface finish, which was the requirement of the industrial sponsor.

The results presented in this section could be used as a tool for the achievement of the desired surface finish on samples of SS316. This analysis and subsequent further development could be applied to other metal alloys and it is an important step towards the understanding of the ECM process and the adequate prediction of the resulting surface finish. Moreover, the accurate determination of the fundamental relationships between power, overpotential, interelectrode

gap, current density, and electrolyte flow rate and temperature will lead to more accurate computational simulations of the ECM process (presented in section 2.3), and it will support the tool design techniques. Additional experimental work however would help to corroborate the results showed here.

## 2.3. *Simulation of ECM in a 3D environment*

### 2.3.1. Introduction

The complexity of experimentally controlling the ECM parameters in section 2.2 emphasises the need for the development of a computational model that allows the simulation the ECM process in full. A two dimensional (2D) ECM computational simulation model has already been developed in section 2.1 of this work; it is clear however, that its application is limited for real-world problems which are based on three-dimensional (3D) environments. In an attempt to solve this problem, the same simulation technique explained in section 1.6, was used for the development of a 3D ECM simulation model. The aim of this model was to understand and forecast the ECM results by performing in a virtual environment the machining. This will prevent, and eventually solve, the problems that the ECM process may present *a priori* the experimental work, hence reducing the time and cost of the ECM set-up.

As mentioned before, ECM is the result of a complex interaction of various physical and chemical phenomena [2], e.g. electrodynamics, mass transfer, heat transfer, fluid dynamics and electrochemistry. These high interrelated phenomena make different the material dissolution rate at each point of the workpiece surface profile [17], thus making difficult the correct prediction of the final geometry of the workpiece. Diverse experimental [28], [68], [103], [134], [191] and theoretical [2], [17], [21], [24], [129], [136] work had been carried out in order to solve this problem. And various computational ECM simulation models [2], [10], [44] had also been developed in order to forecast or control the ECM process, however in most of these studies the ECM problem was reduced to a two dimensional (2D) geometry. This was done due to the goals of the simulation, the available input data, and the computational resources. Hence there is still need for the development of an accurate three dimensional (3D) simulation model of the ECM process that can integrate all the physic and chemistry of ECM.

In this section, the development of a 3D ECM computational simulation model is presented. The advancement of computer aided design (CAD) and finite element analysis (FEA) technologies has given the opportunity to overcome some of the limitations of the previous work. And as a result, a finite element based simulation model of the ECM process in a 3D environment could be developed in this work. First the theory for the 3D ECM model is introduced, and then a commercial CAD software, SolidEdge®, and FEA package, COMSOL Multiphysics®, are used for the computational simulation of the ECM process in a 3D environment. The advantage of this model over previous ones is that the different physical and chemical phenomena during the process can be applied using the diverse modules of the FEA package and the results merged into a single solution. For validation, the output data was compared with experimental

published results and the work done in collaboration with pECM Systems Ltd® from Barnsley, UK presented in section 2.2.

Especially in ECM processes, the variation on the machining parameters leads to an evident change in the resulting workpiece, therefore the ECM simulation presented in this work has the advantage of allowing the user to foresee the behaviour of ECM at any time during the process and to predict the final profile of the workpiece. Results showed a good agreement with the experimental works; however some improvement can still be implemented in order to enhance the accuracy of the results.

### 2.3.2. ECM theory for three-dimensional problems

As explained in Chapter 1, the formulation of the ECM process depends on the scheme of the problem. pECM Systems Ltd was interested on the effect of the machining parameters on the surface finish of the pipes internal face without needing to change the tool shape, hence for this work the direct problem, where the tool has a fixed geometry and is used to shape a static workpiece [34], [60], was considered. The ECM parameters, e.g. material of the work piece, voltage applied, $V_1$, electric current, $I$, feed rate of the tool (velocity at which the tool approaches to the workpiece), $f$, etc., should be stablish before the simulation starts.

When a constant $V_1$ is applied between the electrodes, electric current crosses the interelectrode gap, $y$, carrying metal ions from the workpiece surface towards the tool. The quantity of material dissolved, $m$, obeys Faraday's laws and is based in the following assumptions [136]:

i. tool and workpiece are uniformly covered by electrolyte,
ii. electrolyte flow velocity regime in the interelectrode gap do not change in the flow direction, the flow is said to be fully developed,
iii. electric field with the interelectrode gap is quasi-stationary,
iv. workpiece material does not include impurities and is homogeneous,
v. dissolution of metal is only reacting on the anode and there are no other sub-reactions,
vi. the metal is removed by only dissolution.

Hence, $m$ is directly related to the amount of current, $I$, flowing between the electrodes and can be expressed by [23]:

$$m = \frac{M}{z_n F} It \qquad \textbf{(2.3-1)}$$

, where $m$ (kg) is the dissolved mass; $M$ (kg/mol) is the molar mass of the anode metal; $z_n$ is the dissolution valence of the anode material; $F$ is Faraday's constant (96 458 C/mol); $I$ (A) is the electric current; and $t$ (s) is the total process time.

The applied voltage, $V_1$, is assumed sufficient for the establishment of field lines perpendicular to the electrodes, hence the current across the interelectrode gap and carried by the electrolyte is given by Ohm's law [192]:

$$I = \frac{k_e (V_1 - V_0) A}{y} \qquad \textbf{(2.3-2)}$$

, where $k_e$ (S/m) is the electrolyte conductivity, $y$ (m) is the interelectrode gap, $V_0$ (V) is the overpotential (minimal voltage required at the two electrodes to drive the reaction), and $A$ ($m^2$) is the tool surface area.

Assuming that the current produces solely the workpiece dissolution, the local variation of the anode dissolution, $\Delta y$ (m), for a certain time step, $\Delta t$, is:

$$\frac{\Delta y}{\Delta t} = \frac{M}{z_n F \rho_a} J \qquad \textbf{(2.3-3)}$$

, where $\rho_a$ ($kg/m^3$) is the anode density and $J$ ($A/m^2$) is the current density through the electrolyte [192].

Electrolyte flows rapidly within the interelectrode gap at high enough flow rate, $Q$, flushing away the machining products so they not affect significantly the electrolyte conductivity, therefore $k_e$ is assumed constant throughout the experiment. The distribution of the electrical potential, $\phi$, can be described by Laplace's equation [24], [134]:

$$\frac{\partial^2\phi}{\partial x^2}+\frac{\partial^2\phi}{\partial y^2}+\frac{\partial^2\phi}{\partial z^2}=0 \qquad \textbf{(2.3-4)}$$

According to Faraday's laws and Ohm's law, the anode and cathode boundaries should satisfy particular machining conditions:

$$\phi_{anode}=V_1-V_0 \qquad \textbf{(2.3-5)}$$

$$\phi_{cathode}=0 \qquad \textbf{(2.3-6)}$$

$$nJ_{side}=0 \qquad \textbf{(2.3-7)}$$

, where $\phi_{anode}$ and $\phi_{cathode}$ are the electric potential at the workpiece and tool respectively, and $nJ_{side}$ is the normal current density at the side boundaries of the model.

The aim is to find an anode boundary which can satisfy the Laplace equation for the electric potential distribution $\nabla^2\phi$, within ECM gap domain, and all boundary conditions listed in equations (2.3-5)-(2.3-7) [24].

### 2.3.3. Computational model for the simulation of ECM in a 3D environment

The work developed here is a continuation from previous work developed by the ECM group in the University of Edinburgh. Experimental work [27], [113], [114], [148] in order to understand the ECM process, especially on stainless steels, was carried out and provided useful data for the inclusion of the overpotential behaviour during the process in the present ECM simulation model.

Curry, D. [118] gave the fundamentals for the development of this simulation model. He developed a time-dependent simulation of the ECM process based on boundary FE techniques, and used MATLAB and FEMLAB FEA solver 3.0 to construct the simulation model. MATLAB was used for the ECM material removal calculations and geometry manipulation, and FEMLAB FEA solver 3.0 was applied for handling the meshing of the geometries and solution of Laplace's equation. Most of Curry's work was developed in a 2D environment, however at the end of his work, his 2D simulation model was adapted for a 3D machining environment.

In Curry's work, a 3D geometry of the interelectrode gap was constructed for the simulation. The tool and the workpiece were the top and bottom boundaries respectively, and they were connected laterally by vertical walls. The geometry was developed in a CAD software and then

imported to FEMLAB. The mesh of the geometry was done by FEMLAB, but due to restrictions of the software, the workpiece boundary needed to be decomposed into square faces, affecting the resolution of the mesh. With a suitable mesh geometry in place and definition of the boundary conditions complete, the FE analysis of the model was then carried out. The solution data was then exported from FEMLAB to MATLAB. In MATLAB, the material removal was calculated, and in consequence, the movement of the moving boundaries could be calculated. Based on this information, a new surface boundary was constructed. Before the new geometry of the interelectrode gap could be built up, the points of the surface boundary should be realigned to form a uniform grid. This step was complex and required manual manipulation of the information. Once the new geometry was ready, it was imported back into FEMLAB in order to carry out a second iteration of the ECM process.

As it can be observed, the ECM simulation developed by Curry, was a long, complex and iterative process. It required manual manipulation of the data, and experimental validation was still needed. To this extent, the work developed in this section is a continuation of Curry's work. His results and the 2D model developed in section 2.1 were used as a first step for the development of this 3D ECM simulation model, and the experimental work presented in section 2.2 was used for its validation.

#### 2.3.3.1. System analysis

The same experimental set up than the one used for the experimental work presented in section 2.2, was considered, where ECM was applied on the internal face of SS316 pipes. Figure 2.2-3 illustrates the ECM array consisting of a cylindrical solid tool and a pipe (workpiece) placed vertically and concentric to each other on the bedplate of the ECM machine. The tool was held by the machine head and the workpiece was fixed to the bedplate by a non-conductive vise. Both, tool and pipe, were connected to a DC power supply by conductive clamps. The electrolyte was pumped into the system and flows from the top and between the pipe and the tool. The system was positioned in such a fashion that the electrolyte could exit the array and be collected in the electrolyte reservoir.

As before, there was no need for modelling all the elements in the ECM system, but only the interelectrode gap. The tool and the workpiece were the boundaries of the model which was filled with uniform flowing electrolyte. The pump and the electrolyte collection were represented by the "electrolyte flow rate" input parameter, and the DC Power supply by the electric constraints applied to the model.

#### 2.3.3.2. Model generation

The workpiece was a commercial stainless steel 316 (SS316) pipe of 17 cm in length and 3.81 cm diameter, which was manufactured by rolling and welding. The original material, prior to processing, was dark, opaque and uniform along the pipe. The welding process left behind a weld-flash at the interior face of the pipe, evident in right side of Figure 2.3-1 c). The exterior of the pipe was not treated.

The weld-flash was of interest because it caused a step (weld-step) on the surface of the pipe that affects locally the ECM process. Additionally, the client was willing to get rid of this weld mark and at the same time to ensure a reflective and bright surface finish.

Figure 2.3-1 (a), (b) and (c) are photographs of the pipe, and below, the corresponding CAD models constructed using SolidEdge®, are displayed in Figure 2.3-1 (d), (e) and (f). In the Figure 2.3-1(c) the weld mark is evident as a dark line in the left side of the pipe, and a small step in Figure 2.3-1(f).

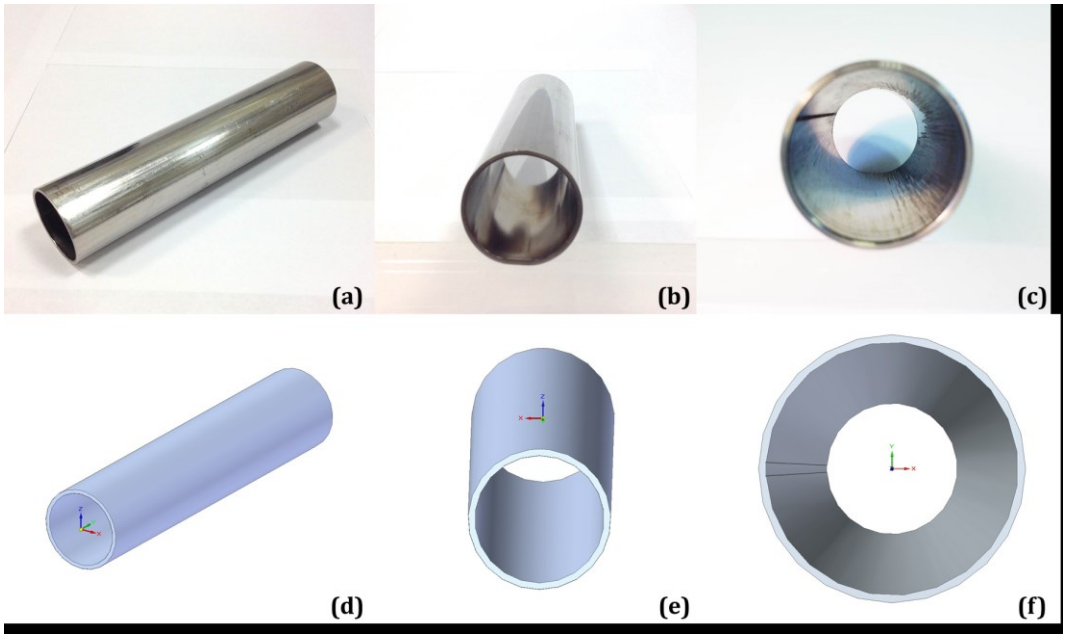


***Figure 2.3-1 Photographs of the pipe used as workpiece ((a), (b)) and its corresponding CAD model ((d), (e)). (c) The internal face view of the SS316 pipe after ECM is presented. The weld-step is visible in the left side, and flow marks are evident at the right side of the pipe. (f) The internal face view the CAD model is presented, the weld-step is visible in the left side.***

The tool was a cylindrical solid bar of stainless steel, with the same diameter of the inner diameter of the pipe but undersized by 2, 4, or 8 mm, according to the sample (2 mm for the present example). This difference in diameters between the tool and the pipe was the interelectrode gap.

***Adapt model for computer simulation***

The geometry defined for this work described the shape of the interelectrode gap, space between the tool and the pipe (workpiece). The tool was the inner boundary, and the pipe was the outer boundary of the model. The required profiles for this work were constructed using SolidEdge®, however any computer aided design (CAD) software might be used. Figure 2.2-3 shows the complete ECM system. From it, only the tool (pink cylinder in Figure 2.3-2) and the pipe (blue cylinder in Figure 2.3-2) will be modelled. The white space between the tool and the workpiece is the interelectrode gap and the area of interest.

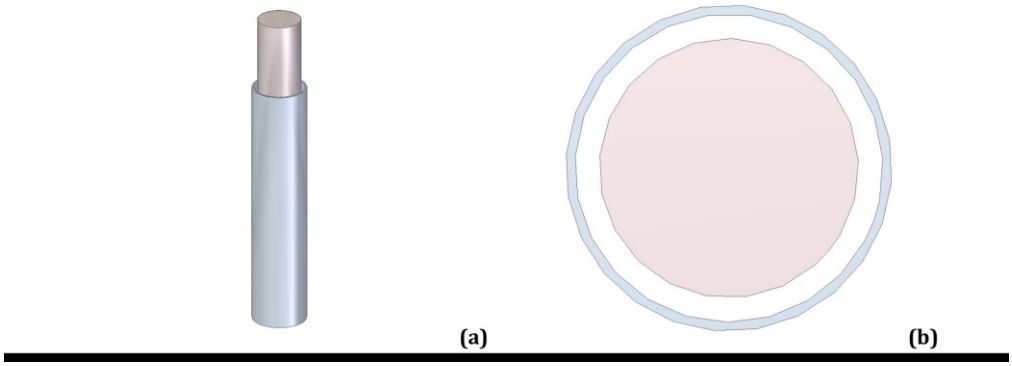


***Figure 2.3-2 Model of the ECM system. (a) Isometric view of the array, (b) Top view of the array. The tool (pink cylinder) is placed concentric to the workpiece (blue ring). The interelectrode gap is the white area between the tool and the workpiece in (b).***

**Geometry symmetries**

Due to symmetry, not all the interelectrode gap needed to be simulated. The voltage is applied uniformly and constant on all the surface of the tool and workpiece. The flow is considered uniform along the cross section area (ring-shape) of the interelectrode gap. Hence, only a section of 30˚ could be taken at the area close to the weld-step. The two profiles, tool and workpiece, were connected with straight lines in both sides. Figure 2.3-3 shows this 30˚ section. In Figure 2.3-3(a) the interelectrode gap is the white area limited on the inside by the tool (pink circle), on the outside by the pipe (blue ring), and on the sides for the two blue straight lines. In Figure 2.3-3(b) this area is highlighted in grey. Figure 2.3-3(c) presents a close view of the weld-step.

One of the advantages of developing a computational simulation model is that knowing the corresponding input parameters, it is possible to simulate any section of the pipe, 30 mm for this case, where all the physics and chemistry can be applied regardless of the size and position of the section in the actual pipe. Figure 2.3-4 shows the final 30˚ of the circumference and 30 mm along the pipe model used for this simulation.

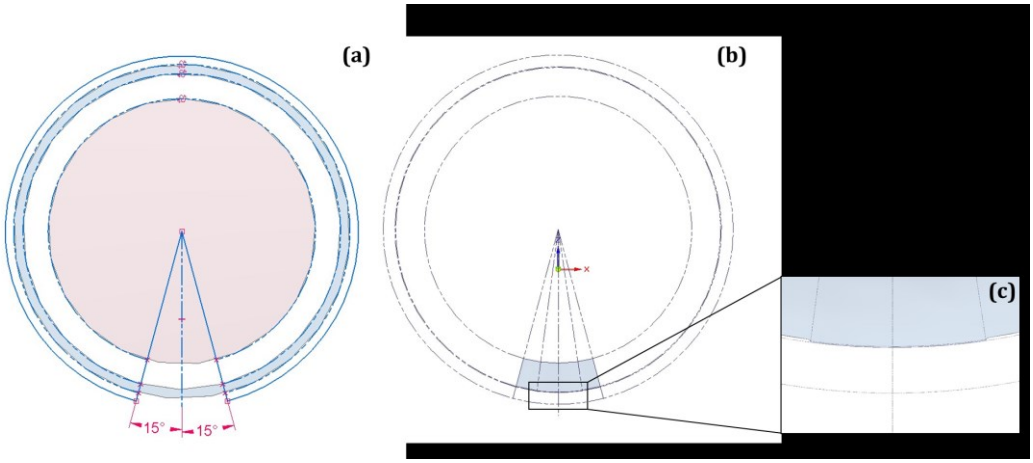


***Figure 2.3-3 Section of 30˚ modelled for the computational simulation of the ECM process. (a) Tool in pink, workpiece in blue and interelectrode gap in white. (b) Section of 30˚ of the interelectrode gap modelled. (c) close view of the weld-step.***

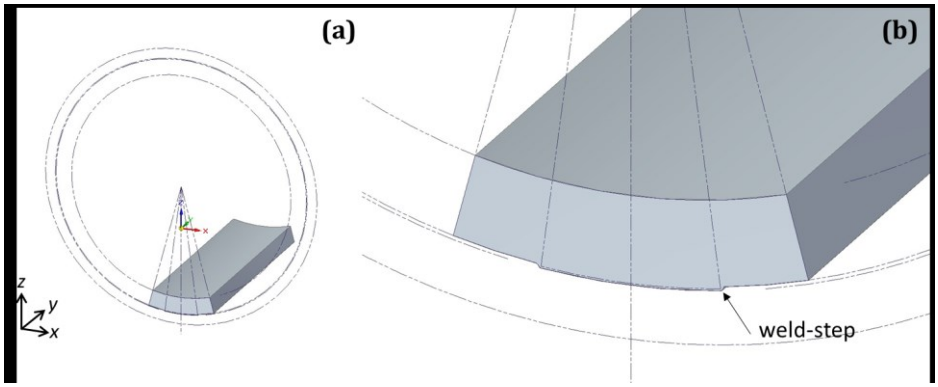


***Figure 2.3-4 Section the 2 mm interelectrode gap of 30˚ of the circumference and 30 mm along the pipe modelled for the computational simulation of the ECM process in 3D perspective.***

The final model displayed in Figure 2.3-4 was then imported into COMSOL Multiphysics®. All the parameters specified in the CAD software, such as dimensions and orientation, were also imported into the FE package.

Three different gaps were modelled for this simulation, Figure 2.3-5(a) 2 mm, (b) 4 mm and (c) 8 mm.

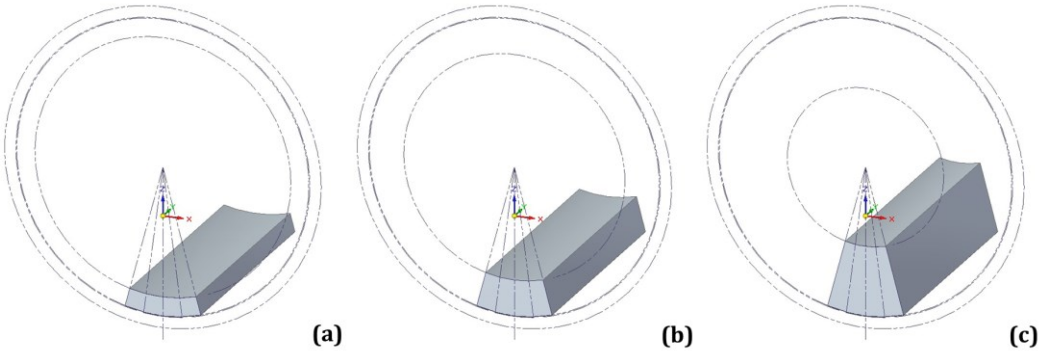


***Figure 2.3-5. Interelectrode gap variations modelled for the ECM simulation, (a) 2 mm, (b) 4 mm and (c) 8 mm in the narrower part. Weld-step of 0.1mm. Parts modelled in SolidEdge® and imported to COMSOL Multiphysics®.***

**Definitions**

In order to define the model properly, names were given to each part. The labelling of the parts gave an easy access and selection to the parts for the physics application and display of results. Figure 2.3-6 shows (a) the 'tool' boundary, (b) the 'workpiece' boundary and (c) the 'electrolyte' lateral boundary. This labelling was especially useful for the workpiece boundary which was formed by several small boundaries. The labelling grouped them in a single selection.

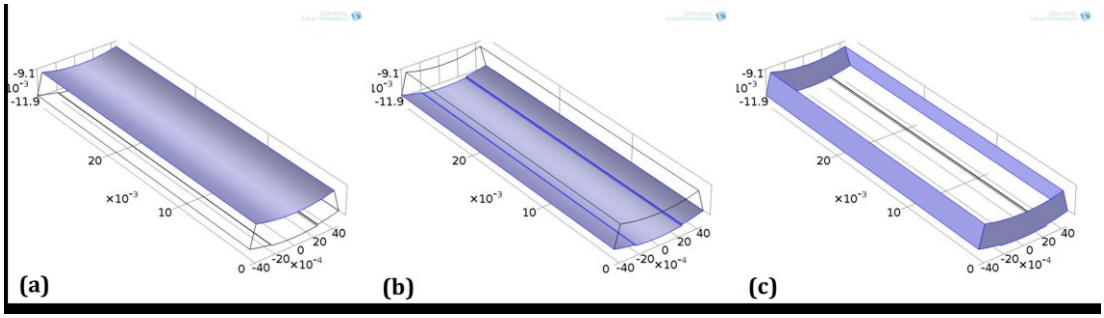


***Figure 2.3-6 Selections and labelling for the 2mm interelectrode gap model in COMSOL Multiphysics®: (a) tool, (b) workpiece, (c) electrolyte.***

#### 2.3.3.3. Model set up

***ECM governing equations***

ECM is based on Faraday's laws for electrolysis, summarized below:

$$v = K_1 J \qquad \textbf{(2.3-8)}$$

, being

$$K_1 = \frac{A_1}{z_{n1} F_1 Rho_1} \qquad \textbf{(2.3-9)}$$

, and $A_1$ (kg/mol) is the molar mass, $z_{n1}$ (1) is the valence, and $Rho_1$ (kg/m$^3$) is the density of the workpiece, and $F_1$ (C/mol) is Faraday's constant. Note that the notation used in the table is the actual one used for introducing the equations into the FE package. Table 2.3-1 presents the equations used for the simulation of ECM on SS316 pipes.

***Table 2.3-1 Equations used in ECM on SS316 simulation model.***

| | Value | Name |
|---|---|---|
| K1 | A1/(zn1*F1*Rho1) | Electrochemical constant |
| dx | x-X | x-displacement |
| dy | y-Y | y-displacement |
| dz | z-Z | z-displacement |

Additionally, each of the physics applied to the model, e.g. fluid dynamics and Joule heating, had their own default equations associated, which were already included in COMSOL Multiphysics®. These equation needed to be customised in order to apply them into the model.

***Workpiece material***

For the ECM simulation, the workpiece material properties should be defined. The material used for this example was stainless steel 316 and the properties of interest for the ECM process were: molar mass ( $A_1$ =5.62x10$^{-2}$ kg/mol), valence ( $z_{n1}$ =3.5), and density ( $Rho_1$ =7870 kg/m$^3$) [176]. Table 2.3-2 below presents the values and nomenclature used in the simulation. Again, note that the notation used in the table is the one used for introducing the equations into the FE package.

***Table 2.3-2 SS316 properties used for the ECM simulation model, data taken from*** [176]***.***

| | Value | Name |
|---|---|---|
| zn1 | 3.5 | Valence Stainless Steel 316 (for shiny surface [27]) |
| A1 | 56.2e-3[kg/mol] | Molecular mass of WP SS316 |
| Rho1 | 7870[kg/(m^3)] | Density of the WP SS316 |

For other applications, some materials are already contained in COMSOL Multiphysics® and can be chosen from the material browser library, or the characteristics of a special material can be added manually by the user.

***Feed rate***

The feed rate, $f$, is the velocity at which the tool moves towards the workpiece during the simulation. For the present example, the tool was static, thus $f$ = 0 m/s.

***Electrolyte***

The type of electrolyte and its characteristics have to be introduced as a constraint for the ECM process simulation model. Electrolyte inlet temperature and, in order, its electrical conductivity, $k_e$, were the properties of interest for this simulation. Additionally the electrolyte flow rate, $Q$, had to be established. The electrolyte electrical conductivity and density are temperature dependent, hence, the initial temperature, $T_e$, was introduced in the equations (2.3-10) and (2.3-11):

$$k_e = M_k T_e + B_k \qquad \textbf{(2.3-10)}$$

$$Rho_e = M_{Rho} T_e + B_{Rho} \qquad \textbf{(2.3-11)}$$

, where $T_e$ is inlet electrolyte temperature, $k_e$ is the electrolyte conductivity, $M_k$ is the gradient of the conductivity equation, $B_k$ is the *y*-intercept of the conductivity equation, $Rho_{Ele}$ is the density of the electrolyte, $M_{Rho}$ is the gradient of the density equation, and $B_{Rho}$ is the *y*-intercept of the density equation.

ECM was considered to be performed using a solution of Sodium Nitrate ($NaNO_3$) as electrolyte, S.G. 1.15, concentration about 22%. Electrolyte flow rate, $Q$, was set to 10, 25, 40, and 60 l/min. And the inlet temperatures considered were 7 °C and 15.3 °C. The values for equation (2.3-10) and (2.3-11) were extracted from experimental published values from [177] and presented in section 2.2 (Figure 2.2-5). The electrolyte was pumped into the system, thus it had a velocity which was dependant on the size of the interelectrode gap and the electrolyte flow rate. Table 1.6-3 presents the nomenclature, values and equations used for this work.

***Table 2.3-3 $NaNO_3$ electrolyte characteristics for the multiphysics ECM on SS316 simulation model.***

| | Value | Name |
|---|---|---|
| T | Te | Inlet electrolyte temperature |
| Mk | 0.336[S/(K*m)] | Gradient Conductivity |
| Bk | -82.964[S/m] | Origin Conductivity |
| sig1 | (Mk*Te[K])+Bk | Conductivity $NaNO_3$ |
| MRho | -0.6357[kg/(K*m^3)] | Gradient Rho of $NaNO_3$ |
| BRho | 1371.5[kg/m^3] | Origin Rho of $NaNO_3$ |
| rho | ((MRho*Te[K])+BRho) [kg/m^3] | Density of $NaNO_3$ |
| *y* | 4[mm] | Interelectrode gap |
| Ve1 | 25[l/min] | Electrolyte flow rate |
| Vin1 | (Ve1/(π*(0.0179[m]-0.5*Gap[m])^2)) [m/s] | Electrolyte flow velocity |

***Electrodes voltage***

The reference voltage was set at the tool and an overpotential, $V_0$, was assumed to be generated at the workpiece during the ECM process. The potential difference applied, $V_1$, to the system had to be provided as a constraint and could be added as a global definition of the model. The voltage was assumed to be uniform during all the simulation and the overvoltage was dependent on the current density during the process, as shown in equation (2.3-12).

$$J = k_e(V_1 - V_0) \qquad \textbf{(2.3-12)}$$

Previous work [42], [81], [85] highlighted the effect of the overpotential on the ECM behaviour, namely high overpotential favours non-uniform surface finish, and low overpotential favour the removal of the characteristic oxide film at the SS316 surface, as it can be observed in section 2.2.5.1. Moreover, Muir [114] demonstrated that the overpotential is dependent on the current density, $J$, and the electrolyte type, as it is depicted in Figure 2.3-7 for ECM on Inconel 718 (In718).

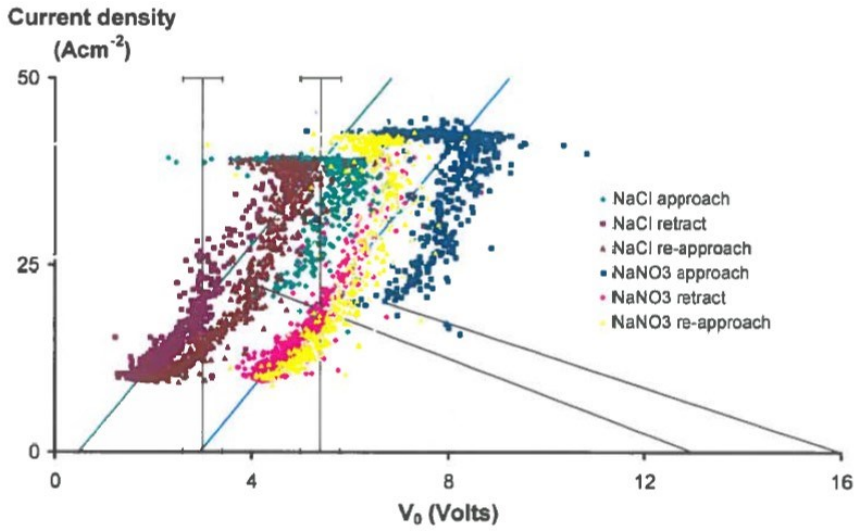


***Figure 2.3-7 Current density and overvoltage data for ECM on In718 using NaCl and NaNO3 as electrolyte. Image taken from*** [114]

The above highlight the importance of including the overpotential behaviour in the simulation model. The overpotential behaviour used for the present simulation model was determined by extracting experimental data from [42], and parametrised them into equation (2.3-13).

$$V_0 = 2.514x10^{-5} J + 1.746 \qquad \textbf{(2.3-13)}$$

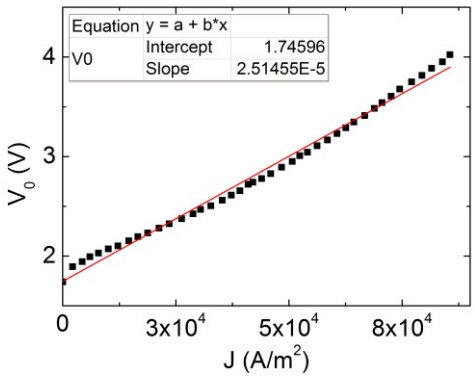


***Figure 2.3-8 Overpotential $V_0$, in relation of the current density $J$, in experiments with $NaNO_3$. Data extracted from*** [42]***. The red line shows the fitting line and equation that describes the overvoltage behaviour.***

#### *Machining time*

The length of the simulation was given by the machining time. Therefore an exit condition of 10 s, same as the actual machining time, was established for the present example.

***Assumptions***

Upon running the ECM process, some parameters had to be provided or assumed. The main parameters to consider were the workpiece material specifications, Table 2.3-2, and electrolyte characteristics, Table 2.3-3. Additional parameters considered for the ECM process are presented in Table 2.3-4.

***Table 2.3-4 Parameters assumed for ECM on SS316 pipes.***

| | Value | Name |
|---|---|---|
| $\eta$ | Current efficiency | 100 % |
| e1 | 80 | Relative permittivity of water |
| $y$ | 4[mm] | Initial gap |
| $F1$ | Faraday's Constant | 96500 C/mol |
| | Electrolyte | $NaNO_3$ at 22% mass percent |

***Physics application***

COMSOL Multiphysics® has the capability to allow the development of simulations using coupled multiphysics phenomena. A fully developed coupled model using electric currents, electrolyte flow, moving boundaries and Joule Heating is constructed in this section. The tool, upper boundary, was considered static. The workpiece, lower boundary, was attached to a moving mesh which simulates the dissolution of material due to ECM. $V_1$ was considered uniform and constant. The dissolution of the workpiece profile depends on the material properties of it, $M$, $z$ and $\rho$, and on $J$ and $V_0$ during the process. For this work, these parameters were extracted from literature [60], [176], published experimental work [27], [42], [131] and previous experimental work presented in section 2.2. The interelectrode gap was assumed to be filled with uniform electrolyte flowing in a laminar fashion from the front to the back of the geometry. The lateral sides were considered open and insulated. Figure 2.3-9 depicts the boundary conditions built up for this simulation.

**Electrolyte flow**

High electrolyte flow was pumped into the interelectrode gap, hence a fully developed velocity profile was assumed for ECM simulation [60]. Ideally, the electrolyte sweeps away the ECM products, hence the effect of any sludge in the electrolyte could be considered negligible due to the small volume ratio. The electrolyte was assumed incompressible and laminar [44], [140], and the fluid profile should met the equation (2.3-14) [169]:

$$\rho u \cdot \nabla u = \nabla\left[-p\mathrm{I} + \mu(\nabla u + \nabla u)^T\right] + F \qquad (2.3\text{-}14)$$

, where $\rho$ (kg/m$^3$) is the electrolyte density, $u$ (m/s) is the electrolyte velocity, $p$ (N/m$^2$) is the pressure of the electrolyte, $\mathrm{I}$ is the identity matrix, $\mu$ (kg/m s) is the electrolyte dynamic viscosity, and $F$ (N/m$^3$) is the volume force. $F$, between the electrodes and the electrolyte was assumed to be small enough to be ignored.

The initial temperature, $T_e$, was set to 15.3 ˚C or 7 ˚C, and the electrolyte and workpiece material properties were specified as input parameters (already defined in the previous section). Due to the fact that just one section of the pipe length was considered, the initial values were not zero but the electrolyte velocity at ideal uniform conditions, $V_{in1}$. The inlet and the outlet of the electrolyte flow were the front and the back faces of the model respectively, and the electrolyte was pumped at a uniform flow rate, $Q$, of 10, 25, 40, and 60 l/min. The outlet had a boundary condition of null pressure ( $P_0 = 0$ Pa). The tool (upper boundary) and the workpiece (lower boundary) were defined as walls of the model, and the short lateral sides were considered open boundaries.

Moreover, previous work [26], [27] had demonstrated that the electrolyte flow affects the overpotential during the ECM process, and in turn the final surface finish of the workpiece.

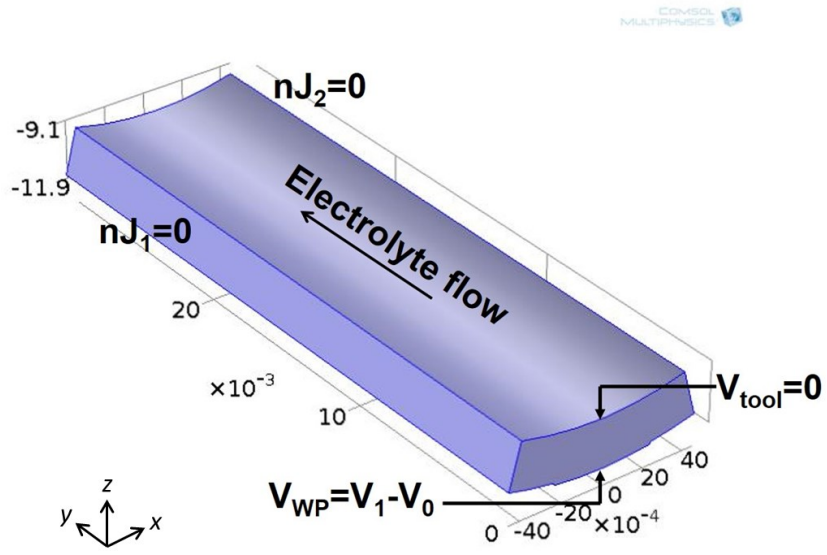


***Figure 2.3-9 Boundary conditions and fluid flow direction of the electrolyte for ECM on SS316 pipes simulation. Interelectrode gap 2 mm.***

**Joule Heating**

Joule heating, $q$, is the generation of heat by passing an electric current through a conductive material. Inputs include electric current, voltage and material resistivity [175]. For the present work, the conductive material was the electrolyte, whose properties were defined before. The electrolyte electric conductivity, $k_e$, is temperature dependent, thus the inlet electrolyte temperature, $T_e$, had to be established first. During ECM, $q$ should met equation (2.3-15) [169]:

$$q = JE \qquad \textbf{(2.3-15)}$$

$J$ depends on the machining parameters, e.g. $V_1$, $I$ and $y$; and the properties of the electrolyte, e.g. $k_e$ and $T_e$. On the other side, $E$ depends on the potential difference and the resistivity of the electrolyte [169]. And in turn, the electrolyte temperature during the process, $T$, varies according to equation (2.3-16) [140], [169], [175]:

$$q = \rho C\left[\frac{\partial T}{\partial t} + u\nabla T\right] - \nabla\cdot\left(k\nabla T\right) \qquad \textbf{(2.3-16)}$$

, where $\rho$ (kg/m$^3$) is the electrolyte density, $C$ (J/kg K) is the specific heat, $T$ (K) is the temperature, $u$ (m/s) is the velocity and $k$ (W/m K) is the thermal conductivity of the electrolyte. Additionally, the surface-to-ambient radiation emissivity, $\varepsilon$, of SS316 had to be defined.

**Electric currents**

The electrode surfaces are equipotentials, where the boundary conditions are:

$$V_{tool} = 0 \qquad \textbf{(2.3-17)}$$

$$V_{WP} = V_1 - V_0 \qquad \textbf{(2.3-18)}$$

$$n\vec{J}_{1,2} = 0 \qquad \textbf{(2.3-19)}$$

, where $V_{tool}$ is the electric potential at the cathode (tool), $V_{WP}$ is the electric potential at the anode (workpiece), $V_1$ is the voltage applied to the system (18, 27, and 36 V), $V_0$ is the

overpotential at the workpiece during the ECM process, and $n\vec{J}_{1,2}$ is the normal current density at the sides of the model. Figure 2.3-9 shows these boundary conditions.

**Moving boundaries**

For the simulation of the movement of the tool and the dissolution of the workpiece, therefore the deformation of the interelectrode gap, an Arbitrary Lagrangian-Eulerian (ALE) formulation was used. The model was developed in a global coordinate system, allowing free deformation of all the system. The mesh attached to the tool was fixed, thus their velocity in each axis direction, $v_x, v_y$ and $v_z$, was equal to 0 m/s, with respect to the global coordinate system. The mesh attached to the workpiece moved in relation to the boundary system, and according to equations (2.3-1) and (2.3-2) [13]. The mesh attached to the walls is fixed in directions $x$ and $y$, hence $v_x$ and $v_y$ =0 m/s, and free in $v_z$ with respect to the global coordinate system, see Figure 2.3-10.

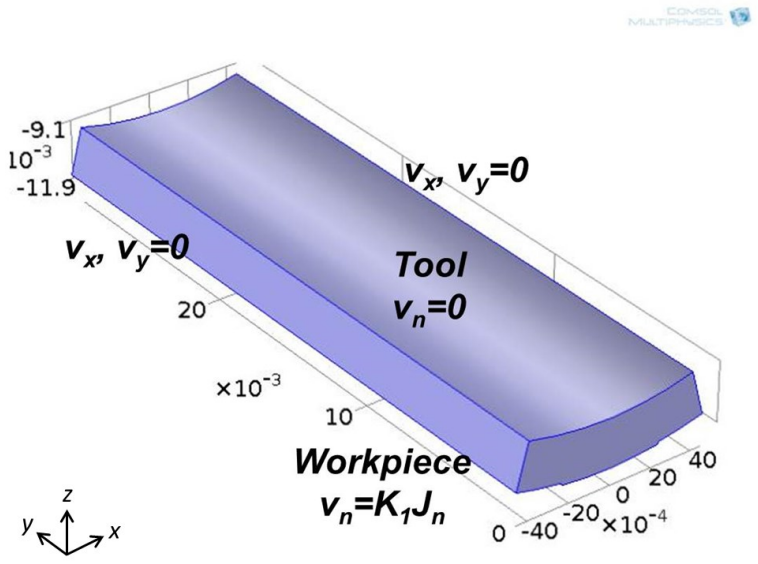


***Figure 2.3-10 Moving mesh boundary conditions for ECM on SS316 pipes simulation. Interelectrode gap 2 mm.***

#### 2.3.3.4. Computer simulation

***Meshing***

The mesh for the FEM was constructed using the adaptive mesh by refinement option in COMSOL Multiphysics®. This mesh was denser (finer) in the weld-step of the geometry. The increase of the mesh elements in the areas of interest helps to observe with higher accuracy what it is happening in that area; but it also keeps the rest of model with a "coarse" mesh in an

attempt to optimise it, and therefore saving computational resources and time. Figure 2.3-11 displays the meshed interelectrode gap where the elements can be readily noticed to become finer and the mesh denser in the area close to the weld step. The element size established were maximum 0.002 m and minimum $2.5x10^{-4}$ m. The maximum element growth rate was 1.7. This change in size and growth rate can be modified using the simple input interface of the FE package. The element shape was tetrahedral.

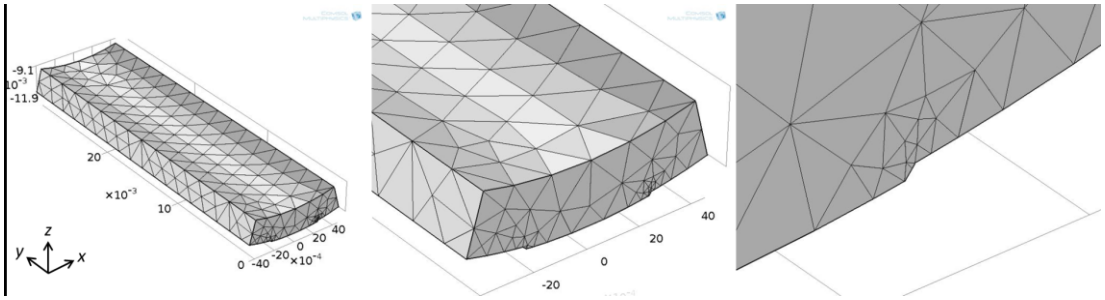


***Figure 2.3-11 Tetrahedral adaptive mesh example for an interelectrode gap of 2 mm at t=0s using COMSOL Multiphysics®. Complete model and close views of the weld-step area where a denser (finer) mesh is present.***

***Simulation steps***

COMSOL Multiphysics® is able to solve the various physical and chemical phenomena of the system in a process called 'coupling'. For a correct coupling, the study has to follow a sequence. This sequence will depend on the physics applied and the interaction between them. The sequence followed for the present work is explained below.

The electrolyte flow was independent of the Joule heating and the electric current. Assuming that the change in geometry of the workpiece was small, thus ignoring its effect on the electrolyte velocity flow profile, the electrolyte flow was set as the first step of the simulation. The results of the electrolyte flow were considered as the initial values for the second step, Joule heating. The third step, electric currents and moving mesh, depends on the temperature of the electrolyte from the second step. The solutions of each step were coupled into a single solution, and in turn, the results could be displayed using the interface of COMSOL Multiphysics®. Additionally, these results could be exported as text, image or spreadsheet files.

***Simulation time***

The length of the simulation was given by the machining time. Therefore an exit condition, $t$ = 10 s, was established.

### 2.3.4. Results and Discussion

The experimental work carried out in section 2.2 was used as benchmarking for the 3D simulation model developed in this work. Table 2.3-5 presents a summary of the variables which were controlled: interelectrode gap was varied between 2, 4, and 8 mm, voltage, $V_1$, between 18, 24, and 36 V, electrolyte flow rate $Q$, between 10, 25, 40 and 60 l/min, and inlet electrolyte temperature $T_e$, between 7 and 15.3 °C.

***Table 2.3-5 Variables for the ECM simulation tests.***

| | Name | Value |
|---|---|---|
| $y$ | Interelectrode gap | 2, 4, 8 mm |
| $V_1$ | Voltage | 18, 27, 36 V |
| $Q$ | Electrolyte flow rate ($Ve_1$) | 10, 25, 40, 60 l/min |
| $T_e$ | Inlet electrolyte temperature | 7, 15.3 °C |

#### 2.3.4.1. Electric potential distribution $\phi$, and overpotential, $V_0$

Figure 2.3-12 depicts the electric potential distribution within the interelectrode gap. Additionally the overpotential variations (depending on the interelectrode gap and $V_1$ ) can be observed. The results agree with previous work [86] where the overpotential is higher at smaller gaps. Additionally, $V_0$ is directly related to $V_1$ [42], [79], [81], [85]. Figure 2.3-12 (a), (b) and (c) shows an example of this behaviour.

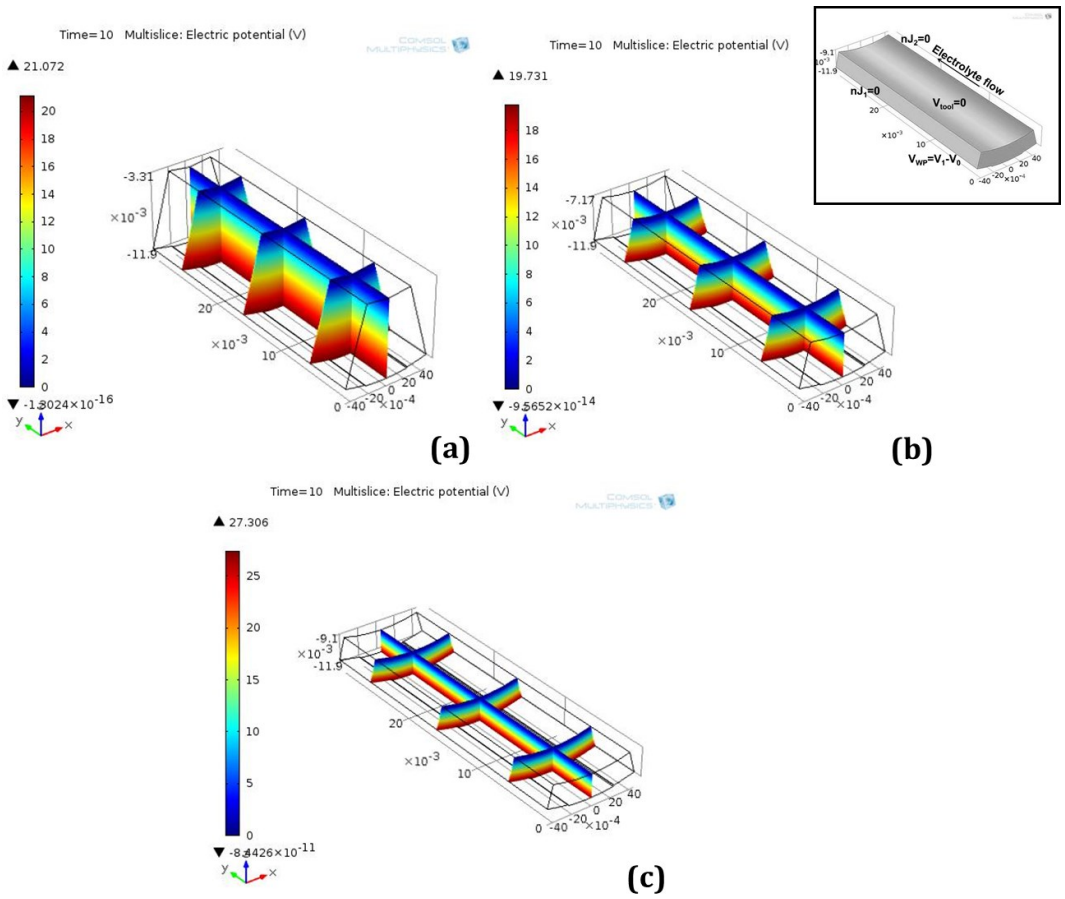


***Figure 2.3-12 Example of the electric potential distribution, $\phi$, for an interelectrode gap at $Q$ = 25 l/min, $T_{in}$ = 15.3 °C and t= 10 s, for (a) Gap = 8 mm and $V_1$ = 18 V; (b) Gap = 4 mm and $V_1$ = 24; and (c) Gap = 2 mm and $V_1$ = 36 V.***

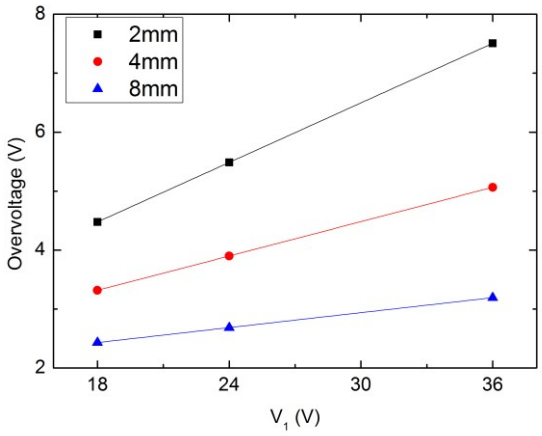


***Figure 2.3-13 Overpotential $V_0$ in relation with electric potential $V_1$ and Gap. Results extracted from the ECM simulation model for a $Q$ = 25l/min and $T_e$ = 7°C.***

#### 2.3.4.1. Current density, $J$

Figure 2.1-13 displays the normal current density at the interelectrode gap. As expected, at the end of the simulation, $t$ =10 s, an almost uniform current density was achieved. $J$ is inversely related to the gap, hence smaller gaps show higher $J$. Figure 2.3-15(d) shows how the current density is different in the weld-step, as "sharp" corners provoke an increase of the current density, this has been observed previously in theoretical work [24] and experimental work [44] in the form of marks (ridges) on the workpiece surface.

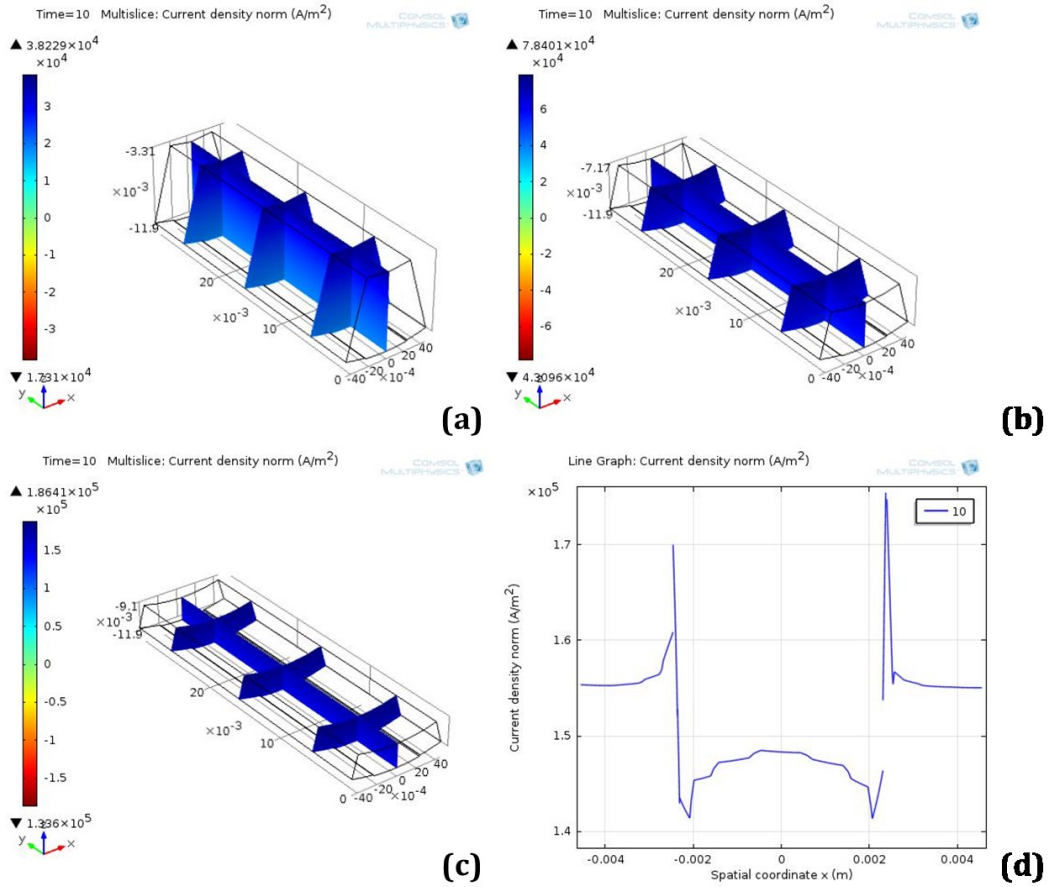


***Figure 2.3-14 Example of the current density $J$, for an interelectrode gap at $Q$ = 25l/min, $T_e$ = 15.3 °C, and t= 10 s, for (a) Gap = 8 mm and $V_1$ = 18; (b) Gap = 4 mm and $V_1$ = 24 V; and (c) Gap = 2 mm and $V_1$ = 36 V; (d) Current density at the workpiece edge, Gap = 2 mm and $V_1$ = 36 V.***

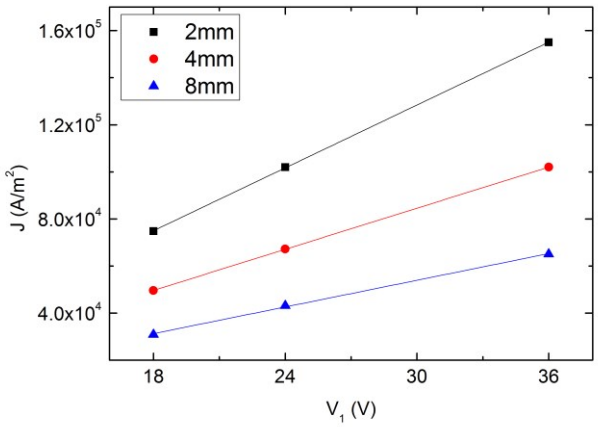


***Figure 2.3-15 Current density $J$ in relation with electric potential $V_1$ and Gap. Results extracted from the ECM simulation model for a $Q$ = 25l/min and $T_e$ = 7°C.***

#### 2.3.4.1. Electrolyte flow rate, $Q$

The electrolyte flow, $Q$, in the interelectrode gap is depicted in Figure 2.3-16. The electrolyte enters at the front of the geometry and exits at the back of it. The inlet flow rate was set uniform, and the entrance effects were neglected. As expected, the highest velocity values were observed in the centre of the interelectrode gap, and the lower ones at the walls (tool and workpiece boundaries), this forms the anticipated parabolic flow profile of the electrolyte. The lateral sides were considered open. Some turbulence was expected close to the weld-step. From Figure 2.3-16(a), it can be observed that at low flow rates (<10 l/min) the laminar boundary layer (layer of fluid in the immediate vicinity of the wall that can affect the ECM accordingly with section 2.2.5.3) was more evident.

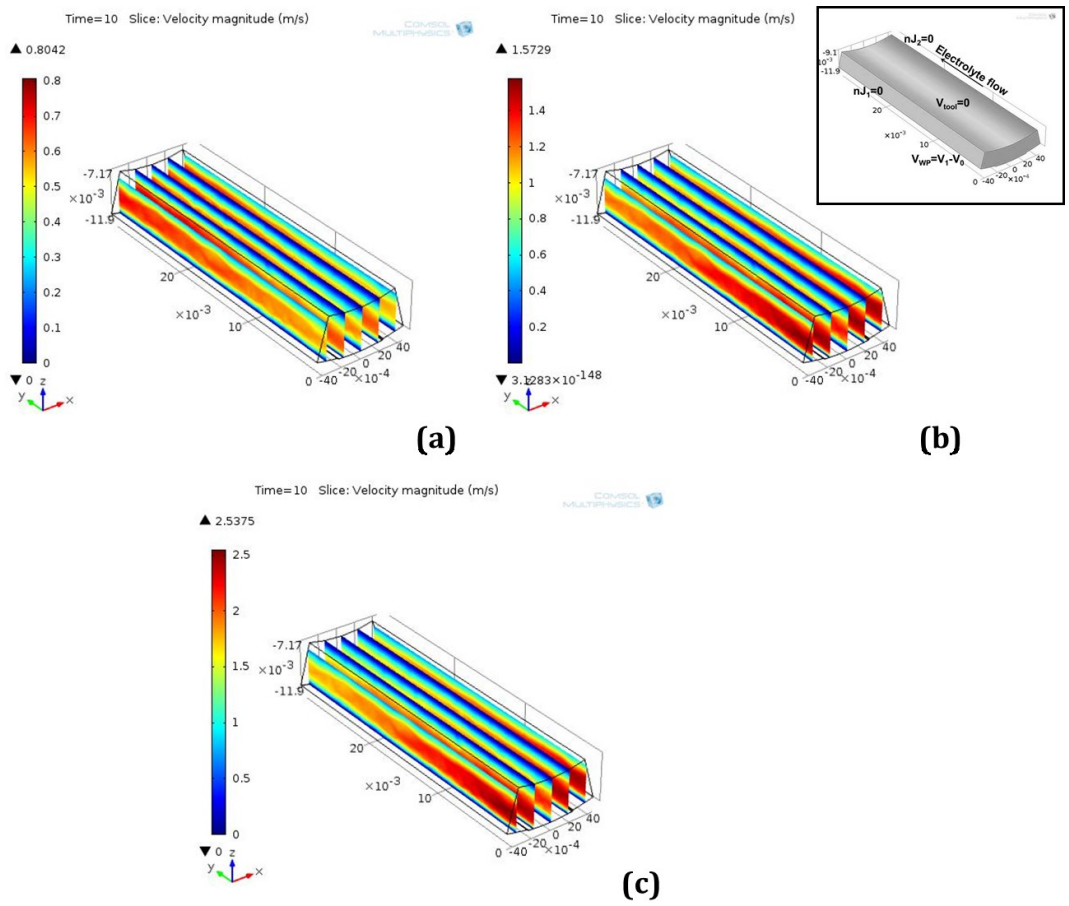


***Figure 2.3-16 Example of the electrolyte velocity, for an interelectrode gap of 4mm and $V_1$ = 24 V at 10 s. (a) $Q$ =10 l/min, (b) $Q$ =25 l/min, and (c) $Q$ =40 l/min.***

#### 2.3.4.1. Temperature, $T$

The workpiece electrochemical dissolution generates heat due to Joule heating. The electrolyte flow controls the temperature of the system, but in parallel, the electrochemical process keeps heating it up due to Joule heating. Deconinck, *et al.* [9], [10] demonstrated that there is an increase of the electrolyte temperature at the vicinity of the tool during ECM. The results in the present work showed a difference of about 1 °C, and the same behaviour was observed. Additionally, the increase of the electrolyte temperature between the entrance and the exit of the interelectrode gap is depicted in Figure 2.3-17.

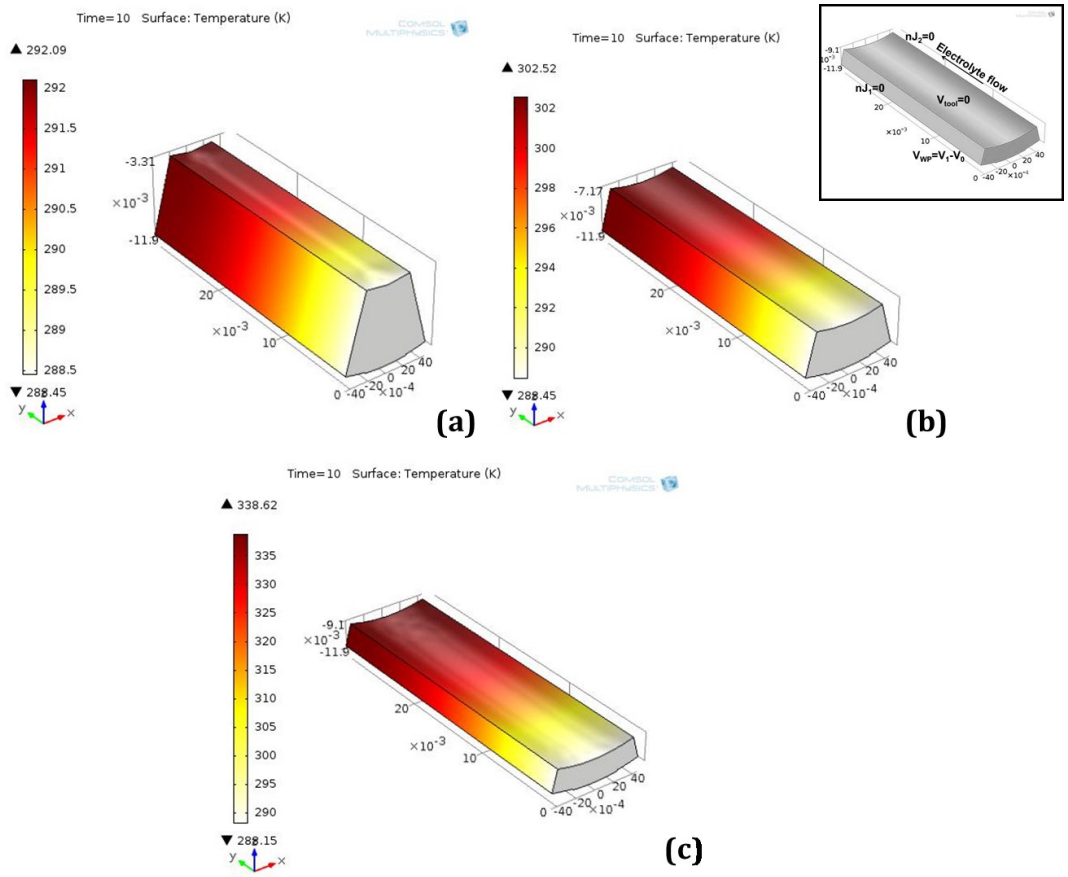


***Figure 2.3-17 Temperature distribution for a $Q$ =25 l/min and $V_1$ = 18 V at 10 s. and $T_e$ = 7 °C (a) 8 mm, (b) 4 mm, (c) 2 mm.***

The electrolyte linear temperature distribution in the interelectrode gap is displayed in Figure 2.3-17. Homogeneous temperature distribution is aimed during ECM in order to maintain $k_e$ stable and, in turn, $J$ [111]. At higher $T$, $k_e$ and $J$ rise, as it was observed in sections 2.2.5.2 and 2.2.5.5.

#### 2.3.4.2. Workpiece dissolution

The workpiece 3D dissolved profile after 10 s of simulated ECM is presented in Figure 2.3-18. As expected, the dissolution was normal to the workpiece surface, but also to the sides of the weld-step. For quantitative geometry analysis, the deformation of the workpiece profile can be related to the material removed from the workpiece. From previous work [60], [86], [193], [194], the material removed (or in the simulation model, the deformation of the workpiece profile), is directly related to $V_1$, $V_0$ and $J$ during the ECM process.

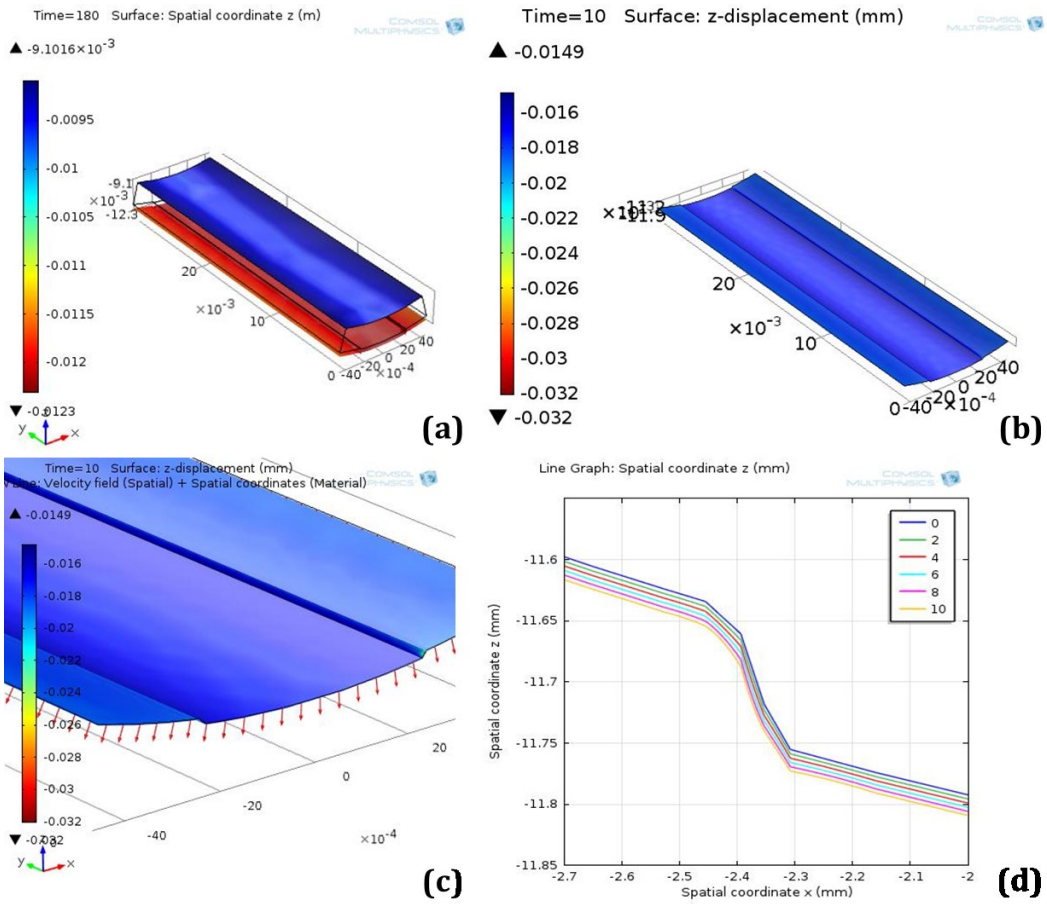


***Figure 2.3-18 (a) deformed profile for an inter-electrode gap of 2mm, Q=25 L/min, $V_1$=24 V, T=15.3 °C and t=10 s; displacement of the tool (upper profile) and the workpiece (lower profile); (b) displacement of the workpiece; (c) close view of the displacement of the workpiece, with arrows indicating the direction of the movement; (d) change in the spatial coordinates in the weld-step.***

As it can be observed in Figure 2.3-18(a), after 10 s, the tool remains static and the workpiece has a deformation (material dissolution) of 0.015-0.020 mm (Figure 2.3-18(b)). Figure 2.3-18(c) illustrates with arrows the direction of the movement of the workpiece dissolution and give a close view of the weld step. The weld step spatial coordinates are shown in Figure 2.3-18(d) and it can be observed that material dissolution occurs in parallel on the pipe walls and on the weld step lateral wall. This is a normal behaviour expected in ECM, usually called overcut [141].

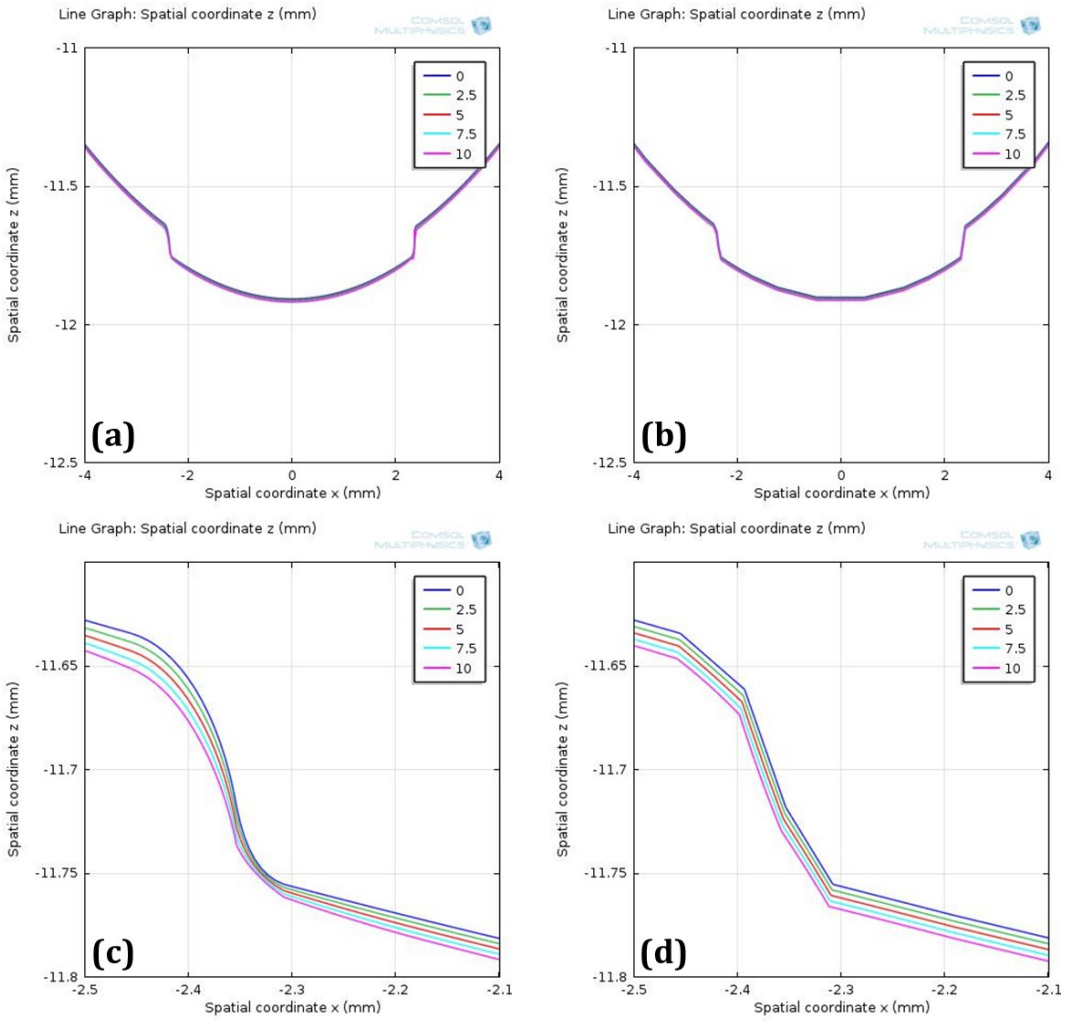


***Figure 2.3-19 Deformed profile for an interelectrode gap of 4mm, $V_1$ = 24 V and $T_{in}$ = 15.3 °C, at t= 10 s, (a) and (c) using a ECM simulation model without fluid dynamics, Joule heating and assuming a constant overpotential, (b) and (d) using the ECM simulation model developed in this thesis.***

The ECM simulation model developed in this thesis has the novelty of adding some of the physical and chemical reactions present during ECM, e.g. fluid dynamics, Joule heating and electrochemical reactions, in order to provide a more accurate prediction of the final workpiece profile. Figure 2.3-19 shows a comparison between the workpiece profiles when these additional physical and chemical reactions are included into the simulation model. Disregarding the smoothness of the profile, which depends on the mesh used, it is evident the difference in the workpiece profiles. Figure 2.3-19 (c) and (d) show a closer view of the weld step. When the enhanced ECM simulation model is used, the expected overcut is attained in the workpiece profile. However, data about the initial dimensions of the pipes studied in section 2.2 and used for this simulation model were not provided, hence the simulation results could not be verified.

### 2.3.5. Conclusions

This section presents an enhanced method for the simulation of the ECM process in a 3D environment. A CAD software, Solid Edge®, was used in order to create the geometry of the problem, and a FEM package, COMSOL Multiphysics®, to create the mesh, apply the boundary conditions and simulate the different phenomena of the ECM process. The workpiece material properties, electrolyte characteristics and machining parameters, i.e. interelectrode gap, voltage applied, electrolyte flow rate, and electrolyte inlet temperature, were provided as input parameters. COMSOL Multiphysics® was able to merge the results into a single solution.

Simulations varying the interelectrode gap, voltage applied, electrolyte flow rate, and electrolyte inlet temperature were carried out, and the FEM package enabled the extraction of information about the ECM process at any time during the ECM simulation. In this work the electric potential distribution, current density, electrolyte flow profile and temperature distribution were extracted. As expected a direct relation between the applied voltage and the current density and the overpotential was observed. Moreover, the final workpiece geometry could be obtained using this simulation model. Although a good agreement was found between the results presented in this section, the experimental work in section 2.2 and the published literature data [10], [44], [79], [81], [85], [86], [193], [194], there are still some discrepancies between the simulation and the experimental results. The main causes affecting the FE solution might be [24]:

i. Lateral boundaries insulation. According to the FE model, the lateral boundaries were insulated as shown in Figure 2.3-9; in the actual ECM process however, these interelectrode gap boundaries are open, meaning the absence of insulation;
ii. Curvature changes. The sharp geometry in the weld-step, generated a concentration point for the electric potential distribution, the current density and the fluid flow, which result in excessive deformation of the local mesh elements and in general affecting the total geometry, an example of this can be seen in Figure 2.3-14

The use of this simulation model allows the user to eliminate beforehand the range of tool-workpiece-machining parameters and configurations that would not deliver the expected result, saving time and resources in ECM and tool design processes. Additionally this model can easily be modified in order to be applied in various geometries and different materials; however more experimental data, such as in situ electrolyte temperature and conductivity, pipe dimensions, and time dependent measurements of the current, are still needed for further development of the model and to enhance the accuracy of the results.

# *Chapter 3*

## *Validation of the 3D ECM simulation model*

*What we see depends mainly*
*on what we look for.*
*-John Lubbock*

## 3.1. *Validation of the ECM simulation model: case 1 and case 2*

### 3.1.1. Introduction

A crucial final step in the development of a simulation of the ECM process is the validation and implementation of the results in the real world. In this section, two samples of the pipes electrochemically machined, presented in section 2.2, were chosen to be simulated. The first sample chosen was one with the reflective and bright surface finish (case 1, hereafter), and the second was one with the passivated surface finish (case 2, hereafter). The same parameters used for the actual machining were used as the input parameter in the simulation model, i.e. voltage applied, interelectrode gap, electrolyte inlet temperature, machining time and electrolyte flow rate. Additionally, some assumptions based in previous work [27] were made: an average valence of 3.5 and 2.1 was considered for case 1 and the case 2 respectively, the electrolyte flowed within the interelectrode gap was laminar, uniform and covered all the volume (no gas bubbles present), and the voltage applied was stable and constant throughout the process. As seen in section 2.2, a reflective and bright electrochemical machined surface finish is usually associated with a higher overpotential at the surface of the anode ($V_0$ > 9 V), a high current density ($J$ > 4.5x10$^4$ A/m$^2$), and a high electrolyte flow rate ($Q$ ≈ 25 l/min). The objective of the present work is to extract these driving parameters (overpotential, current density and mean electrolyte velocity) from the simulation results and compare them with the experimental data, hence validating our simulation model. Moreover, as in section 2.2, these parameters were correlated with the surface finish after the ECM process, so an accurate determination of them within the simulation model, will help to predict the final surface finish of the sample.

### 3.1.2. Experimental setup

The internal face of commercial stainless steel 316 (SS316) pipes (3.81 cm diameter and 17 cm length) was machined electrochemically. The pipe was manufactured by rolling and welding, leaving behind a dark and opaque surface finish, and in some of them, a weld-flash was left by the welding process. The ECM process was applied to the interior face of the pipe with the objective of achieving a reflective and bright surface finish and the removal of the weld-flash.

The input machining parameters for the ECM process are presented in Table 3.1-1. For case 1, an interelectrode gap, $y$ =4 mm, electrolyte flow rate, $Q$ =25 l/min, and a valence, $z_{n1}$ =3.5, were considered. For case 2, an interelectrode gap, $y$ =8 [mm], electrolyte flow rate, $Q$ =10 l/min, and valence, $z_{n2}$ =2.1, were set. In both cases, a voltage, $V_1$ =24 V, was applied for 10 s.

Sodium nitrate ($NaNO_3$) with specific gravity (S.G.) of 1.15 was used as electrolyte with an inlet temperature $T_e$ =15.3 ˚C.

***Table 3.1-1 List of parameters for ECM on SS316 pipes (case 1 and case 2).***

| Parameter | Case 1 (reflective and bright) | Case 2 (passivated) |
|---|---|---|
| Voltage ($V_1$) | 24 [V] | 24 [V] |
| Tool feed rate ($f$) | 0 [m/s] | 0 [m/s] |
| Machining time ($t$) | 10 [s] | 10 [s] |
| Interelectrode gap ($y$) | 4 [mm] | 8 [mm] |
| Electrolyte type | $NaNO_3$ | $NaNO_3$ |
| Electrolyte flow rate ($Q$) | 25 [l/min] | 10 [l/min] |
| Electrolyte inlet temperature ($T_e$) | 15.3 [˚C] | 15.3 [˚C] |

### 3.1.3.Simulation setup

#### 3.1.3.1. Model generation

In order to translate from the real system to the virtual model, some simplifications had to be made, i.e. only the interelectrode gap was considered, and all the other elements that affect this area of interest were included as input parameter or constrains. For example, fluid dynamics within the interelectrode gap were included instead of the including the pump into the simulation, or the workpiece was constrained to be static instead of adding the support bench into the model. A 3D model of the interelectrode gap was constructed using SolidEdge® and then imported to the FEA package, COMSOL Multiphysics®.

Two cases of the anodic dissolution of the internal face of SS316 pipes, of 3.81 cm diameter ($D_{workpiece}$) and 17 cm length, were simulated. The tool, a solid cylinder of stainless steel of diameter $D_{tool}$ and same length of the pipe, was considered static, feed rate $f$ =0 m/s, and placed at the inside the pipe and concentric to it, where

$$D_{tool} = D_{workpiece} - 2y \qquad \textbf{(3.1-1)}$$

, the interelectrode gap, $y$ **,** is the distance between the tool and the inner face of the pipe. 4 mm and 8 mm for case 1 and case 2 respectively.

The interelectrode gap was the area of interest for this work. The main objective of pECM Systems Ltd was to eliminate the flash left by the welding process and to achieve a reflective and bright surface finish at the interior of the pipes. Therefore, the geometry defined describes the shape of this interelectrode gap, especially near to the weld-flash. In Figure 3.1-1, the tool is the inner boundary (pink cylinder) and the pipe (blue cylinder) is the outer boundary of the model. Due to symmetry, not all the interelectrode gap had to be simulated, therefore only a section of 30 mm along the pipe and 30˚ of the circumference was modelled. This area covers the area close to the weld-step.

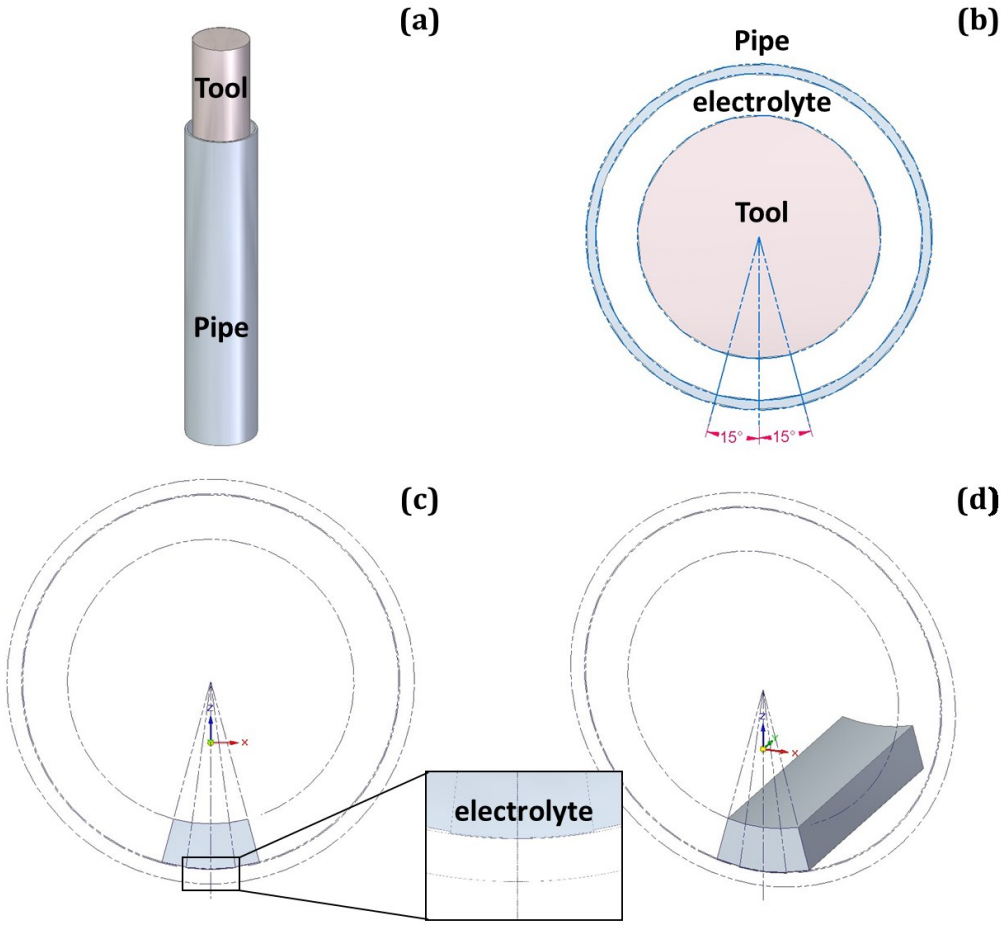


***Figure 3.1-1 Section of 30˚ modelled for the computational simulation of the ECM process. (a) Tool in pink and workpiece in blue. (b) Top view of the model, interelectrode gap in white. (c) 30˚ section of the circumference of the 4mm interelectrode gap modelled and close view of the weld-step. (d) 30˚ section of the circumference and 30 mm along the pipe of the 4 mm interelectrode gap modelled for the computational simulation of the ECM process in 3D perspective.***

#### 3.1.3.2. Model set up

COMSOL Multiphysics® was used for the development of the ECM simulation. For the present work, the boundary conditions appropriate to the real system were set up, and a fully coupled model including electric currents, moving boundaries, Joule heating, fluid flow and electrochemistry, as done in section 2.3, was constructed. The FE package has the advantage of being able to couple all the physics applied in a single solution.

The input parameters for this simulation were the workpiece material properties (Molar mass $M$, density $\rho$, and valence $zn_1$), the machining parameters (Voltage $V_1$, tool feed rate $f$, machining time $t$, and interelectrode gap $y$) and the electrolyte properties (Type, density $\rho_e$, conductivity $k_e$, flow rate $Q$, and inlet temperature $T_e$).

***Table 3.1-2 List of parameters for ECM on SS316 pipes simulation***

| Parameter | Case 1 (reflective and bright) | Case 2 (passivated) |
|---|---|---|
| Molar mass ( $M$ ) | 56.2e-3 [kg/mol] | 56.2e-3 [kg/mol] |
| Workpiece density ( $\rho$ ) | 7870 [kg/m^3] | 7870 [kg/m^3] |
| Valence ( $z_n$ ) | 3.5 | 2.1 |
| Voltage ( $V_1$ ) | 24 [V] | 24 [V] |
| Tool feed rate ( $f$ ) | 0 [m/s] | 0 [m/s] |
| Machining time ( $t$ ) | 10 [s] | 10 [s] |
| Interelectrode gap ( $y$ ) | 4 [mm] | 8 [mm] |
| Electrolyte type | $NaNO_3$ | $NaNO_3$ |
| Electrolyte density ( $\rho_e$ ) | $(-0.635T_e + 1371.5)$ [kg/m^3] | |
| Electrolyte conductivity ( $k_e$ ) | $(0.335T_e - 82.9)$ [S/m] | |
| Electrolyte flow rate ( $Q$ ) | 25 [l/min] | 10 [l/min] |
| Electrolyte inlet temperature ( $T_e$ ) | 288.45 [K] | 288.45 [K] |

From previous work [27], [118] a different surface finish was observed consistent with different dissolution mechanisms and different valencies. For the SS316 electrochemical dissolution, using $NaNO_3$ as electrolyte, a smooth and shiny surface is usually achieved with a high dissolution valence, whereas a rough and passivated surface is commonly found with a low dissolution valence. Therefore, for the simulation developed, the valencies assumed were 3.5

for case 1 and 2.1 for case 2 according to [27]. Table 3.1-2 present the list of parameters used for the simulation.

The electrolyte used was Sodium Nitrate ($NaNO_3$) whose $\rho_e$, and $k_e$, are temperature dependent, and follow equations (3.1-2) and (3.1-3) from [177]:

$$\rho_e = -0.635T_e + 1371.5 \qquad \textbf{(3.1-2)}$$

$$k_e = 0.335T_e - 82.9 \qquad \textbf{(3.1-3)}$$

The electrolyte was pumped into the system with a flow rate of 25 l/min for case 1 and 10 l/min for case 2, in such a fashion that the electrolyte flowed within the interelectrode gap providing the necessary ions to carry the electric current between the electrodes, but also flushing away the material ions (ECM products) dissolved from the workpiece and mitigating the temperature increase of the system. Due to the fact that only a section of 30 mm is modelled, an average velocity of the electrolyte had to be considered as an initial value. From fluid dynamics, this velocity depends on the electrolyte flow rate, $Q$, and the interelectrode gap size, $y$.

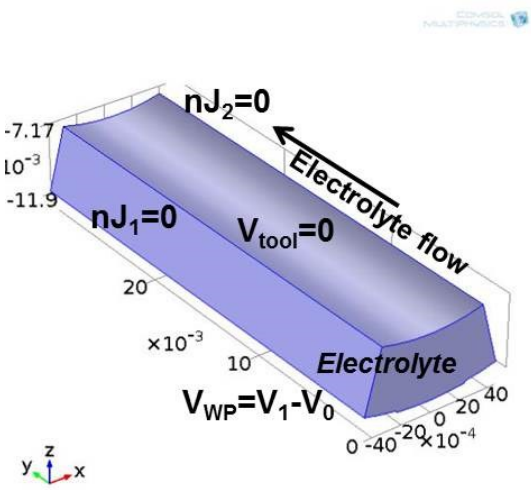


***Figure 3.1-2 Boundary conditions applied on the ECM simulation model. The gap presented is 4 mm.***

A stable and constant voltage, $V_1$=24 V, is applied in both cases, and each simulation lasted for 10 s. Voltage losses associated with the circuit elements are considered negligible. Figure 3.1-2 illustrates the boundary conditions used for these simulations.

#### 3.1.3.3. Meshing

A moving mesh in an Arbitrary Lagrangian-Eulerian (ALE) formulation was used. The tool is considered static, thus a fixed mesh was attached to the tool surface (upper boundary). The workpiece profile changes accordingly with the dissolution of the material, therefore a moving mesh was attached to it. The dissolution of material is dependent on the current density, $J$, according to equation (3.1-4) [60]:

$$\vec{v}_n = K_1 \vec{J}_n \qquad \textit{(3.1-4)}$$

, where $K_1$ is the electrochemical constant that depends on the workpiece material properties.

An adaptive mesh was constructed using the FE package. This mesh has the characteristic of being denser (finer) in the areas of high curvature, close to the weld-step, and coarser in the rest of the model. Figure 3.1-3 displays the meshed interelectrode gap, the elements can be readily noticed to become finer and the mesh denser in the area close to the weld step.

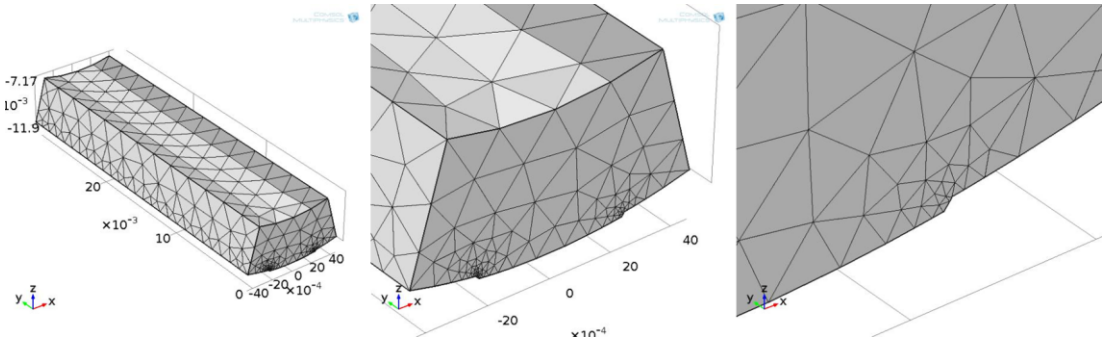


***Figure 3.1-3 Tetrahedral adaptive mesh example for an interelectrode gap of 4 mm at t=0 s using COMSOL Multiphysics®. Complete model and close views of the weld-step area where a denser (finer) mesh is present.***

### 3.1.4. Results and discussion

The final surface finish of the SS316 samples was dependant on the electrochemical dissolution of the oxide film that was formed on their surfaces [13], [27]. An electrochemically polished (reflective and bright) surface is usually associated with the random removal of atoms from the anode surface. A non- or partial breakdown of this film is a common problem during ECM, which results in passivated or non-uniform surface finish of the workpiece [26], [27], [41]. For the present evaluation, two samples with different surface finish were considered, being case 1 with a reflective and bright surface finish and case 2 with a passivated surface finish. Figure 3.1-4 presents the samples chosen.

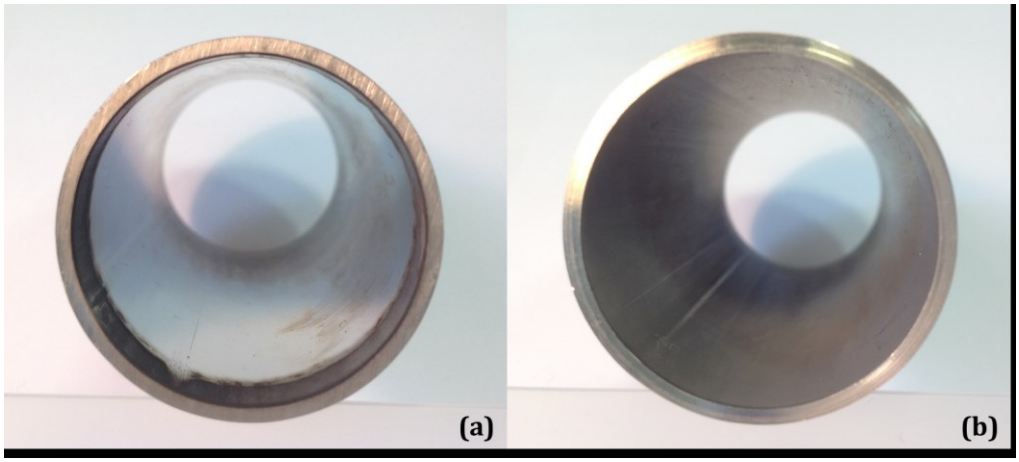


***Figure 3.1-4 Surface finish photograph of the samples for (a) Case 1, surface finish: reflective and bright, 24 V, 25 l/min, 4 mm gap, (b) Case 2, surface finish: passivated, 24 V, 10 l/min, 8 mm gap.***

#### 3.1.4.1. Electrolyte flow velocity

As mention before, the electrolyte was pumped from the top into the system and in between the electrodes at a flow rate $Q$=25 l/min and $Q$=10 l/min for case 1 and case 2 respectively. In the model presented here, the electrolyte inlet was the front face of the geometry and the outlet was the back face. The tool and the workpiece (pipe) were considered static walls. The workpiece surface profile deformation was too small to affect the electrolyte velocity profile, thus it was assumed negligible.

As a first approximation, a fully developed laminar flow was considered in both cases accordingly to [44], [140]. From previous work [26], [27], [60], [117], $Q$ higher than 20 l/min is usually needed for a reflective and bright surface finish. This is in agreement with the experimental results in section 2.2, where $Q$=25 l/min was associated with a reflective and bright surface finish, and $Q$=10 l/min was associated with a passivated surface finish. From the simulation results, a maximum velocity of 1.573 m/s and 1.092 m/s was achieved, Figure 3.1-5. These values correspond to a transitional flow not to a laminar flow as considered initially for the simulation. However, diverse studies [189], [195]–[197] have been developed to ascertain the actual flow regime in a concentric annular pipe similar to the array presented in this work, and an accurate solution is still under development.

In general, once the oxide film from the surface of the SS316 sample is broken by the ECM, the turbulences in the electrolyte flow promotes the removal of the oxide particles, as explained by [186] and in section 2.2.5.3. In a transitional flow however, a laminar boundary layer may be at

the vicinity of the oxide film, hence there is not turbulence to sweep away these particles, generating a non-uniform or a passivated surface finish as observed in Figure 3.1-4 (b). This is particularly evident in Figure 3.1-5 (b) where it can be observed that the flow profile was not fully developed until half way along the sample area of the geometry. Hence the low electrolyte velocity favours this laminar flow layer, and in turn promotes the accumulation of ECM dissolution products, temperature rise, electrolyte conductivity drop, and in consequence, the passivation of the sample.

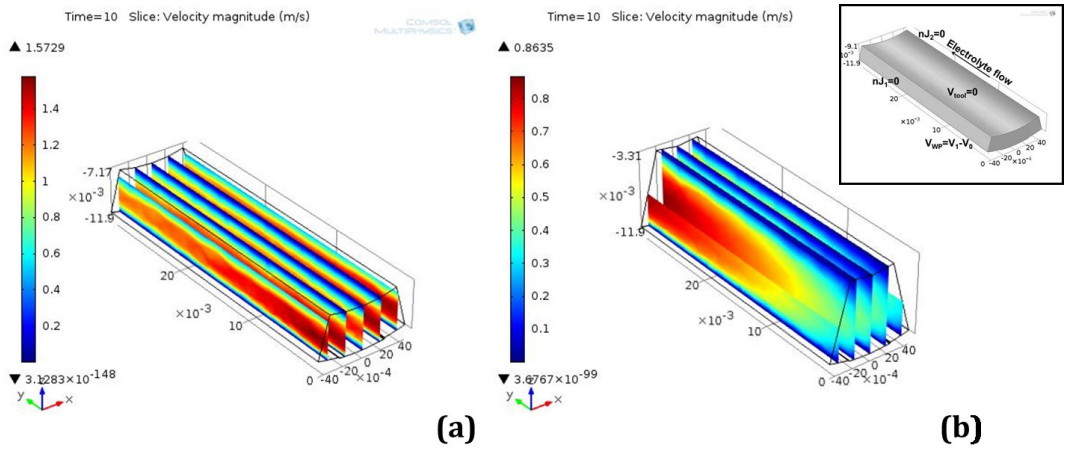


***Figure 3.1-5 Simulation results for the velocity magnitude at t=10 s for (a) Case 1, surface finish: reflective and bright, 24 V, 25 l/min, 4 mm gap. (b) Case 2, surface finish: passivated, 24 V, 10 l/min, 8 mm gap.***

#### 3.1.4.2. Joule heating

The passage of electric current between the electrodes through the electrolyte generates heat. The amount of heat is proportional to the current density, $J$, and the electrolyte electric conductivity, $k_e$. In turn $J$ is dependent on $V_1$ and $V_0$ according to equation (3.1-5),

$$J = \frac{k_e}{y}(V_1 - V_0) \qquad \textit{(3.1-5)}$$

, where $k_e$ is dependent on the electrolyte temperature. Figure 3.1-5 shows the boundary conditions applied on the simulation model.

Previous work [198], [199] demonstrated that electrochemical reactions depend strongly on electrolyte temperature. This is because the electrolyte conductivity is proportional to temperature [181], [191], and this is observed in Figure 3.1-6 for $NaNO_3$. Hence, with the

temperature increase due to Joule heating, the conductivity favour the electrochemical reactions. The objective is to have a $J$ high enough to keep stable the metal ion migration though the oxide film.

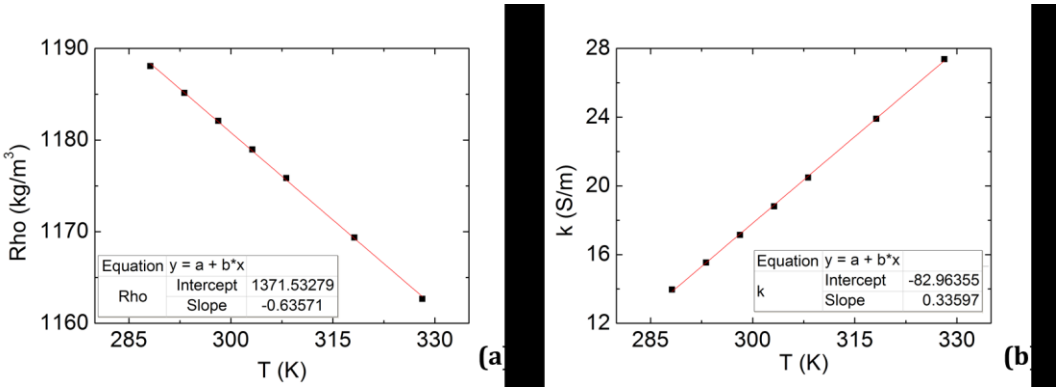


***Figure 3.1-6 Density (a) and conductivity (b) of $NaNO_3$ in relation with the temperature*** [177] ***at 22% mass percent. Fitting line (red line) and equation describing the density and behaviour are presented.***

In the experimental samples, a higher temperature in case 1 was associated with a reflective and bright surface finish, and in case 2 a lower temperature was associated with a passivated surface temperature. Additionally, as expected, there is linear increase of the electrolyte temperature as it flows along the length of the pipe. This difference between the inlet and outlet electrolyte temperature is expected to affect the electrochemical reactions and the surface finish uniformity of the samples, as shown in section 2.2.5.5.

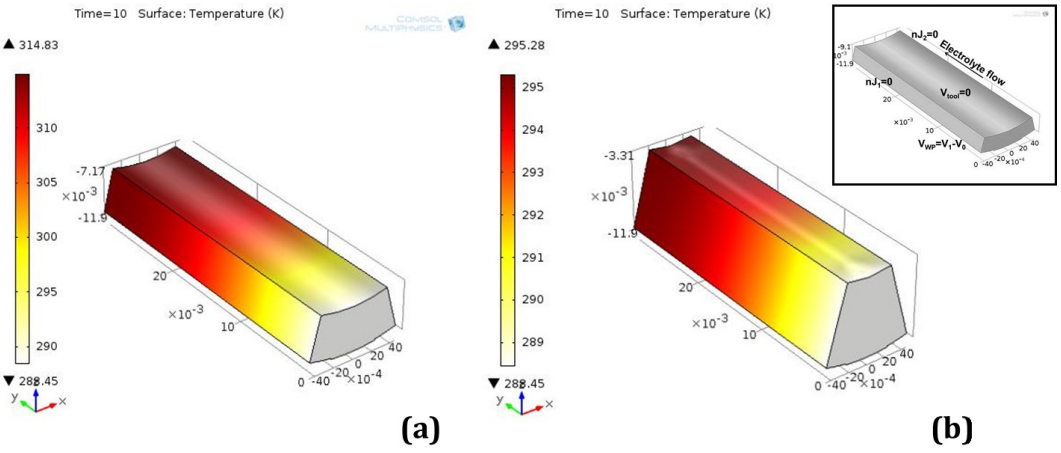


***Figure 3.1-7. Simulation results for the temperature distribution at t=10 s for (a) Case 1, surface finish: reflective and bright, 24 V, 25l/min, 4 mm gap. (b) Case 2, surface finish: passivated, 24 V, 10 l/min, 8 mm gap. Both with electrolyte inlet temperature $T_e$ =15.3 ˚C.***

#### 3.1.4.3. Electric currents

When the electrodes are connected to an external electric source, a current flow (migration of ions) between the electrodes and within the electrolyte is established. The current density, $J$, depends on the rate at which the ions arrive at their respective electrode and is proportional to the applied voltage, electrolyte conductivity, interelectrode gap and tool feed rate [83]. For the present work, a constant and uniform potential difference between the electrodes $V_1$=24 V, was applied in both cases. Additionally at the pipe (workpiece), an overpotential, $V_0$, was expected, that in turn was governed by $J$. For this evaluation, the overpotential behaviour was determined by experimental data from [42] and was parametrised according to equation (3.1-6):

$$V_0 = 2.514x10^{-5} J + 1.746 \qquad \textbf{(3.1-6)}$$

The overpotential was demonstrated to be one of the main parameters that are correlated with the surface finish in SS316 samples machined by ECM, as presented in section 2.2.5.1 and in the literature [13], [27], [41]. From experimental results, $V_0$ higher than 9 V is expected for a reflective and bright surface finish and $V_0$ lower than 6 V is associated with a passivated surface finish. The experimental results showed a $V_0$=8.9 V and a $V_0$=3.9 V for case 1 and case 2 respectively; however from the simulation results $V_0$=4.6 V and $V_0$ 3.1 V for case 1 and case 2 were attained respectively. Figure 3.1-8 displays the simulated electric potential distribution. Although the trend in the simulation results is as anticipated, i.e. a higher overpotential for case 1 and a lower overpotential for case 2, the numerical difference is significant.

This difference between the simulated and the experimental values could be attributed to possible electrical losses, differences in the power supply, gas generation and changes in the electrolyte concentration not considered in the simulation model. Additionally errors in measuring the parameters during the experimental ECM could also had been made. For example, the measurement of the experimental electric current was done in-situ using a data acquisition software provided by pECM systems Ltd®. This software indicated the current in time but did not store the data; therefore the values had to be registered by the user an instant before ECM is finished (t=10 s). This value was assumed as the current for all the process. Previous work [27] however, demonstrated a change on the current in time. This assumption may also be a cause for the discrepancy between the simulation and experimental results. Additionally, it is important to note that the $V_0$ behaviour was extracted experimentally by [42]

in samples of SS304, whose Cr content is higher by 2% than in SS316. The increase of Cr promotes the passivation of the samples.

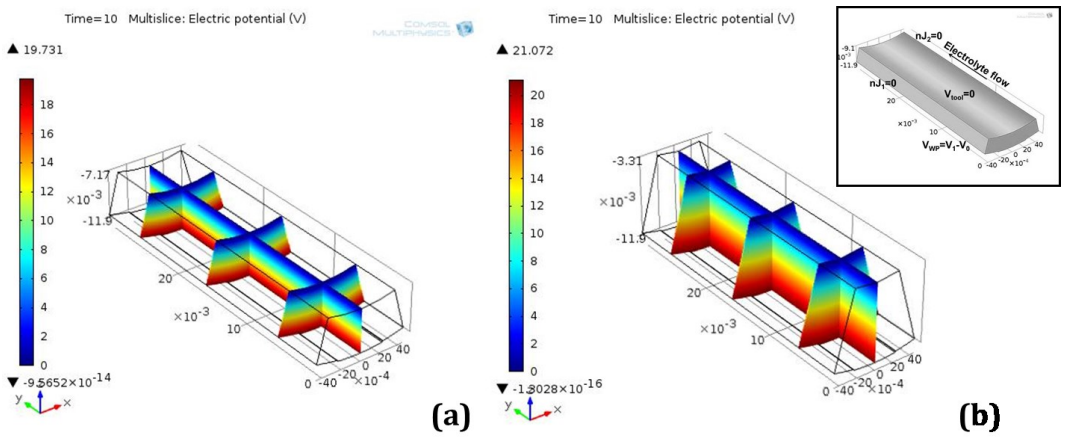


***Figure 3.1-8 Simulated electric potential for ECM on SS316 pipes, (a) Case 1, surface finish: reflective and bright, 24 V, 25l/min, 4 mm gap. (b) Case 2, surface finish: passivated, 24 V, 10 l/min, 8 mm gap. Both with electrolyte inlet temperature*** $T_e$ ***=15.3 ˚C.***

The experimental results show that for a reflective and bright surface finish a high current density ($J > 5x10^4$ A/m²) was needed. If the current density was lower a passivated surface finish was attained. Focussing on this current density, $J$, simulation results agree with the values expected from the experimental work, where $J = 6x10^4$ A/m² for case 1 and $J = 2.7x10^4$ A/m² for case 2. As expected, a higher $J$ is observed for case 1 than for case 2. Figure 3.1-9 illustrates the relationship between the current density, the overvoltage and the surface finish. It is important to highlight that the electrolyte flow of the non-uniform samples (blue rhomboids in Figure 3.1-9) is less than 25 l/min, meaning that the heat and the workpiece dissolution products are not well dissipated, affecting $J$ and in consequence the ECM behaviour.

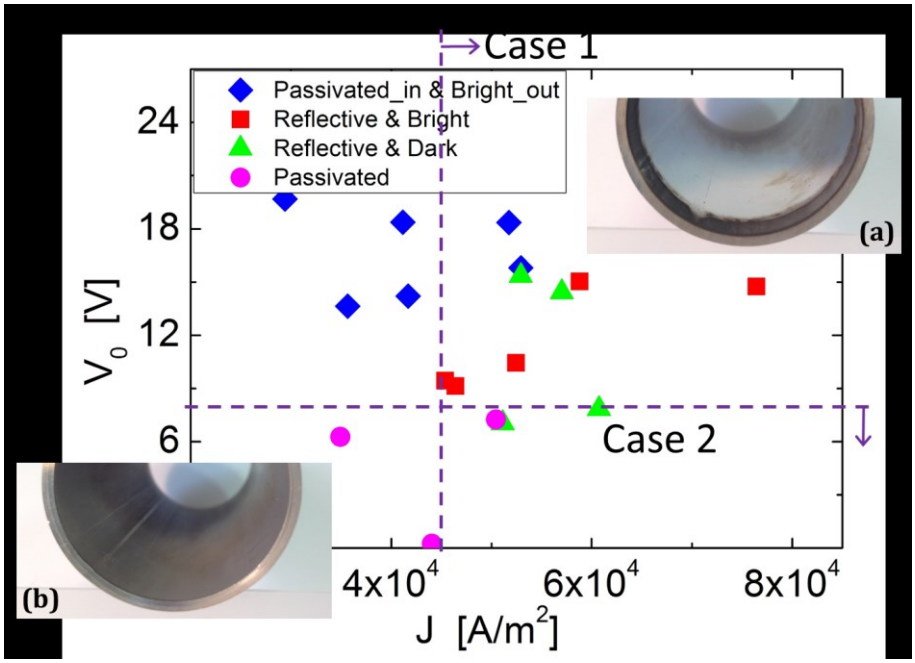


***Figure 3.1-9 Experimental $J$ and $V_0$ for ECM on SS316 pipes, (a) Case 1, surface finish: reflective and bright, 24 V, 25l/min, 4 mm gap. (b) Case 2, surface finish: passivated, 24 V, 10 l/min, 8 mm gap. Both with electrolyte inlet temperature $T_e$ =15.3 ˚C.***

Figure 3.1-10 presents the current density simulation results. It can be observed that there is a higher $J$ in the area where the tool and the pipe are closer (external parts of the graphs in Figure 3.1-10), than in the area of the weld-step. Moreover, in the corners of the weld-step the current density reaches a peak. This behaviour has been explained in previous work [44], [191], where "sharp" corners provoke an increase in the current density, leaving behind ridges on the workpiece surface. Additionally, due to the adaptive mesh used in the FE method, very small elements can also modify the results of the current density, which is dependent on the area where the current is applied.

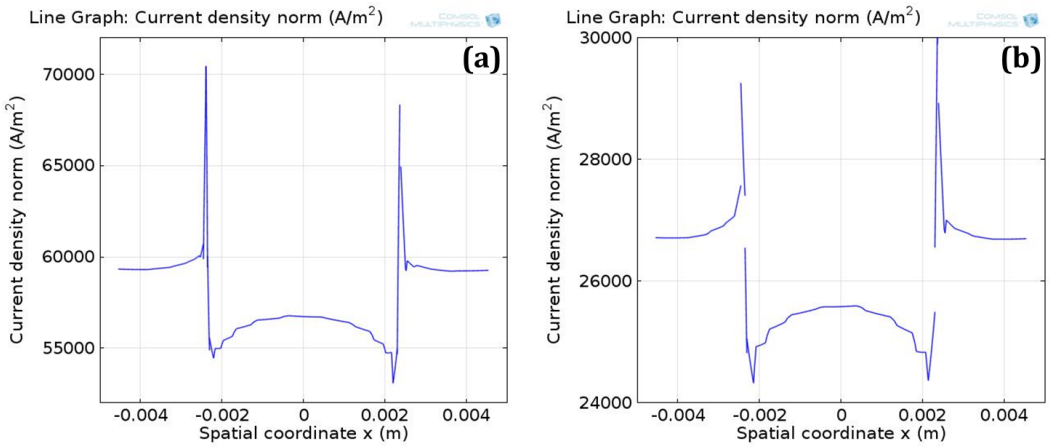


***Figure 3.1-10 Current density simulation results for ECM on SS316 pipes, (a) Case 1, surface finish: reflective and bright, 24 V, 25l/min, 4 mm gap. (b) Case 2, surface finish: passivated, 24 V, 10 l/min, 8 mm gap. Both with electrolyte inlet temperature $T_e$ =15.3 ˚C.***

### 3.1.5. Conclusions

In this section, the simulation and experimental results of two samples of SS316 machined by ECM were compared. A reflective and bright surface finish in case 1 and a passivated surface finish in case 2 were attained experimentally by ECM (section 2.2). For this simulation, the same machining parameters used for the experimental work, i.e. $V_1$ =24 V, $T_e$ =15.3 ˚C, $t$ =10 s, were applied into the ECM simulation model developed in section 2.3. Different gaps, 4 mm and 8 mm, and electrolyte flow rate, $Q$ =25 l/min and $Q$ =10 l/min, for case 1 and case 2 respectively were considered. Moreover, from literature [27] it is known that the average dissolution valence, $z_{n1}$, has a high effect on the surface finish, hence a high dissolution valence ($z_{n1}$ =3.5) was used for case 1 and a low dissolution valence ($z_{n1}$ =2.1) was used for case 2.

The results show a good agreement between the simulation and the experimental work. Simulation results in terms of the current density ($J = 6x10^4$ A/m² for case 1 and $J = 2.7x10^4$ A/m² for case 2) were within the same order of magnitude and trend ($J$ over 5x10⁴ A/m² for case 1 and below for case 2) as experimental and published works. However there were some discrepancies in the overpotential obtained, where the simulation values were lower than expected, about 4 V for case 1 and 0.8 V for case 2. Nevertheless the results followed the expected trend, i.e. higher overpotential and current density for case 1 than for case 2, highlighting the electrochemical effect of the overpotential on the results attained. A reason for these discrepancies might be that the efficiency of the process, the change in the electrolyte concentration and the gas generation were not considered in the ECM simulation model. For

further work, these side reactions should be acknowledged in order to enhance the simulation results; however more experimental work would be needed in order to verify it. This experimental work should also include in time and in situ measurements of the ECM parameters, such as current and temperature along the pipe.

Additionally, the objective of the prediction of the surface finish by the simulation model was achieved. By harvesting the driving parameters of the ECM simulation data, i.e. electrolyte velocity and temperature, overpotential and current density, a good prediction of the surface finish was successfully attained.

Therefore the developed simulation model could be used as a tool for forecasting the behaviour of ECM, the final geometry and surface finish of the sample. Some improvement in the model however can still be done in order to enhance the accuracy of the results and to apply it with different materials and electrolytes.

## 3.2. *Validation of the ECM simulation model: case 3*

### 3.2.1. Introduction

One of the advantages of the present simulation model is the possibility of setting up or modifying the parameters of the ECM process if necessary. For the validation in case 3, the ECM simulation model was applied for the same parameters as on case 1 but using Sodium Chloride (NaCl) as electrolyte instead of Sodium Nitrate (NaNo3). This is an example of the versatility of the developed ECM simulation model. It is well known that the type of electrolyte strongly influences the ECM behaviour and outcome. The machining parameters of case 1 remained the same, e.g. voltage applied, tool feed rate, machining time, interelectrode gap, and electrolyte flow rate, and only the electrolyte input parameters are modified accordingly with the use of NaCl as electrolyte. NaCl is characterised as being very corrosive, but also for having a more stable conductivity than $NaNO_3$. As expected higher current densities were achieved using NaCl, however the temperature of the system also increased. This may have an effect on the surface finish of the sample. The results were compared with published experimental data and a good agreement was found, but more experimental data is still needed in order to enhance the simulation model and its verification.

### 3.2.2. Simulation setup

#### 3.2.2.1. Model generation

The same geometry used for case 1 in section 3.1 is used for the case 3 validation, Figure 3.1-1. A 3D model of the 4 mm interelectrode gap was constructed using SolidEdge® and then imported to the FEA package, COMSOL Multiphysics®. The tool was a static solid cylinder of stainless steel, which was placed inside and concentric to the workpiece, a SS316 pipe.

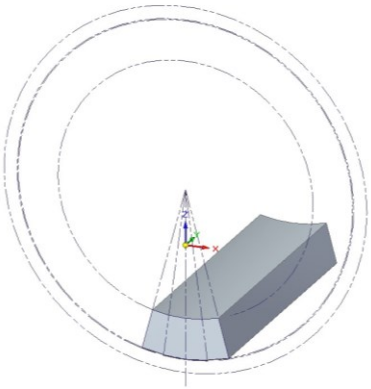

***Figure 3.2-1 Section of 30˚ of the circumference and 30 mm along the pipe of the 4mm interelectrode gap modelled for the computational simulation of the ECM process in 3D perspective.***

The interelectrode gap is 4 mm, and it is the area of interest for the present work, especially in the area close to the weld-step. In Figure 3.2-1, shows the modelled section of 30 mm along the pipe and 30° of the circumference of the 4mm interelectrode gap. This area covers the area close to the weld-step.

#### 3.2.2.2. Model set up

COMSOL Multiphysics® was used for the development of the ECM simulation. For the present work, the boundary conditions appropriate to case 1 were set up, but NaCl was added as electrolyte instead of $NaNO_3$. A fully coupled model including electric currents, moving boundaries, Joule heating, fluid flow and electrochemistry was built.

The input parameters for this simulation were the workpiece material properties ( $M$ , $\rho$ , and $zn_1$), the machining parameters ( $V_1$, $f$ , $t$ , and $y$ ) and the electrolyte properties ( $\rho_e$ , $k_e$ , $Q$ , and $T_e$ ).

The electrolyte used was Sodium Chloride (NaCl) whose density $\rho_e$ , and conductivity $k_e$ , are also temperature dependent, and follow equation (3.2-2) and (3.2-3) from [181], [182]:

$$\rho_e = -0.368T_e + 1145.5 \qquad \textit{(3.2-1)}$$

$$k_e = 0.573T_e - 149.9 \qquad \textit{(3.2-2)}$$

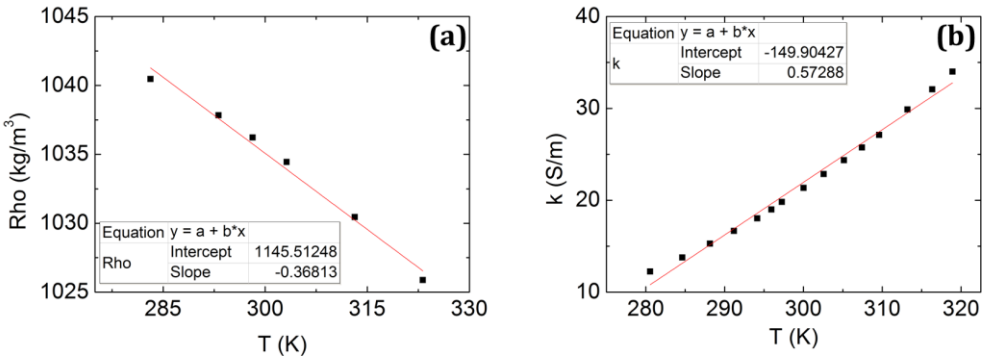


***Figure 3.2-2 Density (a) and conductivity (b) of NaCl in relation with the temperature*** [181], [182] ***The solid line shows linear best fit and corresponds to equation 3.2-1 and 3.2-2.***

The electrolyte was pumped into the system with a flow rate of 25 l/min, and due to the fact that only a section of 30 mm was modelled, an average velocity of the electrolyte was considered as an initial value. This velocity depends on $Q$, and $y$.

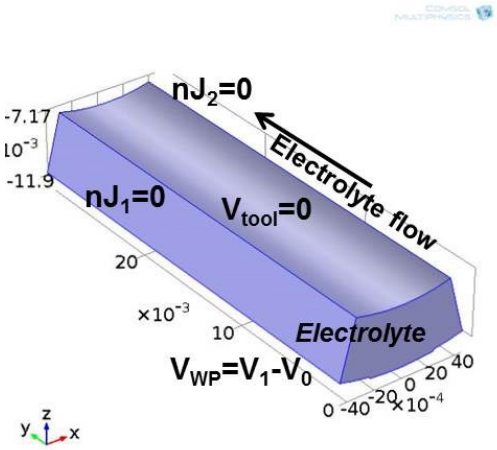


***Figure 3.2-3 Boundary conditions applied on the ECM simulation model. The gap presented is 4 mm.***

A stable and constant voltage $V_1$=24 V was applied, and the simulation lasted for 10 s. Voltage losses associated with the circuit elements were considered negligible. Figure 3.2-3 shows the boundary conditions used for the present example. Table 3.2-1 present the list of parameters used for the simulation.

***Table 3.2-1 List of parameters for ECM on SS316 pipes simulation with NaCl as electrolyte***

| Parameter | Case 3<br>(NaCl as electrolyte) |
|---|---|
| Molar mass ( $M$ ) | 56.2e-3 [kg/mol] |
| Workpiece density ( $\rho$ ) | 7870 [kg/m^3] |
| Valence ( $z_n$ ) | 3.5 |
| Voltage ( $V_1$ ) | 24 [V] |
| Tool feed rate ( $f$ ) | 0 [m/s] |
| Machining time ( $t$ ) | 10 [s] |
| Interelectrode gap ( $y$ ) | 4 [mm] |
| Electrolyte type | NaCl |
| Electrolyte density ( $\rho_e$ ) | $(-0.368T_e[K]+1145.5)$ [kg/m^3] |

| | |
|---|---|
| Electrolyte conductivity ( $k_e$ ) | ( $0.573T_e - 149.9$ ) [S/m] |
| Electrolyte flow rate ( $Q$ ) | 25 [l/min] |
| Electrolyte inlet temperature ( $T_e$ ) | 288.45 [K] |

#### 3.2.2.3. Meshing

As in case 1, the same adaptive moving mesh in ALE formulation was used. The tool was considered static, thus a fixed mesh was attached to the tool surface (upper boundary). The workpiece profile changes according with the dissolution of the material, therefore a moving mesh was attached to it. The dissolution of material was dependent on the current density $J$, according to equation (3.2-4) [60]:

$$\vec{v}_n = K_1 \vec{J}_n \qquad \textbf{(3.2-3)}$$

, where $K_1$ is the electrochemical constant that depends on the workpiece material properties.

### 3.2.3. Results and discussion

#### 3.2.3.1. Electrolyte flow velocity

The electrolyte was pumped from the top into the system and in between the electrodes at a flow rate $Q$=25 l/min. The electrolyte inlet was the front face of the 3D geometry and the outlet was the back face. The tool and the workpiece (pipe) were considered as static walls. The workpiece surface profile deformation due to the ECM dissolution was considered too small to affect the electrolyte velocity profile, thus it was assumed negligible. Figure 3.2-4 presents the electrolyte velocity profile for this case. From previous work [26], [27], [60], [117] under low $Q$ (8 l/min) a high dissolution valence was obtained ($z_n$ =3.5) leading to a smooth, shiny surface. And under high $Q$ (20 l/min), a low dissolution valence was obtained ($z_n$= 2.1), which is usually characteristic of a dull, rough, pitted surface.

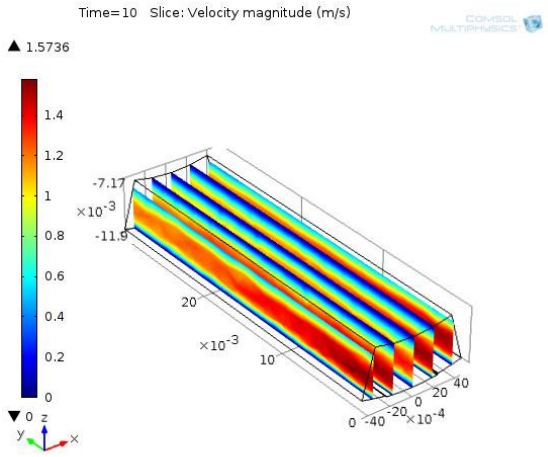


***Figure 3.2-4 Simulation results for the velocity magnitude at t=10 s for case 3, at 24 V, 25l/min, 4 mm gap and NaCl as electrolyte.***

#### 3.2.3.2. Joule heating

The passage of electric current between the electrodes through the electrolyte generates heat. The amount of heat released is proportional to $J$ and $k_e$. In turn $J$ is dependent on $V_1$ and $V_0$, and $k_e$ is dependent on the electrolyte temperature. Figure 3.2-3 shows the boundary conditions applied on the simulation model. Changing the electrolyte from $NaNO_3$ to NaCl, will affect $J$, and in consequence the Joule heating of the system.

$$J = \frac{k_e}{y}(V_1 - V_0) \qquad \textbf{(3.2-4)}$$

, where $k_e$ is in direct relation with $J$, which is expected to be higher in case 3 (where NaCl was used as electrolyte) than in case 1 (where $NaNO_3$ was the electrolyte); hence, setting the rest of the parameters the same as in case 1, the temperature was also expected to be higher. This is depicted on Figure 3.2-5. Additionally, it can be observed that the electrolyte temperature increases linearly as the electrolyte flows along the length of the pipe.

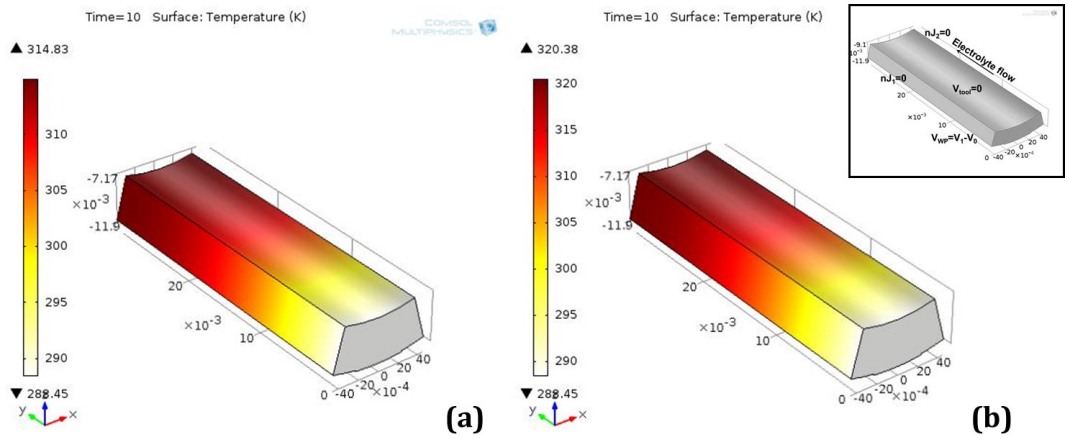


***Figure 3.2-5 Temperature distribution simulation results for ECM on SS316 pipes at t=10 s for 24 V, 25l/min, 4 mm gap, and $T_e$=15.3 ˚C, using (a) Case 1, $NaNO_3$. (b) Case 3, NaCl.***

#### 3.2.3.3. Electric currents

Current density, $J$, depends on the rate at which ions arrive at the respective electrode, and is proportional to $V_1$, $k_e$, $y$, and $f$ [83]. For the present work, a constant and uniform potential difference between the electrodes, $V_1$=24 V, was applied, and at the workpiece the $V_0$ behaviour was determined by experimental ECM on samples of SS304, according to [42] and parametrised into equation (3.2-6):

$$V_0 = 2.25x10^{-5} J + 0.68 \qquad \textit{(3.2-5)}$$

From experimental work [27] in SS316 samples machined by ECM with NaCl as electrolyte and $Q$ over 20 l/min, $V_0$ at the workpiece should be between 4.4 and 6.7 V. Figure 3.2-6 displays the electric potential distribution and it can be observed that $V_0$=3.7 V. As expected from [114] this value was lower than that obtained using $NaNO_3$ as electrolyte (4.6 V), but it was also lower than expected from the literature.

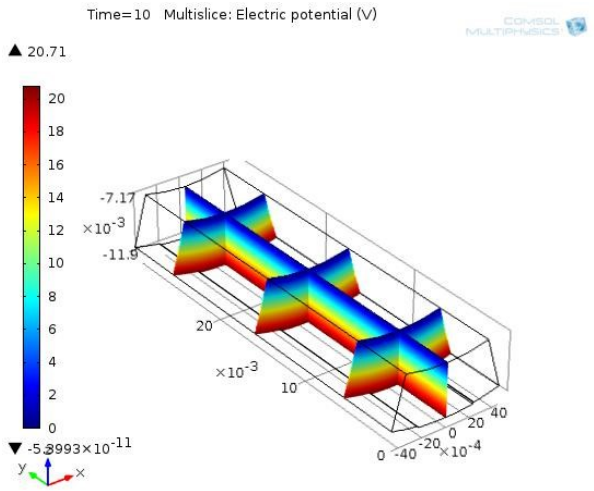


***Figure 3.2-6 Simulated electric potential for ECM on SS316 pipes at t=10 s for 24 V, 25l/min, 4 mm gap, and $T_e$=15.3 ˚C, using NaCl.***

Focussing on the current density $J < 5.5x10^4$ A/m² was expected for NaCl, and according to equation (3.2-5), $J$ was also expected to be higher in case 3 than in case 1. The results agree with this and it can be observed in Figure 3.2-7

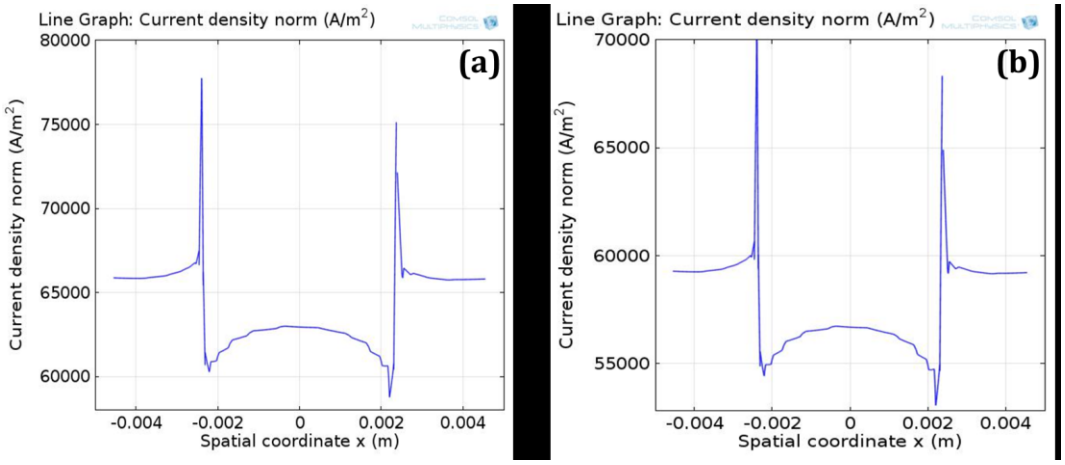


***Figure 3.2-7 Current density simulation results for ECM on SS316 pipes, at t=10 s for 24 V, 25l/min, 4 mm gap, and $T_e$=15.3 ˚C, using (a) Case 3, NaCl, (b) Case 1, $NaNO_3$.***

### 3.2.1. Conclusions

In order to demonstrate the versatility of the ECM simulation model developed in this work, the 3D ECM simulation model was applied using NaCl as electrolyte instead of $NaNO_3$. The electrolyte (NaCl or $NaNO_3$) type has a strong influence in the ECM behaviour, e.g. the current density when NaCl is used as electrolyte, increased by more than 5x10³ A/m², for the same

parameters when $NaNO_3$ was used. In consequence, the temperature of the system was also affected.

Results agree with the published literature data; however the overpotential is lower than expected by approx. 0.5 V. This discrepancy can be explained by the difference in size between the interelectrode gap used for this validation (4 mm) and the ones used in the published works (0.8 mm), and as before, the current efficiency, the electrolyte concentration and the gas generation was not included in the simulation model and affect the results attained. Despite the variations between the simulation results and the expected ones, the present simulation model has demonstrated to be useful for the understanding and forecast of the ECM behaviour. There is still experimental work needed in order to have enough data for the improvement and further development of this ECM simulation model, and this is a motivation for further work in the ECM study.

## 3.3. *Validation of the ECM simulation model: case 4*

### 3.3.1. Introduction

In order to comply with the needs of the industrial partner, i.e. to eliminate the weld step of the internal face of the pipe, this ECM simulation model has the objective of predicting the final geometry of the workpiece. The 3D ECM simulation model developed in section 2.3 has the advantage of allowing the prediction of this final workpiece. Moreover this model allows the setting up or modification of the ECM simulation parameters in order to ensure that the final geometry will be as close as possible to the one expected for the client. In the present section, the 3D ECM simulation model developed in this thesis was applied for simulating ECM on the internal face of a SS316 pipe whose surface finish after the process was reflective and bright (case 1 in section 3.1). The same machining parameters, e.g. voltage applied, tool feed rate, interelectrode gap and electrolyte flow rate, were used, but the machining time was modified. For this validation (case 4 hereafter), the simulation was run until the final geometry was smooth, i.e. the weld step was eliminated or reduced enough without compromising the geometry of the rest of the pipe. The aim was to ascertain an optimum machining time where there was balance between a good geometry and the time needed to be achieved.

The use of this ECM simulation model has the advantage of avoiding the multiple iterative experimental tests usually associated to find this optimum machining time. Furthermore, this model could be a tool for solving the problems that may occur during the process before the experimental work. However, further experimental data still is needed in order to enhance the simulation model and its verification.

### 3.3.2. Simulation setup

#### 3.3.2.1. Model generation

The same geometry used for case 1 in section 3.1 was used for this validation. A 3D model of the interelectrode gap was constructed using SolidEdge® and imported to the FEA package, COMSOL Multiphysics®. The tool was a static solid SS cylinder, placed at the inside and concentric to a SS316 pipe (workpiece). The area of interest for this simulation was the interelectrode gap, especially in the area close to the weld-step. The objective was to reduce or eliminate this weld step. Figure 3.3-1 presents the modelled section of 30 mm along the pipe and 30˚ of the circumference of the 4 mm interelectrode gap. This area covers the weld step. Tool and workpiece are the top and bottom boundaries of the model respectively.

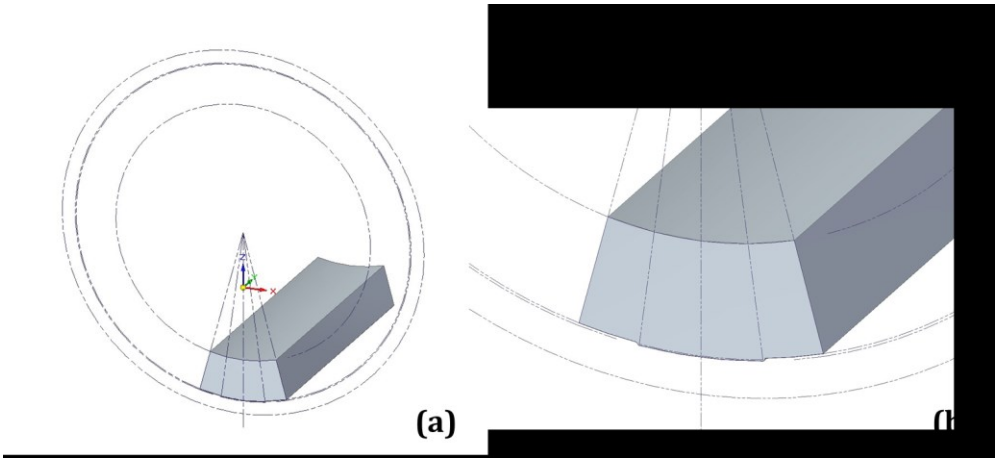


***Figure 3.3-1 Section of 30° of circumference and 30 mm along the pipe of the 4 mm interelectrode gap modelled for the computational simulation of the ECM process in 3D perspective.***

#### 3.3.2.1. Model set up

COMSOL Multiphysics® was used for the development of the ECM simulation. The boundary conditions and input parameters, same as in case 1, were the workpiece material properties ($M$, $\rho$, and $zn_1$), the machining parameters ($V_1$ and $y$) and the electrolyte properties ($\rho_e$, $k_e$, $Q$, and $T_e$). The simulation was run for a machining time, $t$, long enough to reduce the weld step without compromising the ECM process and the rest of the workpiece. Table 3.3-1 present the list of parameters used for this simulation, and Figure 3.3-2 the boundary conditions considered. A fully coupled model including moving boundaries, electric currents, fluid flow, heat transfer and electrochemistry was developed.

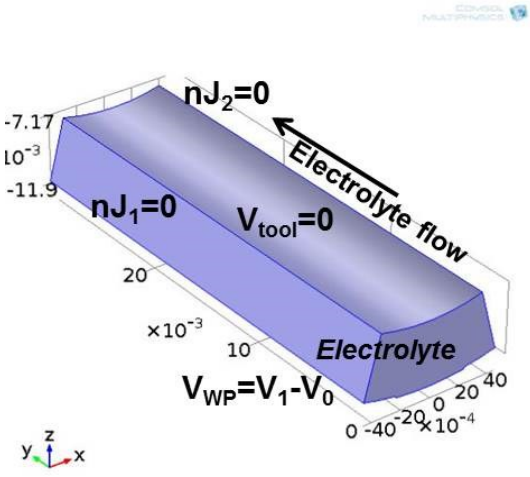


***Figure 3.3-2 Electrolyte model of y=4 mm, showing the boundary conditions used for the ECM tool-design.***

***Table 3.3-1 List of parameters for ECM on SS316 pipes simulation***

| Parameter | Case 4 (reflective and bright) |
|---|---|
| Molar mass ( $M$ ) | 56.2e-3 [kg/mol] |
| Workpiece density ( $\rho$ ) | 7870 [kg/m^3] |
| Valence ( $z_n$ ) | 3.5 |
| Voltage ( $V_1$ ) | 24 [V] |
| Tool feed rate ( $f$ ) | 0 [m/s] |
| Machining time ( $t$ ) | 10 [s] |
| Interelectrode gap ( $y$ ) | 4 [mm] |
| Electrolyte type | $NaNO_3$ |
| Electrolyte density ( $\rho_e$ ) | ( $-0.635T_e + 1371.5$ ) [kg/m$^3$] |
| Electrolyte conductivity ( $k_e$ ) | ( $0.335T_e - 82.9$ ) [S/m] |
| Electrolyte flow rate ( $Q$ ) | 25 [l/min] |
| Electrolyte inlet temperature ( $T_e$ ) | 288.45 [K] |

The electrolyte used was Sodium Nitrate ($NaNO_3$) whose $\rho_e$, and $k_e$, are temperature dependent, and follow equations (3.3-2) and (3.3-3) from [177]:

$$\rho_e = -0.635T_e + 1371.5 \qquad \textbf{(3.3-1)}$$

$$k_e = 0.335T_e - 82.9 \qquad \textbf{(3.3-2)}$$

The electrolyte was pumped into the system with a flow rate of 25 l/min. A stable and constant voltage $V_1$ =24 V was applied and the simulation lasted for $t$ =210 s. Voltage losses associated with the circuit elements were considered negligible.

#### 3.3.2.2. Meshing

As in previous cases, an adaptive moving mesh in ALE formulation was used. A fixed mesh was attached to the tool surface (upper boundary) and the workpiece profile (lower boundary) changed according with the dissolution of the material, therefore a moving mesh was attached to it. The change in the workpiece profile was dependent on the current density $J$, according to equation (3.3-3) [60]:

$$\vec{v}_n = K_1 \vec{J}_n \qquad \textbf{(3.3-3)}$$

, where $K_1$ is the electrochemical constant that depends on the workpiece material properties.

### 3.3.3. Results and discussion

The workpiece profile displacement is displayed in Figure 3.3-3. As expected, higher dissolution can be observed in the external areas, where the tool (blue surface in Figure 3.3-3 (a)) and workpiece (red surface Figure 3.3-3 (a)) were closer, and a lower dissolution was achieved on the central area where the electrode were farther. Figure 3.3-3 (b) shows a closer view of this smoothing of the surface at for $t$ =210 s. Figure 3.3-3 (c) depicts the front view of the workpiece profile at intermediate steps from 0 to 210 s. From Figure 3.3-3 (c) however, it is evident that the complete smoothing of the workpiece was not yet achieved. A closer view of the weld step is presented in Figure 3.3-3 (d). The weld step is evidently smaller, however there is also a dissolution of the rest of the workpiece. This dissolution at 210 s is of 0.25 mm. The pipes used as workpiece had a standard wall thickness of 1.65 mm, hence the wall loss is already 15% and to carry on with the dissolution of material would compromise its performance. Moreover, 210s of machining time is already 20 times longer than the usual machining time for these particular samples. Another important factor to consider is that the material dissolution is inversely related to the interelectrode gap. Hence, as the dissolution proceeds, the gap keeps increasing with time, reducing the efficiency of the process.

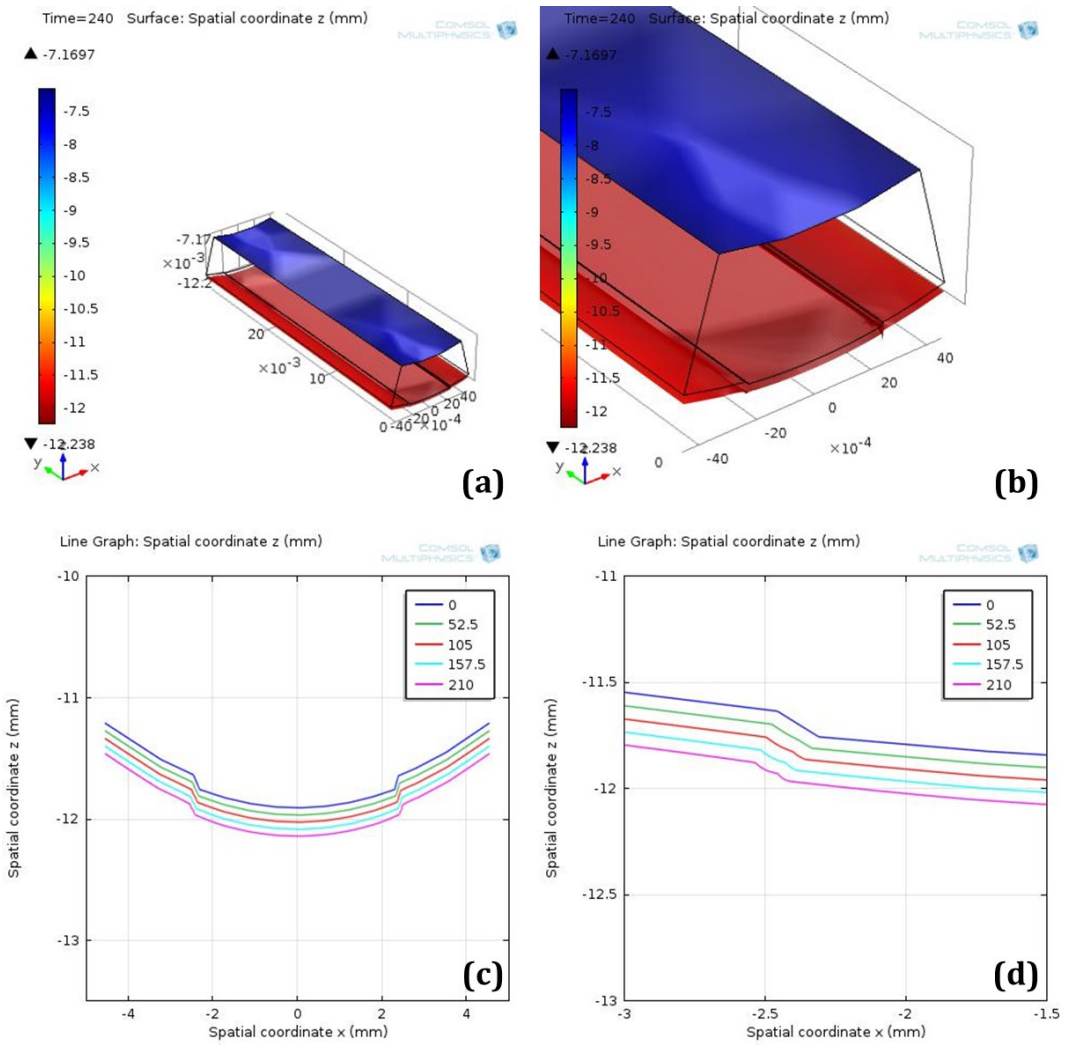


***Figure 3.3-3 Deformed profile of the interelectrode gap of 4 mm, $V_1$ =24 V and $T_e$ =15.3 ℃, at t = 210 s: (a) tool (blue) and workpiece (red), (b) closer view of the tool and workpiece. For (a) and (b), the colour scale represent the position of the surfaces in the global space; (c) change in spatial coordinates of the workpiece at t =0, 52.5, 105, 157.5, and 210 s, (d) closer view of the weld step at the same times than (c).***

Figure 3.3-4 presents a comparison between the workpiece profile at 10 s, which is the experimental machining time used in case 1, and the simulation time of 210 s in case 4. It can be observed that the workpiece profile in case 4 is smoother than the one in case 1, complying with the objective of this work. However it can also observed that there is a small kink in the lower green line at 210 s. A plausible explanation of this imperfection could be the concentration of current density lines (perpendicular to the tool profile) in this area, or that the meshing resolution was not good enough in order to copy accurately the tool profile.

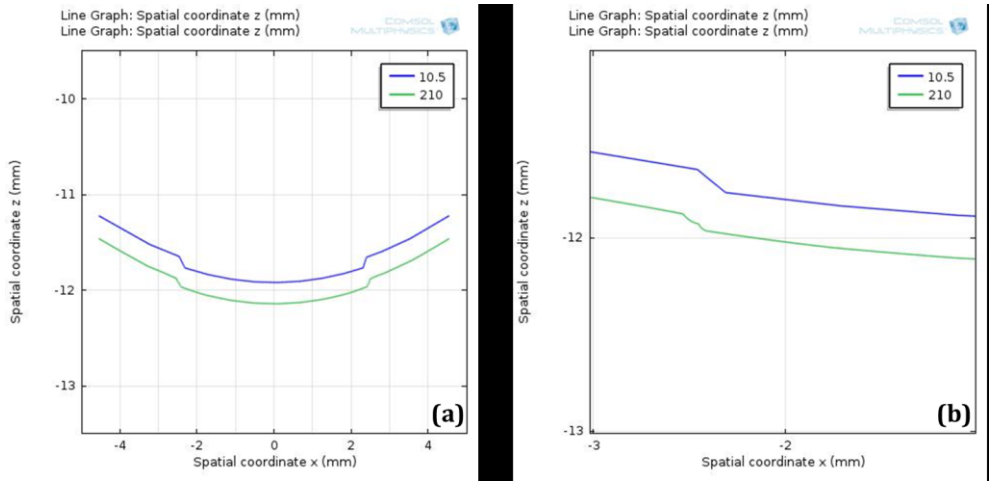


***Figure 3.3-4 Comparison of the workpiece profiles between case 1 (blue upper line) and case (4) (green lowe line).***

As done in industry experimentally, the change in the tool profile can be done and is expected to have an effect on the surface profile attained. In the experimental tests of section 2.2, the tool was varied accordingly in order to have an interelectrode gap of 2mm, 4mm and 8 mm. Hence, for this section, the interelectrode gap was also varied but this time inside the virtual environment. The objective was to identify the effect of the interelectrode gap on the resulting workpiece profile if the ECM was carried out at different gaps and for longer time. The results would help in determining the tool dimensions that would better provide the workpiece desired. This approach would be costly and time consuming if done experimentally. Additionally, the virtual work could identify and prevent errors during the experimental tests.

Figure 3.3-5 shows the workpiece profiles when the electrolyte gap is varied from 2mm (Figure 3.3-5 (a) and (b)), 4 mm (Figure 3.3-5 (c) and (d)), and 8 mm (Figure 3.3-5 (e) and (f)). As expected, ECM had better results when a smaller gap was used. However, this is limited by the practical factors during the ECM process, i.e. the correct set up and alignment of the tool inside the pipe.

Additionally, a larger simulation time could also be needed for an accurate smoothing of the workpiece profile, but as it can be observed in Figure 3.3-5 (f), the small defects in the tool geometry are also copied on workpiece, hence there are areas where the dissolution was concentrated and are evident after 210 s. This is in agreement with the high current density also observed in this area (side walls of the weld step) as presented in section 2.3.4.1

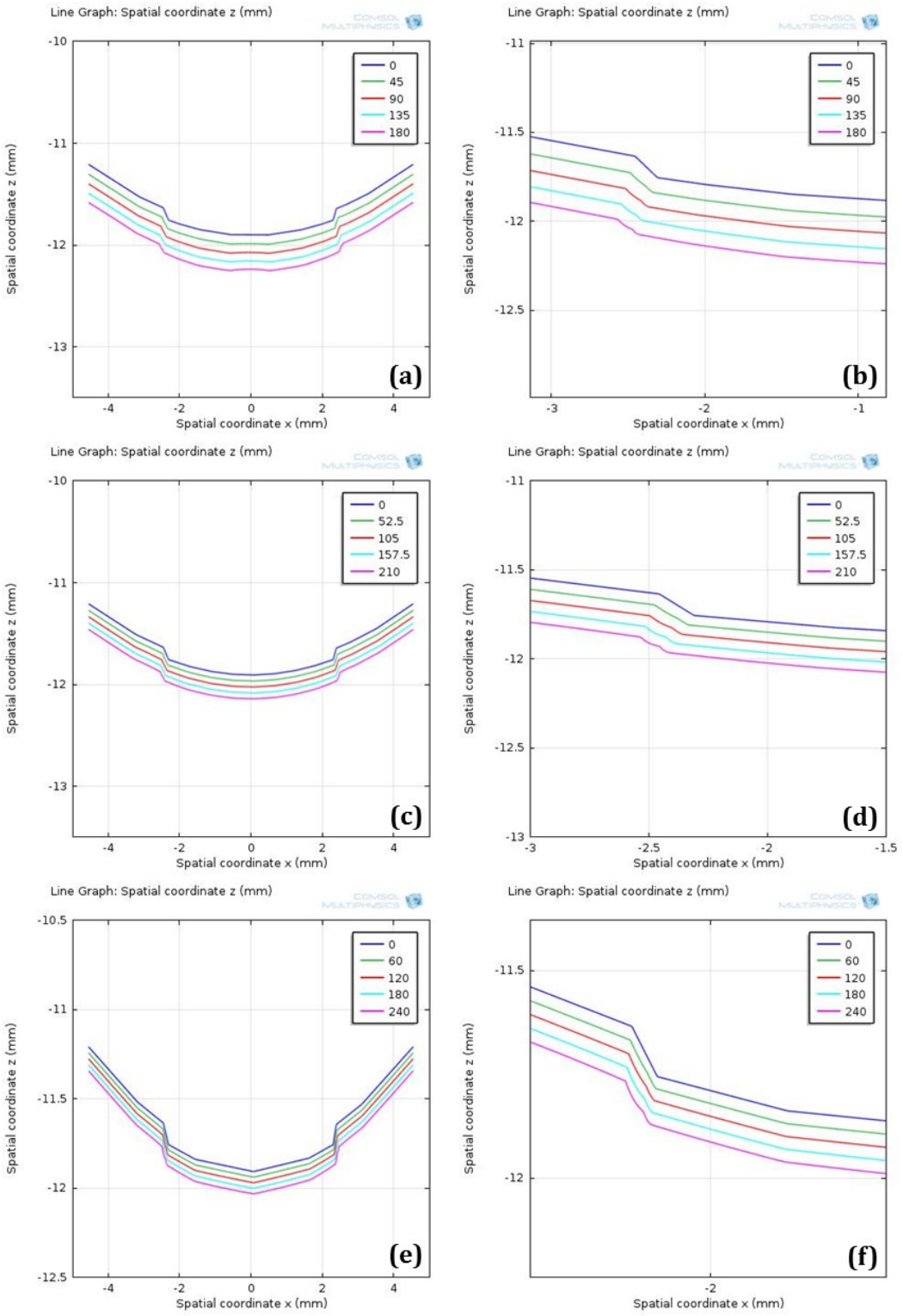


***Figure 3.3-5 Workpiece profiles when the electrolyte gap is varied from 2mm ((a) and (b)), 4 mm ((c) and (d)), and 8 mm ((e) and (f)).***

Results show that the tool-design problem, even in its simpler version when just a change in the diameter was done, is a more demanding problem that the prediction of the workpiece profile. Additionally, this simulation requires experimental validation, in order to verify its accuracy.

### 3.3.4. Conclusions

This section presents the application of the 3D ECM simulation model for machining of the internal face of a SS316 pipe under the same machining conditions of case 1, but for a longer machining time. The simulation was run until the final geometry was smooth, i.e. the weld step was reduced enough, without compromising the geometry and performance of the rest of the pipe. The simulation of the ECM process was developed applying $V_1$=24 V, $T_e$=15.3 °C, and $Q$=25 l/min. Results show that the objective of smoothing the workpiece is possible, but requires an increment in the machining time of over 2000%, and the dissolution of material is of 15% of the wall thickness, compromising the performance of the pipe.

A variation on the electrolyte gap, i.e. to have a smaller gap by increasing the tool diameter, could be also a solution for achieving a smoother workpiece, but it is limited by the ECM experimental implementation. To change the geometry of the tool, where the erosion of material is concentrated at the weld step, could be also another solution. However this solution is difficult to implement due to the non-uniformity of the weld step across the samples.

Nonetheless, the use of a virtual process for the solution of this problem instead of an experimental one will save time and reduce the costs related to the ECM process. Experimental validation is still needed, and it could be a good starting point for the further development of ECM in industry.

# *Chapter 4*

## *Conclusions and future work*

*A man who doesn't think for himself,*
*does not think at all.*
*-Oscar Wilde*

### *Conclusions*

The complexity of electrochemical machining (ECM) is the main reason for the development of the computational simulation of the process in this thesis. This simulation is based on the theoretical background presented in Chapter 1, and agrees with the experimental results of Chapter 2. Additionally, the model has demonstrated to be self-consistent and versatile, as demonstrated in Chapter 3.

The computational simulation model of ECM developed fulfils the ECM theory and was supported by experimental and published data. A computer aided design (CAD) software, SolidEdge®, was used for the construction of the geometry of the problem, and a finite element (FE) package, COMSOL Multiphysics®, was used to solve the diverse phenomena involved in ECM, such as fluid dynamics, heat transfer, electrodynamics, mass transfer and electrochemistry. FEM demonstrated to be a useful tool for their solution and by using COMSOL Multiphysics®, a coupled solution including the multiple phenomena of the process was possible. In this way, a single solution can show the process in full.

A clear methodology for the ECM simulation had been established. This methodology was mainly divided in five sections: system analysis, model generation, model set up, computer simulation and analysis of results. The systematic use of this methodology allows the modeller the correct application of the ECM simulation model and the achievement of consistent and accurate results.

The versatility of the ECM simulation model constructed and the methodology were proved by applying them in the simulation of the process: in a two dimensional environment, in a three dimensional environment, and in a real-world application. The simulation results of the 2D ECM simulation were compared with published simulation data and with previous work developed within the University of Edinburgh ECM group. A good agreement was found. One of the main advantages of the work described in this thesis is that it makes possible the extraction of further information about the process without the need for a third software or manual manipulation of the data. Machining input parameters, e.g. voltage, electrolyte flow rate, machining time, etc., could be easily modified using the user friendly interface of the FE package, and the information about the ECM process, such as electric potential distribution, current density, workpiece profile deformation, etc., could be extracted for any time during the machining.

These encouraging results were the first step for the work in collaboration with industry: pECM systems Ltd. form Barnsley, UK. The objective of the joint work was to enable the control of the process and to forecast the surface finish of pipes made of stainless steel 316 (SS316), which interior face was machined by ECM. The simulation techniques developed until now had the limitation of not being able to predict surface finish of the pieces, especially for the electrochemically machined SS alloys where the surface finish depends on the machining parameters and the behaviour of metal and electrolyte during the process.

In order to address the above problem, the experimental analysis presented in section 2.2 was developed. In this experimental work, the ECM machining parameters were varied in order to ascertain their influence, if any, on the surface finish of the SS316 samples. Once the main parameters were identified, this information can be used for an accurate prediction of the surface finish of SS316 samples machined by ECM. Results highlight the strong relationship between the surface finish and the overvoltage and current density during ECM. These parameters depend in turn on the machining parameters, the electrolyte characteristics and the interelectrode gap dimensions. For example, for a reflective and bright surface finish, a combination of parameters should be accomplish, i.e. overpotential between 9 and 15 V, current density over 4.5 $A/cm^2$, flow rate of 25 l/min, and gap equal or smaller than 4 mm. On the other hand, if the overpotential was below 5 V, or if the gap was too big (8 mm), a passivated surface was usually obtained, or if the flow rate was too high, a dark surface was then commonly observed.

The complexity of controlling these parameters experimentally emphasized the need for an ECM simulation model that would allow the user the development of the process virtually, and to estimate the outcome *a priori* of the experimental work. Therefore, in the last part of Chapter 2, an enhanced simulation model of ECM in a three dimensional (3D) environment was constructed. This new simulation model includes the multiple phenomena occurring during ECM, such as fluid dynamics, Joule heating and electrochemical reactions, as well as information extracted form experimental tests. As within the 2D simulation model, information about the behaviour of the process can be extracted, and this time, the harvesting of the proper data can lead to a good forecast of the surface finish of the sample, as seen in section 3.1. The results attained with the 3D simulation model were also compared with published data, and with the experimental results from the previous section, and good agreement between the experimental and simulation results was found, in terms of potential distribution, current density, electrolyte velocity and temperature.

When the simulation and experimental results of two opposite cases, i.e. reflective and bright, and passivated surface finish, were compared in Chapter 3, a reasonably concordance was observed between the experimental work and the simulation results. As expected, a higher overpotential and current density were related to a reflective and bright surface finish, and a lower overpotential and current density were related to a passivated surface finish. However some discrepancies between the simulation numerical values achieved and the expected were observed, e.g. the overpotential values from the simulation results were lower than the experimental ones by 2 V in average. These discrepancies could be result of not including the electrolyte concentration changes, the bubble generation and the efficiency of the process in the simulation model. More experimental work would be useful in order to verify it.

The 3D ECM simulation model was additionally applied for one reflective and bright surface finish case but using a different electrolyte, i.e. NaCl instead of NaNO3. The results agreed with published data, and this verifies the flexibility of the simulation model developed. It is expected that this model can also be applied for different materials. Still there is more experimental work that needs to be carried out and further development of the model is desirable in order to enhance the accuracy of the results.

At the end of this work, the model was applied as a means for forecasting the optimal machining time and profile that can be achieved by ECM on the SS316 samples. The results were encouraging but there is still experimental work to be done in order to verify the results and develop further this simulation model.

***Future work***

Although an enhanced three dimensional ECM simulation model was developed in this thesis, there is still room of improvement of it, and this will go hand in hand with the further experimental study of the ECM process.

From Chapter 1, more in depth research in the physical and chemical reactions that occur during the ECM process should be studied. The electrodynamics and electrochemistry in the area close to the workpiece surface (double layer) are still under research and not fully understood. Additionally, the type of metal used and the type of electrolyte represent an additional factor that needs to be addressed in order to control better the ECM process.

With the above in mind, a more detailed study on ECM on alloys with high chromium content, such as SS316, still needs to be done. The passivation film that these metals present is still not entirely understood. Moreover, different electrolytes can be used or developed to enhance the ECM results, therefore, a more detailed study of this aspect is also desirable.

The inclusion in the ECM simulation model of more accurate data is also needed. The addition of an overvoltage equation that accurately reproduces its real behaviour is desirable. Additionally, the simulation model requires to be evaluated for more complicated shapes, and for non-deal conditions. The validation of the simulation results with measurements in-situ of the ECM parameters, i.e. a more accurate measurement of the current during the process, and an in-situ measurement of the temperature of the electrolyte, would also be appropriate and could provide important data for the further development of the simulation model.

From Chapter 3, it is evident that the some improvements on the ECM simulation model should be done. The simulation model is considering a uniform laminar flow, and the results show that a transitional and even turbulent flow should be considered. Additionally the electrolyte concentration effects, gas generation and efficiency of the process should be included. Furthermore the modelling of the ECM products, chemical by products and sludge, should be addressed. This information could be used for pre-determining the safety and disposal of the used electrolytes.

Moreover, the tool design is a work in progress. Until now the results are encouraging, but there is still a lot of work to be done in this aspect. This is the most common problem of ECM in industry, and they are still looking for a solution for this problem; therefore, its further investigation is of high priority.

With respect to the work done in collaboration with pECM Systems Ltd®, the implementation of an accurate ECM simulation model that provides *a priori* information about the behaviour of ECM on SS316 samples using NaCl as electrolyte, is still a project under development. Additionally, the electrochemical machining of samples with more complicated geometry, and in different conditions would be a desirable next step.

# References


[1] S. Kalpakjian and S. R. Schmid, *Manufacturing Processes for Engineering Materials*, 5th ed. Singapore: Pearson Education, Inc, 2008.

[2] M. Hackert-Oschätzchen, S. F. Jahn, and A. Schubert, "Design of Electrochemical Machining Processes by Multiphysics Simulation," in *COMSOL Conference 2011*, 2011.

[3] D. Clifton, A. R. Mount, D. Jardine, and R. Roth, "Electrochemical machining of gamma titanium aluminide intermetallics," *J. Mater. Process. Technol.*, vol. 108, no. 3, pp. 338–348, 2001.

[4] J. Kozak, "Thermal models of pulse electrochemical machining," *Bull. Polish Acad. Sci. Tech. Sci.*, vol. 52, pp. 313–320, 2004.

[5] Z. Xu, D. Zhu, L. Wang, and X. Shi, "Study on flow field of turbine blade with flexible 3 - electrode feeding method in ECM," in *Technology and Innovation Conference, 2006. ITIC 2006. International*, 2006, pp. 135–139.

[6] N. S. Qu and Z. Y. Xu, "Improving machining accuracy of electrochemical machining blade by optimization of cathode feeding directions," *Int. J. Adv. Manuf. Technol.*, vol. 68, no. 5–8, pp. 1565–1572, 2013.

[7] S. D. Dhobe, B. Doloi, and B. Bhattacharyya, "Optimisation of ECM process during machining of titanium using quality loss function," *Int. J. Manuf. Technol. Manag.*, vol. 28, p. 19, 2014.

[8] R. Tijun, R. van Tijum, and P. DAP, "Electrochemical Machining in Appliance Manufacturing," *COMSOL News*, 2008.

[9] D. Deconinck, S. Van Damme, J. Deconinck, and S. Van Damme, "A temperature dependent multi-ion model for time accurate numerical simulation of the electrochemical machining process. Part I: Theoretical basis," *Electrochim. Acta*, vol. 60, pp. 321 – 328, 2012.

[10] D. Deconinck, S. Van Damme, C. Albu, L. Hotoiu, and J. Deconinck, "Study of the effects of heat removal on the copying accuracy of the electrochemical machining process," *Electrochim. Acta*, vol. 56, no. 16, pp. 5642 – 5649, 2011.

[11] J. Lu, G. Riedl, B. Kiniger, and E. A. Werner, "Three-dimensional tool design for steady-state electrochemical machining by continuous adjoint-based shape optimization," *Chem. Eng. Sci.*, vol. 106, pp. 198–210, Mar. 2014.

[12] Y. Yang, W. Natsu, and W. Zhao, "Realization of eco-friendly electrochemical micromachining using mineral water as an electrolyte," *Precis. Eng.*, vol. 35, no. 2, pp. 204–213, Apr. 2011.

[13] J. A. McGeough, "Electrochemistry Encyclopedia: Electrochemical Machining (ECM)," *http://electrochem.cwru.edu/encycl/*, 2005. [Online]. Available: http://electrochem.cwru.edu/encycl/art-m03-machining.htm.

[14] K. P. Rajurkar, D. Zhu, J. A. McGeough, J. Kozak, and A. K. M. De Silva, "New Developments in Electro-Chemical Machining," *CIRP Ann. - Manuf. Technol.*, vol. 48, no. 2, pp. 567–579, 1999.

[15] W. Gusseff, "Method and apparatus for the electrolytic treatment of metals," International: B23H3/04; B23H3/10, 1929.

[16] L. A. Williams, "Electrode for electrolytic shaping," US3019178 (A), B23H3/04, B23H3/04, 1959.

[17] H. Hardisty and A. R. Mileham, "Finite element computer investigation of the electrochemical machining process for a parabolically shaped moving tool eroding an arbitrarily shaped workpiece," *Proc. Inst. Mech. Eng. Part B J. Eng. Manuf.*, vol. 213, no. 8, pp. 787–798, 1999.

[18] R. Alkire, T. Bergh, and R. Sani, "Predicting Electrode Shape Change with Use of Finite Element Methods," *J. Electrochem. Soc.*, vol. 125, no. 12, pp. 1981–1988, Dec. 1978.

[19] P. Forsyth and H. Rasmussen, "Solution of Time Dependent Electrochemical Machining Problems by a Co-ordinate Transformation," *Inst. Maths Applics*, no. 24, pp. 411 – 424, 1979.

[20] J. Kozak, K. P. Rajurkar, and R. Balkrishna, "Study of Electrochemical Jet Machining process," *J. Manuf. Sci. Eng. Asme*, vol. 118, no. 4, pp. 490–498, 1996.

[21] G. Alder, D. Clifton, and F. Mill, "A direct analytical solution to the tool design problem in electrochemical machining under steady state conditions," *Proc. Inst. Mech. Eng. Part B J. Eng. Manuf.*, vol. 214, no. 8, pp. 745–750, 2000.

[22] J. Kozak, "Computer simulation system for electrochemical shaping," *J. Mater. Process. Technol.*, vol. 109, no. 3, pp. 354–359, 2001.

[23] M. Purcar, L. Bortels, B. Van den Bossche, and J. Deconinck, "3D electrochemical machining computer simulations," *J. Mater. Process. Technol.*, vol. 149, no. 1–3, pp. 472–478, 2004.

[24] L. Zhiyong and N. Zongwei, "Convergence Analysis of the Numerical Solution for Cathode Design of Aero-engine Blades in Electrochemical Machining," *Chinese J. Aeronaut.*, vol. 20, no. 6, pp. 570–576, 2007.

[25] B. C. Banerjee and P. L. Walker, "Electrolytic Micromachining of Iron Whisker Surfaces," *J. Electrochem. Soc.*, vol. 108, no. 3, pp. 262–265, 1961.

[26] A. R. Mount, P. S. Howarth, and D. Clifton, "The use of a segmented tool for the analysis of electrochemical machining," *J. Appl. Electrochem.*, vol. 31, no. 11, pp. 1213–1220, 2001.

[27] A. R. Mount, P. S. Howarth, and D. Clifton, "The Electrochemical Machining Characteristics of Stainless Steels," *J. Electrochem. Soc.*, vol. 150, no. 3, pp. D63–D69, 2003.

[28] Y. Zhou and J. J. Derby, "The cathode design problem in electrochemical machining," *Chem. Eng. Sci.*, vol. 50, no. 17, pp. 2679–2689, 1995.

[29] A. R. Mileham, H. Hardisty, H. Shirvani, and D. Clifton, "Integrating tool design and manufacture for electrochemical machining (ECM) using process simulation," in *Proc 10th ADM Conference - International Conference on Design Tools and Methods in Industrial Engineering*, 1997, pp. 785–796.

[30] J. McClennan, G. Alder, A. Sherlock, F. Mill, and D. Clifton, "Two-Dimensional Tool Design for Two-Dimensional Equilibrium Electrochemical Machining Die-Sinking Using a

Numerical Method," *Proc. Inst. Mech. Eng. -- Part B -- Eng. Manuf.*, vol. 220, no. 5, pp. 637–645, 2006.

[31] M. Datta and D. Landolt, "Electrochemical saw using pulsating voltage," *J. Appl. Electrochem.*, vol. 13, no. 6, pp. 795–802, 1983.

[32] B. Bhattacharyya, "Recent developments in electrochemical micromachining," *Pulse, PSG Coll. Technol.*, p. 8, 2000.

[33] B. Bhattacharyya and J. Munda, "Experimental investigation into electrochemical micromachining (EMM) process," *J. Mater. Process. Technol.*, vol. 140, no. 1–3, pp. 287–291, 2003.

[34] A. D. Davydov, V. M. Volgin, and V. V. Lyubimov, "Electrochemical machining of metals: Fundamentals of electrochemical shaping," *Russ. J. Electrochem.*, vol. 40, no. 12, pp. 1230–1265, 2004.

[35] L. Bortels, M. Purcar, B. Bossche, and J. Deconinck, "A user-friendly simulation software tool for 3D ECM," *J. Mater. Process. Technol.*, vol. 149, no. 1–3, pp. 486–492, 2004.

[36] J. Deconinck, G. Maggetto, and J. Vereecken, "Calculation of Current Distribution and Electrode Shape Change by the Boundary Element Method," *J. Electrochem. Soc.*, vol. 132, no. 12, pp. 2960–2965, 1985.

[37] O. H. Narayanan, S. Hinduja, and C. F. Noble, "Design of Tools for Electrochemical Machining by the Boundary Element Method," *Proc. Inst. Mech. Eng. Part C J. Mech. Eng. Sci.*, vol. 200, no. 3, pp. 195–205, May 1986.

[38] R. Alkire, D. Reiser, and R. Sani, "Effect of Fluid Flow on Removal of Dissolution Products from Small Cavities," *J. Electrochem. Soc.*, vol. 131, no. 12, pp. 2795–2800, 1984.

[39] H. Hardisty, A. R. Mileham, and H. Shirvani, "Theoretical and computational investigation of the electrochemical machining process for characteristic cases of a stepped moving tool eroding a plane surface," *Proc. Inst. Mech. Eng. Part B J. Eng. Manuf.*, vol. 211, no. 3, pp. 197–210, 1997.

[40] M. Purcar, A. Dorochenko, L. Bortels, J. Deconinck, and B. Van den Bossche, "Advanced CAD integrated approach for 3D electrochemical machining simulations," *J. Mater. Process. Technol.*, vol. 203, no. 1–3, pp. 58–71, 2008.

[41] A. R. Mount, D. Clifton, P. S. Howarth, and A. Sherlock, "An integrated strategy for materials characterisation and process simulation in electrochemical machining," *J. Mater. Process. Technol.*, vol. 138, no. 1–3, pp. 449–454, 2003.

[42] E. Rosset, M. Datta, and D. Landolt, "Electrochemical dissolution of stainless steels in flow channel cells with and without photoresist masks," *J. Appl. Electrochem.*, vol. 20, no. 1, pp. 69–76, 1990.

[43] A. Lozano-Morales, "Niobium Electropolishing Using an HF-free Electrolyte," *Plating & Surface Finishing*, vol. 96, no. 8, NASF, Washington DC, 2009.

[44] B. Bingham and J. Parmigiani, "The effect of Electrolyte Flow Slots in Tooling Electrodes on Final Anode Surface in Electrochemical Machining," in *COMSOL Conference 2013*, 2013.

[45] J. P. Hoare and C. R. Wiese, "Current efficiency during the electrochemical machining of iron and nickel," *Corros. Sci.*, vol. 15, no. 6–12, pp. 435–440, Jan. 1975.

[46] J. A. Westley, J. Atkinson, and A. Duffield, "Generic aspects of tool design for electrochemical machining," *J. Mater. Process. Technol.*, vol. 149, no. 1–3, pp. 384–392, 2004.

[47] M. A. Rosen and H. A. Kishawy, "Sustainable Manufacturing and Design: Concepts, Practices and Needs," *Sustainability*, vol. 4, no. 12, pp. 154–174, Jan. 2012.

[48] M. Groover, *Fundaments of modern manufacturing*, 3rd. ed. McGraw Hill, 2007.

[49] A. De Barr and D. A. Oliver, *Electrochemical Machining*. Macdonald & Company, 1968.

[50] E. O. Ezugwu, J. Bonney, and Y. Yamane, "An overview of the machinability of aeroengine alloys," *Journal of Materials Processing Technology*, vol. 134, no. 2. pp. 233–253, 2003.

[51] D. Jin and Z. Liu, "Damage of the machined surface and subsurface in orthogonal milling of FGH95 superalloy," *Int. J. Adv. Manuf. Technol.*, vol. 68, no. 5–8, pp. 1573–1581, 2013.

[52] R. Kovacevic, M. Hashish, R. Mohan, M. Ramulu, T. J. Kim, and E. S. Geskin, "State of the Art of Research and Development in Abrasive Waterjet Machining," *Journal of Manufacturing Science and Engineering*, vol. 119, no. 4B. p. 776, 1997.

[53] B. Benhabib, *Manufacturing. Design, Production, Automation and Integration*. New York, USA: Marcel Dekker, Inc., 2003.

[54] J. Kozak, K. P. Rajurkar, and Y. Makkar, "Study of Pulse Electrochemical Micromachining," *J. Manuf. Process.*, vol. 6, no. 1, pp. 7–14, 2004.

[55] V. Kirchner, C. Laurent, S. Rolf, and E. Gerhard, "Electrochemical machining of stainless steel microelements with ultrashort voltage pulses," *Appl. Phys. Lett.*, vol. 79, no. 11, pp. 1721–1723, 2001.

[56] H. E. Haring and W. Blum, "Trans. Am.," *Electrochem Soc.*, no. 44, p. 313, 1923.

[57] R. K. Pandey, *Handbook of seminconductor electrodeposition*. New York, USA: Marcel Dekker, Inc., 1996.

[58] C. L. Faust, "Surface Preparation by Electropolishing," *J. Electrochem. Soc.*, vol. 95, no. 3, p. 62C–72C, 1949.

[59] E. Bishop and A. L. Livshits, *Electro-Erosion Machining of Metals*. London: Dept. of Scientific and Industrial Resaerch by Butterworths Inc, 1960.

[60] J. A. McGeough, *Principles of electrochemical machining*. London: Chapman and Hall, 1974.

[61] H. K. Nelson, "Turbine and compressor blades." Google Patents, 21-Feb-1961.

[62] ECM Technologies, "ECM Technologies," *CoC Leeuwarden*, 2013. [Online]. Available: http://electrochemicalmachining.com/technology/processes-application. [Accessed: 09-Oct-2015].

[63] N. Ibl and D. Landolt, "On the Mechanism of Anodic Chlorate Formation in Dilute NaCl Solutions," *J. Electrochem. Soc.*, vol. 115, no. 7, pp. 713–720, 1968.

[64] K. Kinoshita, D. Landolt, R. H. Muller, and C. W. Tobias, "Stoichiometry of Anodic Copper Dissolution at High Current Densities," *J. Electrochem. Soc.*, vol. 117, no. 10, pp. 1246–1251, 1970.

[65] D. Landolt, R. Acosta, R. H. Muller, and C. W. Tobias, "An Optical Study of Cathodic Hydrogen Evolution in High Rate Electrolysis," *J. Electrochem. Soc.*, vol. 117, no. 6, pp. 839–845, 1970.

[66] D. Landolt, "Throwing Power Measurements during High Rate Nickel Dissolution under Active and Transpassive Conditions," *J. Electrochem. Soc.*, vol. 119, no. 6, pp. 708–712, 1972.

[67] M. Datta and D. Landolt, "Surface Brightening during High Rate Nickel Dissolution in Nitrate Electrolytes," *J. Electrochem. Soc.*, vol. 122, no. 11, pp. 1466–1472, 1975.

[68] M. Datta, "Fabrication of an Array of Precision Nozzles by Through Mask Electrochemical Micromachining," *J. Electrochem. Soc.*, vol. 142, no. 11, pp. 3801–3805, 1995.

[69] M. Datta, R. V. Shenoy, and L. T. Romankiw, "Recent advances in the study of electrochemical micromachining," *J. Eng. Ind. - Trans. ASME*, vol. 118, no. 1, pp. 29–36, 1996.

[70] M. Datta and D. Harris, "Electrochemical micromachining: An environmentally friendly, high speed processing technology," *Electrochim. Acta*, vol. 42, no. 20–22, pp. 3007 – 3013, 1997.

[71] M. Datta and D. Landolt, "Fundamental aspects and applications of electrochemical microfabrication," *Electrochim. Acta*, vol. 45, no. 15–16, pp. 2535 – 2558, 2000.

[72] M. Datta, Y. Heights, and T. O'Toole, "Electrochemical metal removal technique for planarization on surfaces.," 1996.

[73] J. Bannard, "On the electrochemical machining of some titanium alloys in bromide electrolytes," *J. Appl. Electrochem. Soc.*, vol. 6, no. 6, p. 477, 1976.

[74] J. B. Mathieu, H. J. Mathieu, and D. Landolt, "Electropolishing of Titanium in Perchloric Acid Acetic Acid Solution: I . Auger Electron Spectroscopy Study of Anodic Films," *J. Electrochem. Soc.*, vol. 125, no. 7, pp. 1039–1043, 1978.

[75] A. R. Mount, K. L. Eley, and D. Clifton, "Theoretical analysis of chronoamperometric transients in electrochemical machining and characterization of titanium 6/4 and inconel 718 alloys," *J. Appl. Electrochem.*, vol. 30, no. 4, pp. 447–455, 2000.

[76] D. Clifton, A. R. Mount, G. Alder, and D. Jardine, "Ultrasonic measurement of the inter-electrode gap in electrochemical machining," *Int. J. Mach. Tools Manuf.*, vol. 42, no. 11, pp. 1259–1267, 2002.

[77] M. Matlosz and D. Landolt, “Shape Changes in Electrochemical Polishing: The Effect of Temperature on the Anodic Leveling of Fe2 4Cr,” *J. Electrochem. Soc.*, vol. 136, no. 4, pp. 919–929, 1989.

[78] L. Ponto and D. Landolt, “Electropolishing of chromium in phosphoric acid-sulphuric acid electrolytes,” *J. Appl. Electrochem.*, vol. 17, no. 1, pp. 205–214, 1987.

[79] T. Haisch, E. Mittemeijer, and J. W. Schultze, “Electrochemical machining of the steel 100Cr6 in aqueous NaCl and NaNO3 solutions: microstructure of surface films formed by carbides,” *Electrochim. Acta*, vol. 47, no. 1–2, pp. 235 – 241, 2001.

[80] M. M. Lohrengel, I. Klüppel, C. Rosenkranz, H. Bettermann, and J. W. Schultze, “Microscopic investigations of electrochemical machining of Fe in NaNO3,” *Electrochim. Acta*, vol. 48, no. 20–22, pp. 3203 – 3211, 2003.

[81] S. K. Mukherjee, S. Kumar, P. K. Srivastava, and A. Kumar, “Effect of valency on material removal rate in electrochemical machining of aluminium,” *J. Mater. Process. Technol.*, vol. 202, no. 1–3, pp. 398–401, 2008.

[82] A. Ruszaj, “Investigations on the process of electrochemical sinking, taking into account the randomness of the phenomena occuring in the machining area.,” *Wear*, no. 147, pp. 25–40, 1991.

[83] S. K. Mukherjee, S. Kumar, and P. K. Srivastava, “Effect of over voltage on material removal rate during electrochemical machining,” *Tamkang J. Sci. Eng.*, vol. 8, no. 1, pp. 23–28, 2005.

[84] J. C. da Silva Neto, E. M. da Silva, and M. B. da Silva, “Intervening variables in electrochemical machining,” *J. Mater. Process. Technol. 179, 1/3; 92-96, Brazilian Congr. Manuf. Eng. COBEF 2005, 3rd, Brazilian Congr. Manuf. Eng. COBEF 2005*, p. 5 Pages, 2006.

[85] R. Muir, D. Curry, F. Mill, A. Sherlock, and A. R. Mount, “Real-time parameterization of electrochemical machining by ultrasound measurement of the interelectrode gap,” *Proc. Inst. Mech. Eng. Part B J. Eng. Manuf.*, vol. 221, no. 4, pp. 551–558, 2007.

[86] M. Schneider, S. Schroth, S. Richter, S. Höhn, N. Schubert, and A. Michaelis, “In-situ investigation of the interplay between microstructure and anodic copper dissolution under near-ECM conditions - Part 2: The transpassive state,” *Electrochim. Acta*, vol. 56, no. 22, pp. 7628 – 7636, 2011.

[87] M. Schneider, S. Schroth, N. Schubert, and A. Michaelis, "In-situ investigation of the surface-topography during anodic dissolution of copper under near-ECM conditions," *Mater. Corros.*, vol. 63, no. 2, pp. 96–104, 2012.

[88] V. Bakhir, "Electrochemical Systems and Technologies," *Vitold Bakhir, www.bakhir.com*, 2014. [Online]. Available: http://www.bakhir.com/other/1thzayavka1/. [Accessed: 28-Oct-2014].

[89] D. T. Chin and C. H. Tsang, "Mass Transfer to an Impinging Jet Electrode," *J. Electrochem. Soc.*, vol. 125, no. 9, pp. 1461–1470, 1978.

[90] M. S. Amalnik and J. A. McGeough, "Intelligent concurrent manufacturability evaluation of design for electrochemical machining," *J. Mater. Process. Technol.*, vol. 61, no. 1–2, pp. 130–139, 1996.

[91] K. P. Rajurkar, D. Zhu, and B. Wei, "Minimization of Machining Allowance in Electrochemical Machining," *CIRP Ann. - Manuf. Technol.*, vol. 47, no. 1, pp. 165–168, 1998.

[92] K. P. Rajurkar and D. Zhu, "Improvement of Electrochemical Machining Accuracy by Using Orbital Electrode Movement," *CIRP Ann. - Manuf. Technol.*, vol. 48, no. 1, pp. 139–142, 1999.

[93] S. P. Pavlinich, "The outlook for application of pulse electrochemical machining in the manufacturing of gas turbine engine parts," *Ufa State Aeronaut. Univ.*, vol. 11, no. N2(29), pp. 105–115, 2008.

[94] Y. Zhang, "Investigation into current efficiency for pulse electrochemical machining of nickel alloy," University of Nebraska, 2010.

[95] L. Blaine, "Application of pulsed electrochemical machining to micromold fabrication," in *SPE/ANTEC 2000*, 2000.

[96] A. N. Zaytsev, V. P. Zhitnikov, and T. V. Kosarev, "Formation mechanism and elimination of the workpiece surface macro-defects, aligned along the electrolyte stream at electrochemical machining," *J. Mater. Process. Technol.*, vol. 149, no. 1–3, pp. 439–444, 2004.

[97] P. V. Jadhav and D. S. Bilgi, "Improvement of electrochemical machining accuracy by using rotating electrode movement.," *International conference on total engineering analysis and manufacturing technologies*. IISC, Bangalore, 2007.

[98] T. Kurita, C. Endo, Y. Matsui, H. Masuda, K. Terasawa, F. Tanaka, H. Ikeda, K. Oguchi, and K. Kobayashi, "Mechanical/electrochemical complex machining method for efficient, accurate, and environmentally benign process," *Int. J. Mach. Tools Manuf.*, vol. 48, no. 15, pp. 1599–1604, 2008.

[99] C. Senthilkumar, G. Ganesan, and R. Karthikeyan, "Parametric optimization of electrochemical machining of Al/15% SiCp composites using NSGA - II," *Trans. Nonferrous Met. Soc. China*, vol. 21, no. 10, pp. 2294–2300, 2011.

[100] H. Hocheng, Y. H. Sun, S. C. Lin, and P. S. Kao, "A material removal analysis of electrochemical machining using flat-end cathode," *J. Mater. Process. Technol.*, vol. 140, no. 1, pp. 264–268, 2003.

[101] M. Sen and H. S. Shan, "A review of electrochemical macro- to micro-hole drilling processes," *Int. J. Mach. Tools Manuf.*, vol. 45, no. 2, pp. 137–152, 2005.

[102] M. Sen and H. S. Shan, "Analysis of hole quality characteristics in the electro jet drilling process," *Int. J. Mach. Tools Manuf.*, vol. 45, no. 15, pp. 1706–1716, 2005.

[103] B. Bhattacharyya and J. Munda, "Experimental investigation on the influence of electrochemical machining parameters on machining rate and accuracy in micromachining domain," *Int. J. Mach. Tools Manuf.*, vol. 43, no. 13, pp. 1301–1310, 2003.

[104] B. Bhattacharyya, J. Munda, and M. Malapati, "Advancement in electrochemical micro-machining," *Int. J. Mach. Tools Manuf.*, vol. 44, no. 15, pp. 1577–1589, 2004.

[105] P. Domanowski and J. Kozak, "Direct and inverse problems of shaping by electrochemical generating machining," *J. Mater. Process. Technol.*, vol. 107, no. 1–3, pp. 300–306, 2000.

[106] J. Kozak, L. Dabrowski, K. Lubkowski, M. Rozenek, and R. Slawinski, "CAE-ECM system for electrochemical technology of parts and tools," *J. Mater. Process. Technol.*, vol. 107, no. 1–3, pp. 293–299, 2000.

[107] P. Forsyth and H. Rasmussen, "High order perturbation solution of the electrochemical smoothing problem," *Comput. Appl. Math.*, vol. 6, no. 1, 1980.

[108] R. Sautebin, H. Froidevaux, and D. Landolt, "Theoretical and Experimental Modeling of Surface Leveling in ECM under Primary Current Distribution Conditions," *J. Electrochem. Soc.*, vol. 127, no. 5, pp. 1096–1100, 1980.

[109] G. A. Prentice and C. W. Tobias, "Simulation of Changing Electrode Profiles," *J. Electrochem. Soc.*, vol. 129, no. 1, pp. 78–85, 1982.

[110] M. Hackert-Oschätzchen, G. Meichsner, and A. Schubert, "Simulation of the Shape of Micro Geometries generated with Jet Electrochemical Machining," in *COMSOL Conference 2008*, 2008.

[111] M. Hackert-Oschätzchen, N. Lehnert, M. Kowalick, G. Meichsner, and A. Schubert, "Analysis of the Electrochemical Removal of Aluminium Matrix Composites Using Multiphysics Simulation," in *2014 COMSOL Conference in Cambridge*, 2014.

[112] X. Li, J. Wang, and W. Li, "Current state and prospect of micro-machining," in *Proceedings of the IEEE International Conference on Automation and Logistics, ICAL 2007*, 2007, pp. 1414–1419.

[113] P. S. Howarth, "The electrochemistry of Electrochemical Mahcining," The University of Edinburgh, 2003.

[114] R. Muir, "The Parameterisation of Electrochemical Machining," The University of Edinburgh, 2006.

[115] H. A. El-Hofy, *Fundamentals of Machining Processes: Conventional and Nonconventional Processes*. Florida, USA, 2007.

[116] V. K. Jain and P. C. Pandey, "CAD of ECM tools," *Comput. Des.*, vol. 12, no. 6, pp. 309–315, 1980.

[117] D. Clifton, A. R. Mount, F. Mill, and P. S. Howarth, "Characterization and representation of non-ideal effects in electrochemical machining," *Proc. Inst. Mech. Eng. J. Eng. Manuf.*, vol. 217, no. Article, pp. 373–385, 2003.

[118] D. Curry, "Time-Dependent simulation of electrochemical machining under ideal and non-ideal conditions," The University of Edinburgh, 2007.

[119] M. Burger, L. Koll, E. A. Werner, and A. Platz, "Electrochemical machining characteristics and resulting surface quality of the nickel-base single-crystalline material LEK94," *J. Manuf. Process.*, vol. 14, no. 1, pp. 62–70, 2012.

[120] John Brown Automation Ltd, "Automated 360° ECM Cell for Rolls-Royce Compressor Blade Manufacture," *Aircr. Eng. Aerosp. Technol.*, vol. 57, no. 11, pp. 14–15, Nov. 1985.

[121] W. Xu, J. Song, J. Sun, Q. Dou, and X. Fan, "Fabrication of superhydrophobic surfaces on aluminum substrates using NaNO3 electrolytes," *J. Mater. Sci.*, vol. 46, no. 18, pp. 5925–5930, 2011.

[122] E. Technologies, "ECM Technologies," 2013. [Online]. Available: http://www.electrochemicalmachining.com/. [Accessed: 31-Oct-2014].

[123] Stankonfinexpo, "Stankofinexpo," 2014. [Online]. Available: http://stankofinexpo.com/application-field/aircraft-building-aircraft-engine-industry-automobile-industry/. [Accessed: 31-Oct-2014].

[124] R. Van Tijum and P. T. Pajak, "COMSOL Technical Papers and Presentations," *COMSOL Conference 2008*, 2008. [Online]. Available: http://www.comsol.com/paper/simulation-of-production-processes-using-the-multiphysics-approach-the-electroch-4896. [Accessed: 31-Oct-2014].

[125] J. M. Fitz-Gerald and J. A. McGeough, "Mathematical Theory of Electrochemical Machining 1. Anodic Smoothing," *IMA J. Appl. Math.*, vol. 5, no. 4, pp. 387–408, Dec. 1969.

[126] J. A. McGeough and H. Rasmussen, "On the Derivation of the Quasi-steady Model in Electrochemical Machining," *IMA J. Appl. Math.*, vol. 13, no. 1, pp. 13–21, Feb. 1974.

[127] A. A. Lacey, "Tool Design for Electrochemical Machining in the Presence of Overpotentials," *IMA J. Appl. Math.*, vol. 35, no. 3, pp. 357–364, Nov. 1985.

[128] T. Ozis, "An efficient approach to the solution of the two-dimensional electrochemical machining problem," *J. Comput. Appl. Math.*, vol. 36, no. 2, pp. 239–246, 1991.

[129] J. Kozak, A. F. Budzynski, and P. Domanowski, “Computer simulation electrochemical shaping (ECM-CNC) using a universal tool electrode,” *J. Mater. Process. Technol.*, vol. 76, no. 1–3, pp. 161–164, 1998.

[130] J. Kozak, M. Chuchro, A. Ruszaj, and K. Karbowski, “The computer aided simulation of electrochemical process with universal spherical electrodes when machining sculptured surfaces,” *J. Mater. Process. Technol.*, vol. 107, no. 1–3, pp. 283–287, 2000.

[131] A. K. M. De Silva, H. S. J. Altena, and J. A. McGeough, “Precision ECM by Process Characteristic Modelling,” *CIRP Ann. - Manuf. Technol.*, vol. 49, no. 1, pp. 151–155, 2000.

[132] R. Temur, T. J. Coole, and C. Bocking, “Simulation of the Electrochemical Machining Process,” in *Proeedings of the Solid Freeform Fabrication Symposium*, 2001, pp. 486–496.

[133] R. Temur, C. Bocking, and T. J. Coole, “Building Tool Electrodes for Electrochemical Machining,” in *Net Shape Manufacturing Conference*, 2001.

[134] D. Curry, A. Sherlock, A. R. Mount, and R. Muir, “Time-dependent simulation of electrochemical machining under non-ideal conditions,” in *Simulation of Electrochemical Processes*, R. A. Adey, Ed. SOUTHAMPTON: WIT PRESS, 2005, pp. 133–142.

[135] L. W. Hourng and C. C. Chen, “Numerical simulation and analysis of the electrochemical machining,” *J. Chinese Soc. Mech. Eng. Trans. Chinese Inst. Eng. Ser. C/Chung-Kuo Chi Hsueh K. Ch’eng Hsuebo Pao*, vol. 13, no. 1, pp. 52–61, 1992.

[136] T. Fujisawa, K. Inaba, M. Yamamoto, and D. Kato, “Multiphysics Simulation of Electrochemical Machining Process for Three-Dimensional Compressor Blade,” *J. Fluids Eng.*, vol. 130, no. 8, p. 81602, 2008.

[137] M. H. Wang and D. Zhu, “Simulation of fabrication for gas turbine blade turbulated cooling hole in ECM based on FEM,” *J. Mater. Process. Technol.*, vol. 209, no. 4, pp. 1747–1751, Feb. 2009.

[138] N. Wan, K. Du, R. Mo, and T. Chen, “The Electrochemical Machining Analysis of Aeroengine Blade Based on Isogeometric Method,” *Adv. Mech. Eng.*, 2014.

[139] Z. W. Fan and L. W. Hourng, “Electrochemical micro-drilling of deep holes by rotational cathode tools,” *Int. J. Adv. Manuf. Technol.*, pp. 555–563, 2011.

[140] M. H. Wang, W. Liu, and W. Peng, "Multiphysics research in electrochemical machining of internal spiral hole," *Int. J. Adv. Manuf. Technol.*, vol. 74, no. 5–8, pp. 749–756, 2014.

[141] R. Thanigaivelan, R. M. Arunachalam, B. Karthikeyan, and P. Loganathan, "Electrochemical Micromachining of Stainless Steel with Acidified Sodium Nitrate Electrolyte," *Procedia CIRP*, vol. 6, no. 0, pp. 351–355, 2013.

[142] R. Ganjir and C. K. Biswas, "Optimisation of Process Parameters in ECM by using Rotary U Shaped Tool," National Institute of Technology Rourkela, Orissa, India, 2011.

[143] M. K. Das, K. Kumar, T. K. Barman, and P. Sahoo, "Optimization of Surface Roughness and MRR in Electrochemical Machining of EN31 Tool Steel Using Grey-taguchi Approach," *Procedia Mater. Sci.*, vol. 6, pp. 729–740, 2014.

[144] L. Gordon, "Surface finish in special metals, such as stainless steel, is still not entirely predictable.," *Penton Media, Inc.*, 2010. [Online]. Available: http://machinedesign.com/manufacturing-equipment/advanced-manufacturing-different-twist-electrochemical-machining. [Accessed: 11-Feb-2015].

[145] M. Hackert-Oschätzchen, G. Meichsner, M. Zinecker, A. Martin, and A. Schubert, "Micro machining with continuous electrolytic free jet," *Precis. Eng.*, vol. 36, no. 4, pp. 612–619, 2012.

[146] Z. Liu, Y. Zeng, and W. Zhang, "Fabrication of Metal Microtool Applying Wire Electrochemical Machining," *Adv. Mech. Eng.*, vol. 2014, pp. 1–7, 2014.

[147] T. Kurita and M. Hattori, "A study of EDM and ECM/ECM-lapping complex machining technology," *Int. J. Mach. Tools Manuf.*, vol. 46, no. 14, pp. 1804–1810, 2006.

[148] D. Clifton, "Process Characterisation for Electrochemical Machining," University of Edinburgh, 2001.

[149] Chem Fax, "Electrolysis of Potassium Iodide." Flinn Scientific, Inc., Illinois, USA, 2009.

[150] I. Gardner Business Media, "Pulse power boosts electrolytic machining accuracy," 2012. [Online]. Available: http://www.mmsonline.com/articles/pulse-power-boosts-electrolytic-machining-accuracy. [Accessed: 28-Oct-2014].

[151] U. Mallick and C. K. Biswas, "Estimation of MRR Using U-Shape Electrode in Electrochemical Machining," NATIONAL INSTITUTE OF TECHNOLOGY, Roukela, India, 2009.

[152] A. C. Fischer-Cripps, *The electronics companion*. London: Institute of Physics, 2004.

[153] Sakshat Virtual Labs, "Study of Electrochemical machining process," 2014. [Online]. Available: http://coep.vlab.co.in/?sub=34&brch=105&sim=1423&cnt=1. [Accessed: 03-Nov-2014].

[154] H. S. Shan and P. C. Pandey, *Modern Machining Process*, First Edit. New Delhi: Tata McGraw-Hill Education Pvt. Ltd., 1980.

[155] J. P. Hoare, M. A. LaBoda, M. L. McMillan, and A. J. Wallace, "An Investigation of the Differences Between NaCl and NaClO3 as Electrolytes in Electrochemical Machining," *J. Electrochem. Soc.*, vol. 116, no. 2, pp. 199–203, Feb. 1969.

[156] E. J. Bergquist and L. J. Jennings, "Electrolyte for electrochemical machining of nickel base superalloys," 3975245, 1976.

[157] D. Pletcher and F. Walsh, *Industrial Electrochemistry*, Paperback. Glasgow: Blackie Academic & Professional, 1993.

[158] Y. A. Cengel, R. H. Turner, and R. Smith, "Fundamentals of Thermal-Fluid Sciences," *Applied Mechanics Reviews*, vol. 54. p. B110, 2001.

[159] M. & M. E. Aerospace, "Entrance length," *University of Sydney*, 2005. [Online]. Available: http://www-mdp.eng.cam.ac.uk/web/library/enginfo/aerothermal_dvd_only/aero/fprops/pipeflow/node9.html. [Accessed: 19-Apr-2014].

[160] B. Wei, K. P. Rajurkar, and S. Talpallikar, "Identification of Interelectrode Gap Sizes in Pulse Electrochemical Machining," *J. Electrochem. Soc.*, vol. 144, no. 11, pp. 3913–3919, Nov. 1997.

[161] A. J. Bard, G. Inzelt, and F. Scholz, *Electrochemical dictionary*, vol. 54. 2012.

[162] I. I. T. Kharagpur, "Non conventional machining: Electro Chemical Machining," *IIT Kharagpur*, no. Version 2 ME. p. 15, 2015.

[163] D. Landolt, R. H. Müller, and C. W. Tobias, "High Rate Anodic Dissolution of Copper," *J. Electrochem. Soc.*, vol. 116, no. 10, pp. 1384–1390, Oct. 1969.

[164] D. Landolt, R. H. Muller, and C. W. Tobias, "TRANSFER PROCESSES IN ECM.," U.S. Atomic Energy Commission, Jan. 1970.

[165] P. B. Saxena, *Chemistry of interhalogen compounds*. Delhi: Sachin Printers, Delhi, 2007.

[166] Z. Gasem, "Kinetics of passivation," *ME 472*, 2014. [Online]. Available: http://ocw.kfupm.edu.sa/ocw_courses/user062/ME4720102/Lecture Notes/chapter4.pdf. [Accessed: 05-Nov-2014].

[167] A. M. Helmenstine, "About Education," *About.com*, 2014. [Online]. Available: http://chemistry.about.com/od/chemistryglossary/a/valencedef.htm. [Accessed: 19-Dec-2014].

[168] A. Keshari, "Advanced Techniques for Monitoring, Simulation and Optimization of Machining Processes," UNIVERSITÀ DEGLI STUDI DI NAPOLI FEDERICO II, 2011.

[169] COMSOL Ltd., *Introduction to COMSOL Multiphysics*, COMSOL 4.2. Cambridge, UK: COMSOL Ltd., 2011.

[170] C. M. Hui, "Energy Performance of Air-conditioned Buildings in Hong Kong," City University of Hong Kong, 1996.

[171] C. Kiliçaslan, "Modelling and Simulation of Metal Cutting by Finite Element Method," İzmir Institute of Technology, 2009.

[172] R. Söderlund, "Finite element methods for multiscale/multiphysics problems," Uppsala University, 2011.

[173] E. H. J. Page, "Simulation Modeling Methodology: Principles and Etiology of Decision Support," Virginia Polytechnic Institute and State University, 1994.

[174] D. Matko, B. Zupancic, and R. Karba, *Simulation and modelling of continuous systems : A case study approach*. New York,N.Y.: Prentice Hall, 1992.

[175] Autodesk, "Joule Heating," *Learning Guide Autodesk Simulation*, 2014. [Online]. Available: http://help.autodesk.com/cloudhelp/2014/ITA/SimCFD/files/GUID-ED418E2B-26BD-4351-886A-E6C0AF8F1EF5.htm. [Accessed: 14-Nov-2014].

[176] ASM.matweb.com, "AISI Type 316 Stainless Steel, annealed sheet," *ASM Aerospace Specification Metals Inc.*, 2007. [Online]. Available: http://asm.matweb.com/search/SpecificMaterial.asp?bassnum=MQ316A.

[177] T. Isono, "Density, viscosity, and electrolytic conductivity of concentrated aqueous electrolyte solutions at several temperatures. Alkaline-earth chlorides, lanthanum chloride, sodium chloride, sodium nitrate, sodium bromide, potassium nitrate, potassium bromide, a," *J. Chem. Eng. Data*, vol. 29, no. 1, pp. 45–52, Jan. 1984.

[178] E. Madenci and I. Guven, *The finite element method and applications in engineering using ANSYS*. Arizona: Springer Science & Business Media LLC, 2006.

[179] H. Tipton, "The dynamics of electrochemical machining.," 1964.

[180] Matweb LLC, "Online Materials Information Resource," *http://www.matweb.com*, 2014. [Online]. Available: http://www.matweb.com/index.aspx. [Accessed: 20-Oct-2014].

[181] P. S. Z. Rogers and K. Pitzer, "Volumetric Properties of Aqueous Sodium Chloride Solutions," *J. Phys. Chem.*, vol. 11, no. 1, 1982.

[182] P. M. Emerson, "Theory and Application of Conductivity." Rosemount Analytical Inc., Irvine, CA USA, 2010.

[183] KCI Publishing B.V. Zutphen, "Stainless Steel world," 2014. [Online]. Available: http://www.stainless-steel-world.net/.

[184] COGNE, "Concrinox (R)," *Cogne Acciai Speciali S.p.a*, 2014. [Online]. Available: http://www.cogne.com/en/concrinox2.asp. [Accessed: 12-Dec-2014].

[185] Y. V. Alekseev, "Development or Stagnation of the Theory of Metal Passivity," *Prot. Met.*, vol. 41, no. 5, pp. 491–505, 2005.

[186] T. Wagner, "High rate electrochemical dissolution of iron-bassed alloys in NaCl and NaNO3 electrolytes," Universitat Stuttgart, 2002.

[187] J. Bannard, "Electrochemical machining," *J. Appl. Electrochem.*, vol. 7, no. 1, pp. 1–29, 1977.

[188] D. Sazou, M. Pavlidou, and M. Pagitsas, "Temporal patterning of the potential induced by localized corrosion of iron passivity in acid media. Growth and breakdown of the oxide

film described in terms of a point defect model.," *Phys. Chem. Chem. Phys.*, vol. 11, no. 39, pp. 8841–54, Oct. 2009.

[189] M. F. Khalil, S. Z. Kassab, I. G. Adam, and M. Samaha, "Laminar Flow in Concentric Annulus with a Moving Core," in *Twelfth International Water Technology Conference*, 2008, pp. 439–457.

[190] A. R. Mileham, "Letter," *Precis. Eng.*, vol. 4, no. 3, p. 124, Jul. 1982.

[191] M. H. Wang, D. Zhu, and W. Peng, "Experimental Research on Electrochemical Micromachining," in *Advanced Design and Manufacture to Gain a Competitive Edge*, X.-T. Yan, C. Jiang, and B. Eynard, Eds. Springer London, 2008, pp. 775–783.

[192] J. Kozak, K. P. Rajurkar, and Y. Makkar, "Selected problems of micro-electrochemical machining," *J. Mater. Process. Technol.*, vol. 149, no. 1–3, pp. 426–431, 2004.

[193] D. Lappin, A. Mohammadi, and K. Takahata, "An experimental study of electrochemical polishing for micro-electro-discharge-machined stainless-steel stents," *J. Mater. Sci. Mater. Med.*, vol. 23, no. 2, pp. 349–356, 2012.

[194] Y. Liu, D. Zhu, and L. Zhu, "Micro electrochemical milling of complex structures by using in situ fabricated cylindrical electrode," *Int. J. Adv. Manuf. Technol.*, vol. 60, no. 9, pp. 977–984, 2012.

[195] J. E. Mott and D. D. Joseph, "Stability of Parallel Flow between Concentric Cylinders," *Phys. Fluids*, vol. 11, no. 10, pp. 2066–2073, 1968.

[196] A. Japper-Jaafar, M. P. Escudier, and R. J. Poole, "Transition to turbulence in a concentric annular pipe," in *ISUD 7 Proceedings*, 2010, pp. 99–102.

[197] M. Avcı and O. Aydın, "Laminar forced convection slip-flow in a micro-annulus between two concentric cylinders," *Int. J. Heat Mass Transf.*, vol. 51, no. 13–14, pp. 3460–3467, Jul. 2008.

[198] M. Datta and D. Landolt, "On the role of mass transport in high rate dissolution of iron and nickel in ECM electrolytes—I. Chloride solutions," *Electrochim. Acta*, vol. 25, no. 10, pp. 1255–1262, Oct. 1980.

[199] M. Datta and D. Landolt, "On the role of mass transport in high rate dissolution of iron and nickel in ECM electrolytes—II. Chlorate and nitrate solutions," *Electrochim. Acta*, vol. 25, no. 10, pp. 1263–1271, Oct. 1980.